UiT The Arctic University of Norway

Faculty of Science and Technology

Neoglacial plateau ice cap behaviour in Central Spitsbergen constrained by subglacially preserved vegetation.

Amélie Roche

Master's thesis in Geology - GEO-3900

June 2021

Abstract

Cold-based glacial ice is well known to preserve underlying landforms produced by earlier processes but can also preserve pre-existing organic material and vegetated ground. With current rapid climate warming, overall glacier retreat in the Arctic is exposing formerly ice-buried in situ vegetation at the margin of cold-based ice bodies. Radiocarbon dating of this vegetation constrains the timing of advance of ice over the specific location where the vegetation was collected. Widespread sampling, identification, and dating of vegetation emerging from various ice bodies can permit the reconstruction of the conditions and timing of the latest ice advance in a specific region. While this method has been used in a range of places in the North American Arctic, its application elsewhere has hitherto been limited.

Here 11 samples of in situ preserved bryophyte patches from the margins of three plateau ice caps are presented: Bassen, Foxfonna, and Frostisen, in central Spitsbergen, Svalbard. While it cannot be stated when their Neoglacial ice growth initiated, we found that Bassen was already advancing between 2.2 and 1.5 cal. ka BP, and Foxfonna and Frostisen between 1.5 and 1.2 cal. ka BP, the ice caps being as large as today already before these periods, implying an earlier onset of the Neoglaciation. All available published data in relation to vegetation buried by glaciers in Svalbard were gathered within the VEGLAS database allowing for a wider comprehension of neoglacial advances in Svalbard. Two main advance phases are identified in this dataset. A first advance between 1650 and 1150 BP, corresponding to the Dark Ages Cold Period, and a second advance between 850 and 500 BP, corresponding to the first half of the Little Ice Age. A high frequency of ice caps not behaving according to these general ice advance phases has been observed, revealing the existence of an unexpected disparity in glacial dynamics for the ice caps present in Svalbard.

Reconstructing constraining ages on the timing and style of Late Holocene glacier readvances enables a clearer understanding of cold-based ice cap responses to climate change and can therefore contribute in developing more nuanced projections for future ice caps behaviour.

Acknowledgements

While finalizing this master thesis, I take measure of the number of people that have been assisting me with different aspects of my work during the past year. I am grateful for all your help and consequently would like to acknowledge:

Mark Furze for your guidance and supervision before and during my thesis. I don't have the words to say how thankful I am for everything you did to help me!

Anders Schomacker for your supervision and your valuable comments on the manuscript.

Jóhanna, Tenna, Mark, Marjolein and Andy for unfailing assistance during long and challenging field days.

Charlie, Audun and Sara Mollie for remarkable boat driving while dropping off, picking up (or attempting to) and rescuing the desperate, wet, and exhausted field team in challenging weather and sea conditions. Thanks for not letting us sleep out there!

Simone Lang for thorough work with species identification of the mosses, lichens and angiosperms collected in the field, and Matthias Ahrens as he helped with identifying the most difficult ones.

Sönke Szidat, from the Laboratory for the Analysis of Radiocarbon with AMS of the University of Bern, Switzerland, for your collaboration to the project and the realization of all the radiocarbon measurements.

Wesley Farnsworth for providing the GPS track from 2015 for the ice margin position of Bassen ice cap and for your attempt to supply additional samples to the study.

Andy Hodson for providing the two samples collected in 2019 at Foxfonna.

Marjolein Gevers for being by my side while we were both going through the long process of writing our respective theses.

Joe Buckby for your helpfulness and your comments on the manuscript.

Erik S. Manerfelt for interesting long-distance discussions about my results, though I miss the face to face ones that we used to have in pre-corona times.

Covid-19 for greatly limiting everything that I could have been doing besides working on my thesis during the past year, therefore making me very dedicated to my task.

The Department of Arctic Geology of the University Centre in Svalbard (UNIS) and the Research Council of Norway (Svalbard Science Forum). This project would not have been possible without the funding they allocated me (Arctic Field Grant ES668276).

And last but not least, thanks to my friends Mari, Charlie, Marie, Elise and Jessica for your support and help with making my life easier during the final phase of this thesis, even when not aware of doing so.

Table of Contents

1 Introduction

Concerns about ice retreat and warming climate are gaining more importance every day and tentative modelling of the future is becoming essential. There is an increasing need for studying palaeo-analogues of existing ice bodies in order to better constrain models of future cryospheric response with field data. The Arctic is particularly sensitive to changes in climate and Svalbard is the area situated in the high Arctic with the easiest access and the fastest warming climate. Since the 1990s, Svalbard has experienced a warming that is more than twice the Arctic average and about seven times the global average for the same period (Nordli et al., 2020). The strong climatic gradient and wide range of topographic features across the archipelago makes for an ideal investigation site for glacier monitoring and palaeo-climatic reconstructions.

Following deglaciation, Svalbard glaciers are believed to have reached their minimum extent sometime during the Mid-Holocene (8.2 to 4.2 ka BP). However, the Holocene Glacial Minimum (HGMin) ice extent cannot be directly reconstructed by looking at glacial landforms and geomorphology, as modern ice is more extensive, and has therefore to be inferred by proxy analysis. At present, the extent of ice that remained in Svalbard during the Mid-Holocene is unknown (Farnsworth et al., 2020).

The Late Holocene is characterized by a series of multi-decadal to century-scale climatic fluctuations, superimposed on an overall decline in temperature (Bradley and Bakke, 2019) caused by a progressive decrease in summer insolation and cooling of Svalbard's surrounding seas (Rasmussen et al., 2012; Renssen et al., 2009; Svendsen and Mangerud, 1997). This long-lived cooling trend led to an extensive period of glacier growth following the HGMin usually referred to as the Neoglaciation (Bradley and Bakke, 2019). To this day, the timing of the Neoglaciation in Svalbard is not known nor are the climatic processes related to glacier expansion (Farnsworth et al., 2020).

Cold-based glacial ice – ice bellow pressure melting point that does not have any basal movement and flows only by internal creep deformation – is well known to preserve underlying landforms produced by earlier processes (Ballantyne and Stone, 2015; Corbett et al., 2016; Davis et al., 2006; Kleman, 1994), but can also preserve vegetation that was growing in the close proximity of expanding ice (Bergsma et al., 1984; La Farge et al., 2013). With current rapid climate warming, overall glacier retreat in the Arctic is exposing formerly ice-buried in situ vegetation at the margin of cold based ice bodies (Blake, 1981; Goldthwait, 1960; Miller et al., 2013). Radiocarbon dating of this

vegetation constrains the timing of advance of ice over the specific location where it was collected. Widespread sampling and dating of vegetation emerging from ice bodies can permit the reconstruction of the timing of the latest ice advance in a given region. While this method has been used in a range of places in the Canadian Arctic and Western Greenland (Briner et al., 2014; Schweinsberg et al., 2015), its application elsewhere has thus far been limited.

A single previous study focused specifically on ice-buried vegetation in relation to ice cap advances in Svalbard (Miller et al., 2017). Miller et al. (2017) identified that persistent snowline lowering happened between 4.0 and 3.4 ka BP and then series of successive snowline lowering episodes occurred between 1710 and 1610 BP, 1540 and 1410 BP, 1280 and 1200 BP, 950 and 730 BP, and between 650 and 500 BP. A handful more studies have been conducted following serendipitous discoveries of vegetation buried under a glacier ca. 1.5 ka ago (Humlum et al., 2005) or moraines (Baranowski and Karlén, 1976; Dzierzek et al., 1990; Furrer et al., 1991).

Acquiring constraining ages on the timing of Late Holocene glacier advances helps to develop a clearer understanding of cold-based ice cap responses to climate change in the high Arctic and can therefore contribute in developing more accurate projections for ice cap behaviour in the future.

This thesis aims to contribute to an improved comprehension of the Holocene glacial fluctuations in Svalbard by investigating the timing of the Neoglaciation. In order to achieve this, this project aims to:

(i) constrain the timing of the initiation of the Neoglaciation in Svalbard

(ii) constrain the timing of glacial expansion phases during the Neoglaciation in Svalbard

In order to provide answers to these research questions, three sub-issues were addressed:

- Determine the best methods to sample and date ice buried vegetation and in order to do so, identify the potential error sources
- Establish how to rightfully interpret the data derived from this method
- Identify what are the limitations and perspectives for the method in Svalbard

With the purpose of answering these questions, three ice caps located in central Spitsbergen, Bassen, Foxfonna and Frostisen (Figure 1) were investigated by sampling and dating formerly ice buried vegetation emerging from their retreating margins. A field campaign was organised in late August 2020

to visit Bassen and Frostisen ice caps and Foxfonna was visited in late November 2020. Identification and sampling in the field allowed for the determining the most suitable methods to sample and date

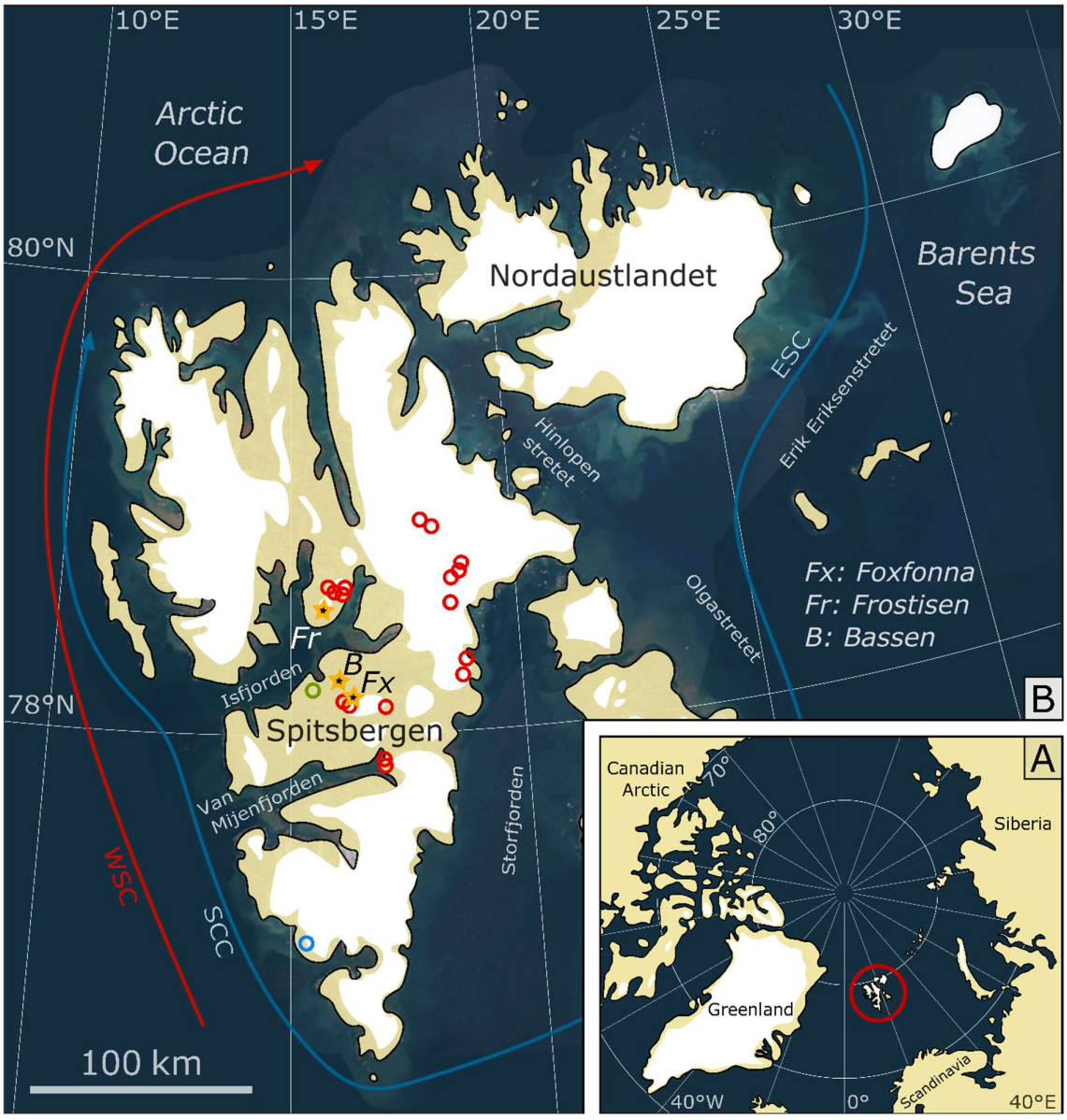

Figure 1. Location map with A) inset map over the North polar region with the Svalbard archipelago circled in red and B) map of Svalbard with the locations of sample sites from previous studies marked with green circles for Humlum et al., 2005, red circles for Miller et al., 2017 and blue circle for Baranowski & Karlén, 1976. Yellow stars mark the sample sites from this study. Oceanic currents after Ślubowska-Woldengen et al., (2007). ESC: East Spitsbergen Current, SCC: Spitsbergen Coastal Current, WSC: West Spitsbergen Current. Base image modified from toposvalbard.no.

ice buried vegetation and with identifying related error sources. In addressing the objective of determining to what extent it is possible to constrain the onset of Neoglaciation in Svalbard as well as the timing of the subsequent ice advance phases, all previously published data concerning vegetation buried by glacial advances in Svalbard were gathered within the VEGLAS (VEgetation Buried by GLAciers in Svalbard) database.

2 Background and theory

2.1 Introduction to Svalbard geology and geography

Located between 74 and 81°N and 10 and 35°E, at the north-west corner of the Barents Sea, the Svalbard archipelago is approximately at the same latitude as Northern Greenland. The mountainous islands are extensively glaciated, with 57% of Svalbard's land area covered by glaciers in the late 2000s (Nuth et al., 2013). The highest mountain, Newtontoppen, reaches 1713 m a.s.l. (Dallmann, 2015).

While the general elevation of Svalbard was the result of tectonic forces caused by the opening of the Arctic and Atlantic oceans, its modern shape was carved out by glacial processes during the successive glaciations of the Quaternary, creating deep submarine troughs, long fjords and large valleys. The local morphology of the mountains is influenced by the type and structure of the bedrock (Dallmann, 2015). Svalbard has been described as a 'geologist paradise' due to the exposure of the complete geologic sequence from the Precambrian to the Quaternary and its extensive fossil record (Hisdal, 1985).

Svalbard has continuous permafrost (Christiansen et al., 2010) with thickness ranging between less than 100 m close to the coasts and in large riverbeds to more than 500 m in mountainous areas (Humlum et al., 2003). Ground ice is present all over the archipelago as rock glaciers, ice-cored moraines, buried glacial ice and within pingos and ice wedges in some valleys (Humlum et al., 2003).

The most continuous ice cover is found on the east of the archipelago, an area that is glacier-favourable due to the association of colder temperatures and moisture input from the Barents Sea. The Austfonna ice cap located on Nordaustlandet is the largest ice cap of the Eurasian Arctic. Large ice fields divided into individual glaciers by mountain ridges and nunataks constitute most of the glaciated areas. Small cirque and valley glaciers are also numerous, especially in the alpine mountain regions of western and central Spitsbergen. In the 1980s, glaciers of an area smaller than 1 km² counted for 56 % of the total amount of individual glaciers, but covered only 1.1 % of the glaciated area (Hagen, 1993). The thickest ice caps have a maximum ice thickness of around 600 m (van Pelt et al., 2013; Navarro et al., 2014, 2016).

2.2 Svalbard glacier cover extent and climate history since the Last Glacial Maximum[1]

2.2.1 From the Last Glacial Maximum to the beginning of the Holocene

During the Last Glacial Maximum (LGM) at around 20 ka BP (Hughes et al., 2016), Svalbard was entirely covered by ice with the exception of some nunataks on the West coast. Deglaciation of the Svalbard-Barents Sea Ice Sheet initiated shortly afterwards and by 14 ka BP the Barents Sea was completely deglaciated, leaving behind two subsidiary ice sheets covering Svalbard (at the exclusion of the already deglaciated Prins Karls Forland) and Franz-Josef Land (Hughes et al., 2016). At the beginning of the Holocene (11.7 ka BP; Walker et al., 2009, 2018), Storfjorden, Erik Eriksenstretet, Olgastretet and a large part of Hinlopenstretet, *id est* most of the deeper marine troughs, were free of ice (Hormes et al., 2013; Farnsworth et al., 2020, Figure 14).

This extensive deglaciation led to a pronounced glacio-isostatic rebound visible along Svalbard's coastline as series of raised marine shorelines. It is possible to establish the formation age of these raised shorelines by radiocarbon dating preserved shells, whale bones and/or driftwood found on or within these raised shorelines. Relative sea level curves quantifying the uplift rates through time can then be established (Salvigsen, 1981; Forman et al., 2004; Schomacker et al., 2019). Differential ice-cover duration, thickness, timing of deglaciation throughout the archipelago as well as later regional ice expansion explain the great variability in uplift observed over Svalbard (Fjeldskaar et al., 2018), with the greatest uplift rates occurring in the Late Pleistocene and the Early Holocene (Forman et al., 2004; Farnsworth et al., 2020).

2.2.2 Early Holocene (11.7 – 8.2 ka BP) and Holocene Thermal Maximum

The Early Holocene coincides with a peak in summer insolation culminating between 9.7 and 7.5 ka BP (Laskar et al., 2004; Renssen et al., 2009). However the peak in Holocene terrestrial summer temperature is observed in the lacustrine archives at around 10 ka BP, with temperatures

[1] For consistency with already published literature, all comparisons with present day climate or temperatures in this review section refer to the old 1960-1990 climate-normal used by the Norwegian Meteorological Institute until the 31st of December 2020. Any comparison with the new climate normal (1990-2020) will be specified (http://met-xpprod.customer.enonic.io/vaer-og-klima/ny-normal-i-klimaforskningen).

reconstructions based on alkenones extracted from lake sediments reaching 7°C warmer than today in North-West Spitsbergen (van der Bilt et al., 2019). The offset between the Holocene Thermal Maximum (HTM) and the maximum summer insolation is due to the strong influence of sea surface temperatures on terrestrial temperatures. Warmer than present temperatures in the Early Holocene are also registered in the sedimentary ancient DNA (*sed*aDNA) found within a lake record from Ringhorndalen, Widjefjorden. Thermophilus arctic plant species had broader distribution during the HTM than at present (Voldstad et al., 2020), and lake sediment plant macrofossil analysis infers that mean July terrestrial temperatures were at least 2°C warmer than today during the first half of the Holocene (Birks, 1991).

The onset of the Holocene is marked by the incursion of warm Atlantic waters around Svalbard due to enhanced northward oceanic heat transport through the Norwegian Atlantic Current (Risebrobakken et al., 2011; Rasmussen et al., 2012; Mangerud and Svendsen, 2018). A major warming of the sea along the western Svalbard margin, between ca. 10.7 and 8.6 ka BP, with subsurface sea temperatures up to 6°C warmer than today, is associated with an increase of the flux of warm Atlantic waters (Ebbesen et al., 2007; Werner et al., 2016). The occurrence of warm-water molluscs fossils in the raised marine sediments along Svalbard's coastlines reveals exceptionally warm sea temperatures for the Arctic in the Early Holocene. The HTM in the sea is marked by the presence of *Zirfaea Crispata* in Svalbard waters, indicating that August sea surface temperatures were around 6°C warmer than present between 10.2 and 9.2 ka BP (Mangerud and Svendsen, 2018). Another study based on stable oxygen isotope ($\delta^{18}O$) from three *Arctica islandica* shells from Dicksonfjorden in central Spitsbergen finds the same 6°C warmer than present temperatures between 10.0 and 9.7 ka BP (Beierlein et al., 2015). A similar warming event is observed in foraminifera within the marine record from fjords and the western Svalbard continental shelf (Hald et al., 2004). High sea temperature lead to a strong reduction of winter and spring sea-ice cover in the waters around Svalbard (Werner et al., 2016; Berben et al., 2017; Allaart et al., 2020) leading to enhanced evaporation of ocean water and therefore enhanced winter precipitation (Kjellman et al., 2020). Following the HTM, the disappearance of *Mytilus edulis* from the fossil record between 9 and 8.2 ka BP indicates a cooling of the sea and temperatures are assumed to have been similar to present during this period (Mangerud and Svendsen, 2018). This cooling has been associated with an inflow of Arctic waters coming from the Arctic Ocean (Ebbesen et al., 2007).

Extensive deglaciation continues through the Early Holocene across Svalbard, with ice margins retreating onto land and ice sheet thickness decreasing dramatically, driving rapid glacio-isostatic

rebound. The rate and amplitude of this uplift is heterogenous in space and time across the archipelago due to variability in ice cover thickness, duration and deglaciation timing (Forman et al., 2004; Sessford et al., 2015; Schomacker et al., 2019; Farnsworth et al., 2020). Svalbard fjords were already half way deglaciated at 11.6 ± 0.2 ka BP, and most fjords were almost entirely deglaciated by 11.0 ka BP (Farnsworth et al., 2020).

As the fjords became deglaciated, several tributary glaciers exhibited re-advances into the fjords and recently deglaciated valleys, reworking shell-rich marine sediments that permits the dating of these re-advances in some instances (Lønne, 2005; Farnsworth et al., 2017, 2018; Larsen et al., 2018). These advances appear to be asynchronous and range between 12 and 9 ka BP, with more than half of the recognised dated re-advances occurring between 11 and 10 ka BP (Farnsworth et al., 2020, Figure 8). The mechanisms behind these advances are yet to be determined, but it is most commonly acknowledged that they may have been driven by ice dynamics as they appear to follow the deglaciation of the fjords, with the oldest ones located at the mouth of fjords and the youngest ones at their heads (Larsen et al., 2018; Farnsworth et al., 2018, 2020).

2.2.3 Mid-Holocene (8.2 – 4.2 ka BP) and Holocene Glacial Minimum

The Mid-Holocene climate is considered to have been warmer than present but had cooled since the temperature peak of the Early Holocene. Sea surface temperatures increased to c. 4°C warmer than present from 8.2 to 6 ka BP and then, as the flow of Atlantic waters progressively decreased, the surface and subsurface sea temperatures cooled down until the end of the Mid-Holocene dropping below modern temperatures around 4.5 ka BP (Rasmussen et al., 2012; Werner et al., 2016; Mangerud and Svendsen, 2018). This progressive cooling of sea temperatures is coupled with an increase in winter sea-ice cover (Ślubowska-Woldengen et al., 2007; Rasmussen et al., 2012; Werner et al., 2016). Similar trends are visible in the terrestrial record. Vascular plant reconstruction based on *sed*aDNA from a lake core from Ringhorndalen shows climatically stable, dry, and warm conditions during most of the Mid-Holocene. A progressive cooling trend through the second half of the Mid-Holocene has been inferred from the same record, starting at ca. 6.5 ka BP (Voldstad et al., 2020).

Svalbard glaciers are believed to have reached their Holocene minimum extent during the Mid-Holocene. However, the Holocene Glacial Minimum (HGMin) ice extent cannot be directly reconstructed from glacial landforms and geomorphology, as modern ice covers any landforms and sediments associated to the HGMin, and has therefore to be inferred by proxy analysis. A number of studies focusing on lake sediment cores observe very low minerogenic inputs during the Mid-

Holocene. This shift in sedimentation is interpreted as the disappearance of the corresponding glaciers from their catchments at the beginning of the Mid-Holocene and already at the end of the Early Holocene for some of them (e.g. Svendsen and Mangerud, 1997; Røthe et al., 2018, 2015; Farnsworth et al., 2020, Figure 9). Sediment core analysis from Femmilsjøen in North-East Widjefjorden shows that glacial meltwater runoff was absent between 10.1 ± 0.4 and 3.2 ± 0.2 cal. ka BP, indicating that a probable complete melt-off of the large Åsgardfonna ice cap occurred during the HGMin given that the ice free catchment of the lake covers a large part of the ice cap's footprint (Allaart et al., 2021).

Fjord records are less conclusive as high sedimentation rate can be caused by tide-water glacier influence or high melt water runoff from tributary glaciers and ice rafted debris (IRDs) can be originated by sea ice, not only icebergs. However, it is assumed that even though some tide-water glaciers fed by bigger ice caps may have survived (Hald et al., 2004), most glaciers disappeared from the archipelago. Supporting this assumption, the findings of relict englacially transported vegetation sampled on the ice surface of Hansbreen, a 16km long tide-water glacier located in South-West Spitsbergen, and dated to 8.0 ± 0.4 and 6.0 ± 0.5 cal. ka BP, Oerlemans et al. (2011) conclude that it is very likely that during the HGMin the main stream of Hansbreen did not exist at all. When gathering the data from these small scale studies, it comes out that the HGMin happened sometime between ca. 8.0 and 6.0 ka ago (Farnsworth et al., 2020), but its extent is still poorly defined due to the difficulties of reconstructing an ice extent that may have never existed during this period or of proving its absence. Further investigations need to be conducted before a somewhat trustworthy estimation of the ice cover extent during the HGMin can be established.

2.2.4 Late Holocene (4.2 ka BP – Present day) and Holocene Glacial Maximum

The Late Holocene in the North Atlantic is characterized by a series of multi-decadal to century-scale climatic fluctuations, superimposed on an overall decline in temperature (Bradley and Bakke, 2019) caused by a progressive decrease in summer insolation and cooling of Svalbard's surrounding seas (Svendsen and Mangerud, 1997; Renssen et al., 2009; Rasmussen et al., 2012). This long-lived cooling trend led to an extensive period of glacier growth usually referred to as the Neoglaciation (Bradley and Bakke, 2019). Sea-ice cover reconstructions based on abundance of the PIP_{25} biomarker index suggest a progressive increase of sea-ice cover throughout the Late Holocene (Müller and Stein, 2014; Allaart et al., 2020).

Fluctuations between cool and warm periods throughout the Late Holocene were interpreted from ice core records from Greenland (Vinther et al., 2009), marine records (Marchal et al., 2002), lake

records (de Wet et al., 2018; van der Bilt et al., 2018) and at vascular plants reconstruction based on *sed*aDNA within a lake record from North Spitsbergen (Voldstad et al., 2020). The warmest period of the Late Holocene, excluding the ongoing warming, occurred between 950 and 700 BP (1000 and 1250 AD) and is usually referred to as the Medieval Warm Period (MWP) but also as the Medieval Climate Anomaly (MCA). The reappearance of *Mytilus edulis* in Svalbard waters at 0.9 ka BP (Mangerud and Svendsen, 2018) is associated with the MWP. The overall cooling culminated in the Little Ice Age (LIA) which followed the MWP (Figure 2.1) and ended before 1900 AD, as shown by the warming observed already in the early 1900s at the very beginning of Svalbard's historical temperature record (Førland et al., 2011; Nordli et al., 2014). The LIA is believed to be a response to the combined effects of orbital forcing, solar activity minima and strong volcanic eruptions (Wanner et al., 2008).

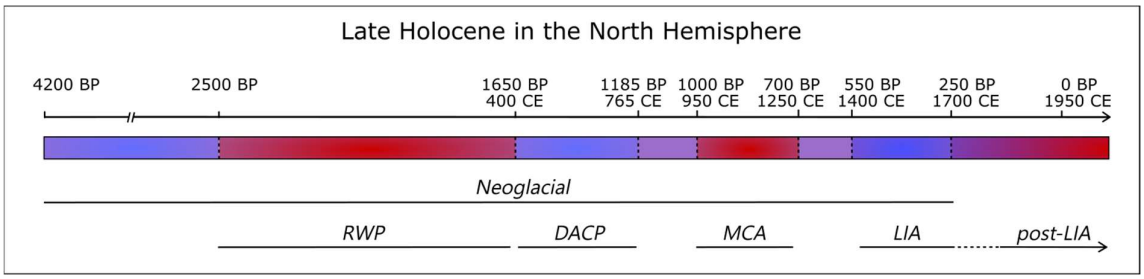

Figure 2.1. Late Holocene timeline. RWP: Roman Warm Period; DACP: Dark Ages Cold Period; MCA: Medieval Climate Anomaly; LIA: Little Ice Age. Timing of the Late Holocene sub-epoch boundaries according to Walker et al., 2018, for the equivalent official Meghalayan sub-epoch. Timing of the RWP according to Wang et al., 2012; of the MCA and the LIA according to Mann et al., 2009 and of the DACP according to Helama et al., 2017.

Higher sedimentation rate and increase in IRD flux in regional waters during the latter part of the Holocene are a consequence of enhanced glacial activity corresponding to the Neoglaciation (Ślubowska-Woldengen et al., 2007; Rasmussen et al., 2014; Flink et al., 2017). A similar sedimentary response is also visible within lacustrine records over Svalbard (Svendsen and Mangerud, 1997; Røthe et al., 2015; van der Bilt et al., 2015). The timing of the onset of the Neoglaciation is still poorly constrained but has been shown locally to have occurred prior to 4 ka BP (Svendsen and Mangerud, 1997; van der Bilt et al., 2015; Miller et al., 2017), while other glaciers started to grow again only by 3.5 ka BP (Røthe et al., 2015).

The paradigm that the end of the LIA coincides with the Late Holocene Glacial Maxima (HGMax; Svendsen and Mangerud, 1997), often as the result of surge events (Schomacker and Kjær, 2008; Flink et al., 2015; Lyså et al., 2018) is increasingly contested as evidences of earlier advances are being identified outside of the LIA moraines in some glacier forefields (eg. Werner, 1993; Reusche et al., 2014; Røthe et al., 2015; Philipps et al., 2017). If it is still true that many, if not most, Svalbard

glaciers reached their HGMax at the end of the LIA, a significant amount of them did so earlier in the Neoglacial. Since the end of the LIA, Svalbard glaciers have been retreating overall (Möller and Kohler, 2018), the retreat being often punctuated by short lived readvances due to surge events (Sevestre et al., 2015; Flink et al., 2015, 2017; Farnsworth et al., 2016, 2017).

2.2.5 Present day climate evolution

Due to the influence of the West Spitsbergen Current (WSC), the northern end of the warm and salty North Atlantic Current (Ślubowska-Woldengen et al., 2007) (Figure 1), and the position of Svalbard along the main North Atlantic cyclone track (Dickson et al., 2000; Isaksen et al., 2016; Wickström et al., 2020), which brings high temperatures and moisture northwards, the archipelago is subject to climatic conditions a lot milder than other land masses located at similar high latitudes. The advection of warm Atlantic waters along the west coast of Svalbard creates a strong West-East temperature and sea ice gradient, with colder temperatures and greater sea ice extent in the East (Førland et al., 2011; Walczowski and Piechura, 2011). There is also an important precipitation gradient between the west coast and central Spitsbergen (Humlum, 2002), with average annual precipitation of 427 mm (Ny-Ålesund) and 191 mm (Longyearbyen) respectively during the 1981-2010 period (Førland et al., 2011).

In the period between 1979, which marked the beginning of satellite monitoring of Arctic sea ice, and 2010, there has been a sea-ice cover loss of 9.2 ± 1.6% decade^{-1} for the Kara and Barents Seas region and 2.1 ± 0.3% decade^{-1} for the Arctic Ocean (Cavalieri and Parkinson, 2012). Since then, both Svalbard and Arctic sea-ice areas have shown enhanced shrinking trends (Figure 2.2). The existence of a strong positive sea-ice cover / temperature feedback relation (Isaksen et al., 2016) is believed to be one of the drivers of the so-called Arctic Amplification phenomenon (Screen and Simmonds, 2010; Pithan and Mauritsen, 2014). The persistent reduction of sea-ice cover is therefore increasing the chances of further rapid warming and sea ice loss. Sea-ice cover is negatively correlated with sea-surface evaporation and precipitation amounts, the shrinking sea-ice cover being thus partly responsible for the observed and projected increase in precipitation (Kopec et al., 2016).

Apart from the colder 1910s and 1960s, mean annual air temperatures on Svalbard have had a rising trend over most of the twentieth century (Nordli et al., 2014). The trend from the 1990s to present is the strongest, with a climate warming of c. 1.7°C per decade, which is more than twice the Arctic average (0.8 °C/decade, north of 66 °N) and about seven times the global average for the same period (Nordli et al., 2020). During the last decades, Svalbard has been experiencing an enhanced

increase of winter temperatures (Isaksen et al., 2016) while annual precipitation amounts also show a significantly positive trend of c. 2% per decade over the last century (Førland et al., 2011).

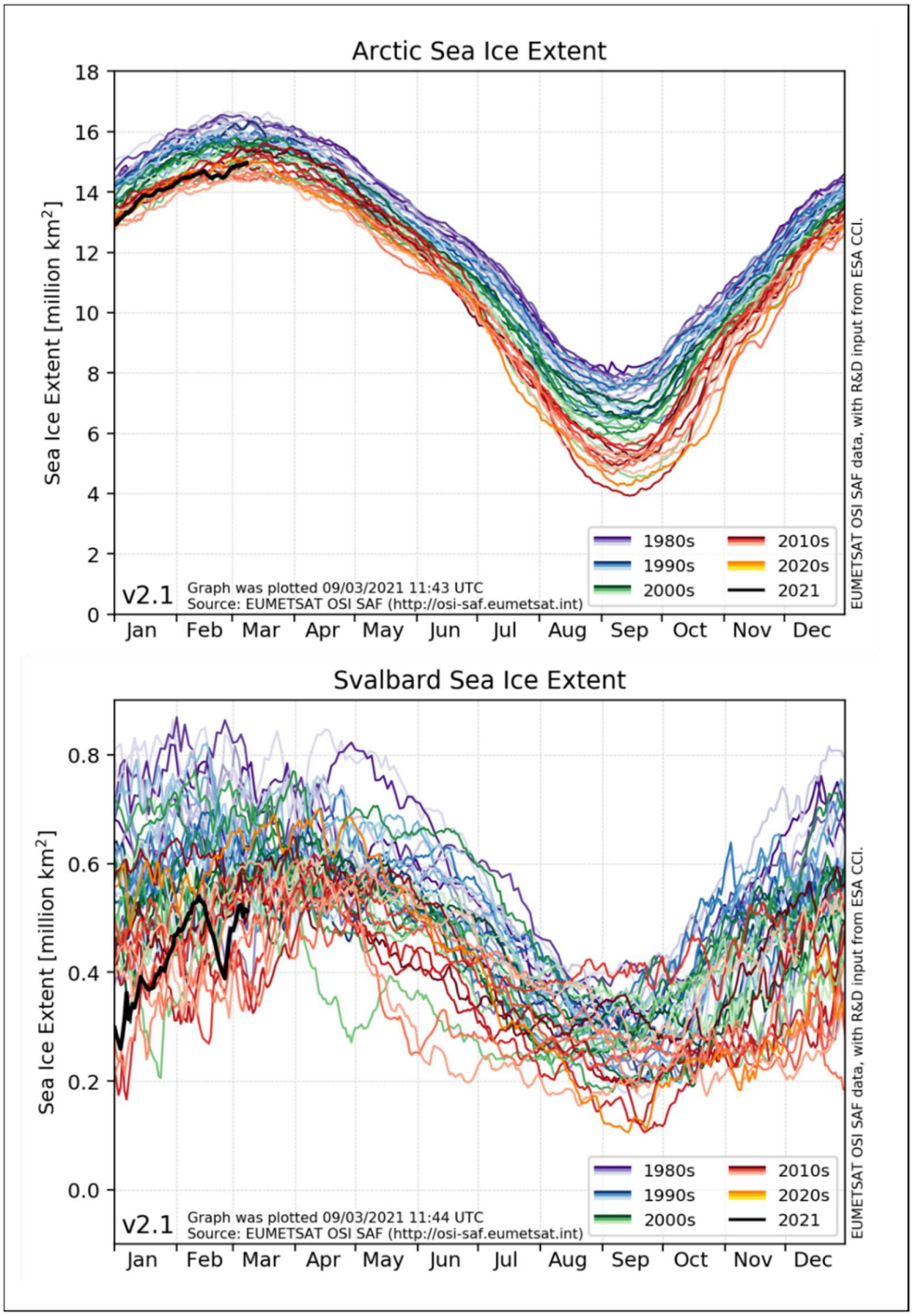

Figure 2.2. Sea ice extent time-series plots from 1979 to 2020 for the arctic region and the Svalbard region based on the new climate indicator of sea ice OSI SAF Sea Ice Index v2.1. (https://osisaf-hl.met.no/v2p1-sea-ice-index).

In steep alpine environments, snow redistribution by the wind is an important factor for snow accumulation over glacierized terrain (Dadic et al., 2010a, 2010b). In Svalbard, precipitation alone is not sufficient to maintain the low equilibrium line altitude (ELA) of many of the glaciers. Wind driven redistribution of the fallen snow on the surface of the glaciers, but also on the overlying slopes causing snow avalanche mass to accumulate at the surface of the glaciers, is a major factor for winter accumulation (Jaedicke and Gauer, 2005). During the past 40 years, wind has been increasing significantly in Svalbard (Wickström et al., 2020). It can then be expected that this phenomenon, coupled with the increase in precipitation, is causing a shift in winter snow cover distribution and thickness. However, even if this shift is favourable to winter accumulation (Kohler et al., 2002), it is still insufficient to overcome the negative effect of increasing temperature on general glaciers mass balance (Kohler et al., 2007). Indeed, between 1980 and 2010, the glacierized area over the entire archipelago has decreased by an average of 80 km^2 yr^{-1} (Nuth et al., 2013) and glaciers have been shown to thin and retreat at increasing rates since the end of the LIA (Kohler et al., 2007; Rachlewicz et al., 2007; Nuth et al., 2010; James et al., 2012; Małecki, 2013; Iverson et al., 2017; Möller and Kohler, 2018; Holmlund, 2021).

2.3 Ice-buried vegetation

2.3.1 Cold ice, an exceptional landscape preservation material

Cold-based glacial ice, *id est* ice below pressure melting point and therefore frozen to the ground, is well known to preserve underlying landforms and sediments produced by earlier processes (Figure 2.3) in Arctic and high alpine environments (Kleman, 1994; Davis et al., 2006; Ballantyne and Stone, 2015; Corbett et al., 2016). This preservation process has the exceptional potential of leaving some parts of high mountain landscapes unchanged through entire glaciations (Staiger et al., 2005).

2.3.2 Multidisciplinary importance of artefacts and organic remains exposed by the ongoing melt of glaciers and ice patches

Besides exposing old landforms, melting cold based ice caps, glaciers and ice patches are revealing a rich variety of botanical and faunal remains as well as human artefacts worldwide, providing material for palaeoenvironmental and archaeological research.

Figure 2.3. Landscape preservation under cold ice. A. Emergence of patterned ground around the retreating margin of Bassen, picture taken from the south side of the ice cap looking westwards. B. Vegetated slope emerging from the downwards receding ice margin of Frostisen South Basin, picture taken from the west side of the ice cap looking southwards.

Ice patch archaeology is a relatively new discipline, developing quickly with the sense of urgency created by the fast disappearance of the ice patches, exposing scientifically valuable fragile organic artefacts to weathering that will lead to their decomposition if they are not found and collected before this fatidic predicament (Reckin, 2013). Some of the artefacts found are going back to the

beginning of the Neolithic (12000 cal. yrs BP), giving unpreceded insights on early humans hunting techniques and technologies in alpine areas (Andrews and MacKay, 2012).

An intense melt episode in the fall of 2006 triggered an ice patch archaeological interest in central southern Norway leading to an ever increasing number of findings and publications (e.g. Nesje et al., 2012; Vedeler and Jørgensen, 2013; Ødegård et al., 2017; Pilø et al., 2020), making this region the most find-rich of the world (Curry, 2014).

Findings from the mountains of Western North America consist essentially of weapons, inferring that Native Americans have used the ice patch areas as hunting grounds since the beginning of the Neolithic (Hare et al., 2012; Lee, 2012; Vanderhoek et al., 2012; Reckin, 2018). This indicates that, as they are still doing today, caribou herds, among other big herbivores, were gathering around the ice patches in summer, seeking cooler temperatures and shelter from mosquitoes (Hare et al., 2004). The weapons findings show a stability in the human hunting technology over seven millennia, when they were using throwing darts, until their sudden replacement by the bow and arrows after 1200 BP (Hare et al., 2012).

The findings from the Alps are generally a lot more diverse than anywhere else as, beside hunting gear, pieces of clothing, fur and tools are also abundant (Rogers et al., 2014). This diversity is explained by the fact that the Alps were not only used as hunting grounds but were crossed by often dangerous transalpine routes connecting the Northern Alps to Italy (Grosjean et al., 2007). Some of these archaeological studies draw conclusions about the local ice patch extent fluctuations through time based on the ages, preservation stages and spatial distribution of the studied artefacts.

The most famous ice patch archaeology discovery belongs to the Alps, where the body of the “iceman” Ötzi was found melting out of an ice patch together with a number of his belongings on the Italian-Austrian border at 3210 m a.s.l. in 1991. Radiocarbon dating of his body gave a death date of ca. 5200 cal. yrs BP (e.g. Kutschera, 1994; Kutschera and Rom, 2000; Dickson et al., 2003; Zink and Maixner, 2019). Analysis of plant macrofossils from Ötzi’s belongings (Oeggl, 2009), DNA analysis of his digestive system content (Rollo et al., 2002) and pollens from his colon (Oeggl et al., 2007) allowed for palaeoenvironmental and botanical reconstructions of the discovery’s area at the time of Ötzi’s life.

In the Yukon, caribou dung pellets found within the ice layers of an ice patch provided pollen and plant macrofossils for analysis and palaeoenvironmental reconstructions, as well as dietary,

genetic, and parasitic information. The abundant distribution of dung within the ice stratigraphy allowed dating of the ice as far as 8300 BP when the snow probably started to accumulate after the HTM. The ice would have accumulated nearly continuously since then, with only two time intervals, at 6700 – 4700 and 920 – 510 BP, when warm and/or dry conditions resulted in no net accumulation (Farnell et al., 2004).

2.3.3 Ice advance timing constrained by dating of formerly ice-buried vegetation

The earliest reports of well-preserved dead vegetation and lichens in the vicinity of or within cold based glaciers are from the Canadian Arctic (Goldthwait, 1960; Beschel, 1961; Bergsma et al., 1984). Blake (1981) used preserved peat deposits to constrain Holocene ice fluctuation of outlet glaciers in Ellesmere Island to show that the ice was advancing at ca. 2.7 cal. ka BP. Bergsma (1984) reports that, though he was more interested by the species composition of the plant community melting out of the margin of Twin Glacier, Ellesmere Island, than by past ice margin behaviour, the emerging vegetation was (once calibrated) dated to be 1500 years old, signifying that the glacier was advancing at that time. He also states that some of his lichens looked remarkably fresh, but assessments of CO_2 efflux by infrared gas analysis indicated no respiration, and therefore qualifies them as dead.

These ice margin past behaviour interpretations rely on the assumption that when cold ice advances over vegetated ground, plants are embedded in the basal ice, this event stopping their carbon exchange with the atmosphere and leading to their death. Now that the ice-margins are retreating, this ice-buried vegetation is being exposed, and can subsequently be sampled and radiocarbon dated to determine its burial time, and thus when the ice margin has been advancing over a sampling location (Figure 2.4). Widespread sampling, identification, and dating of vegetation emerging from various ice bodies can permit the reconstruction of the conditions and timing of the latest ice advance in a region. These cold-based glacier advances are a consequence of persistent snowline lowering that can be due to a cooling climate, enhanced precipitations or a combination of these two factors (Copland, 2011).

Thanks to specific adaptations, bryophytes have a greater capacity to grow in the harsh conditions that are typical to periglacial environments in polar regions than most vascular plants and hence usually represent the greater part of the vegetation being exposed by receding cold-ice bodies.

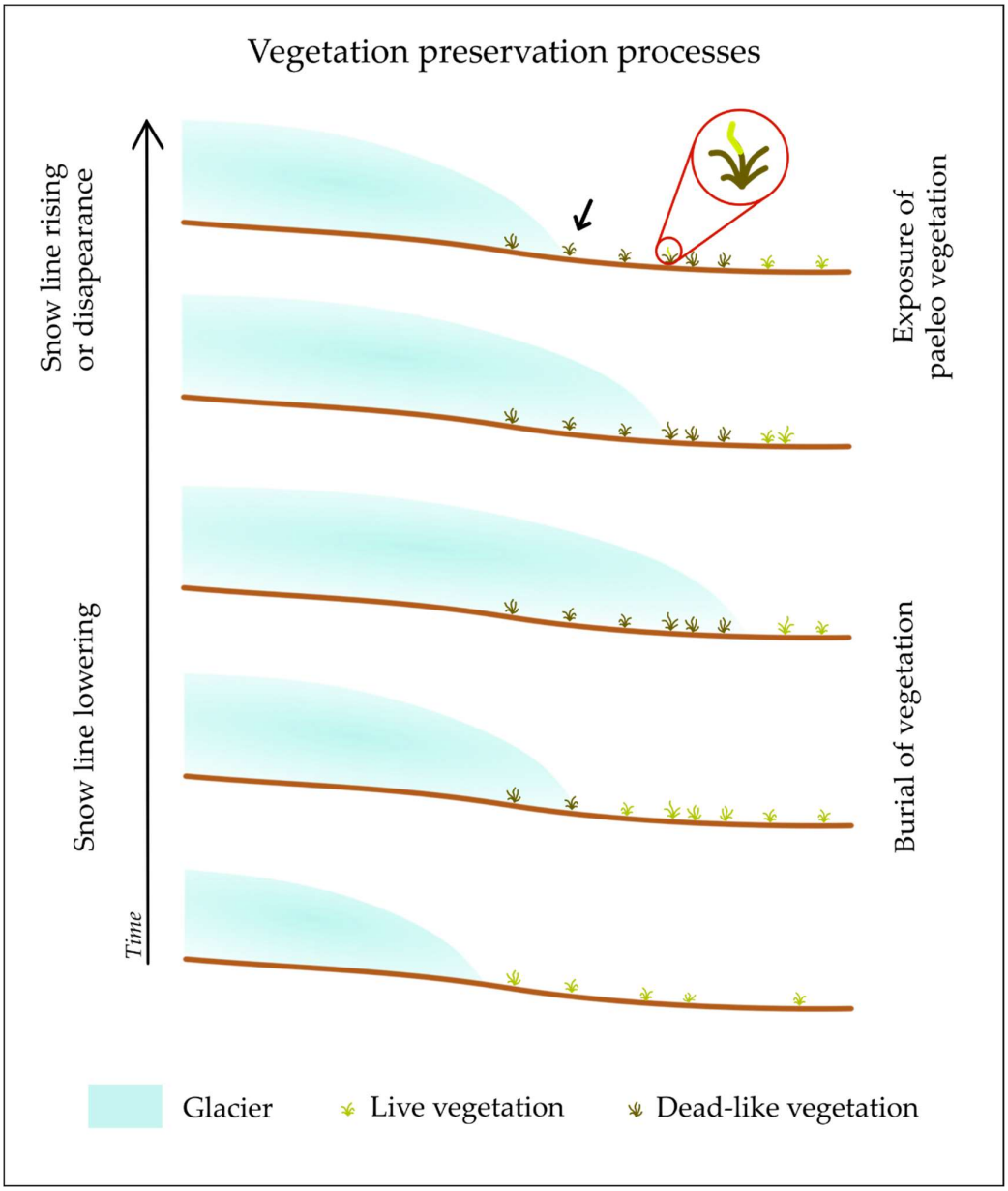

Figure 2.4. Vegetation preservation processes under cold-based ice. The black arrow points towards the ideal sampling zone in order to avoid dating any recolonized or regrowing plant.

2.3.4 Moss "superpowers": Cryptobiosis, Totipotency and Poikilohydrie

Mosses are very resilient organisms that can survive in challenging environments. They possess the remarkable ability to achieve cryptobiosis ("hidden life"), a stage of dormancy, characterized by the cessation of all metabolic processes, brought on by an organism in response to a shift to adverse environmental conditions. This stage between life and death allows for survival until

the environment is favourable to life again (Cannone et al., 2017). Even though still poorly understood, cryptobiosis is most commonly known and studied in relation to the micro-animals known as tardigrades, “water-bears” (Clegg, 2001; Neuman, 2006).

A range of different types of cryptobiosis exists, each defined according to a specific environmental challenge. Cryobiosis (“frozen life”) is a form of cryptobiosis which is triggered by a reduction in temperature and involves the freezing of water within the cells. Though a lot of focus has been put on the study of cryobiosis processes in relation with cryopreservation of Human bodies for space travel (Cerri et al., 2016) and organ banking (Lewis et al., 2016), only three studies have been looking at long term (centennial to millennial) cryobiosis in relation to plants, or more specifically, bryophytes. The idea that bryophytes have the potential to survive for extended periods of time at frozen state, and thus go into cryobiosis, was first brought up by La Farge et al. (2013) when they managed to regrow *in-vitro* bryophytes that they had collected at the margin of the receding Teardrop glacier in the Canadian Arctic after observing *in-situ* regrowth in the field. These bryophytes were radiocarbon dated to be up to 450 years old. This regrowing process is only possible because bryophytes are totipotent and can therefore develop a new organism from one single cell (Borém et al., 2014). Any totipotent cell has the genetic potential to regenerate into a complete organism, a function similar to the one of stem cells in animal organisms (Ishikawa et al., 2011). In Antarctica, bryophytes buried under a glacier and dated to be ca. 600 years old have been observed to show metabolic activity (which was measured using chlorophyll *a* fluorescence) after exposure by the retreating ice, but died in the following years because of too intensive respiration repair processes (Cannone et al., 2017) and light exposure (Lovelock et al., 1995). The oldest mosses that have shown regrowth capacity were bryophytes preserved frozen within a 138 cm long permafrost peat core from the South Orkney Islands in Maritime Antarctica. *In situ* new growth was observed from the clean cut of the core at 110 cm depth after 50 days. Gametophytes sampled right next to the ones exhibiting regrowth were radiocarbon dated to 1620 ± 81 cal. yr. BP (Roads et al., 2014).

The most intensely studied type of cryptobiosis is anhydrobiosis (“life without water”), a form of cryptobiosis initiated by desiccation. It refers to the ability of some organisms to survive the loss of all, or almost all, water and enter a state of suspended life in which their metabolism comes reversibly to a standstill. Various organisms, including plants, yeast, fungal spores, nematodes and brine shrimp can withstand dehydration and remain in anhydrobiotic state for extended periods of time until water becomes available again (Wharton, 2015). Bryophytes have the particularity of being poikilohydrous organisms (i.e. their water content varies with the relative humidity in the environment) (Pugnaire and

Valladares, 1999; Bartels and Salamini, 2001), implying that they go into anhydrobiosis every time they are subject to drought conditions. Anhydrobiosis can be sustained for extended periods of time by plants without causing death. For example, a 1.3 ± 0.3 ka old desiccated lotus seed has been germinated within the same time and conditions as a fresh seed would have (Shen-Miller et al., 1995). Even though poikilohydrie enables long time moss survival, it can lead to potential death following rehydration because of intensive cell respiration necessary to repair the cells, this process costing a lot of energy (Skre and Oechel, 1981). Desiccation duration affects the ability of recovery, and extended desiccation can cause too intense respiration and death (Turetsky et al., 2012). Similar reparation processes follow the exit of cryobiotic stages and can likewise lead to the death of the bryophyte if the damages caused by a long ice-entombment are too important.

2.4 Study area

Central Spitsbergen is deeply incised by Isfjorden, the largest fjord system of the archipelago, allowing the inflow of Atlantic waters to reach far inland in summertime. Summer temperatures are higher there than in the rest of the archipelago (Førland et al., 2011), which is favourable to vegetation growth and development (Shulgina et al., 2011). The low amount of precipitation in central Spitsbergen (191 mm yr^{-1} at Svalbard Airport, Førland et al., 2011) is preventing the development of extensive glaciated areas (Kohler et al., 2002), and therefore numerous, rather small cirque and valley glaciers and plateau ice caps are found in the area. This study focuses on 3 plateau ice caps, two of them, Bassen and Foxfonna, located on either side of Adventdalen, in the vicinity of Longyearbyen on the east side of Isfjorden, and the third, Frostisen, c. 35 km further north in Dickson Land (Figure 1).

2.4.1 Neoglacial snowline descent timing in Svalbard

Only one previous study has focussed specifically on ice-buried vegetation in relation to glacier advances in Svalbard (Miller et al., 2017), and a handful more has been conducted following serendipitous discoveries of vegetation buried under a glacier ca. 1.5 ka ago (Humlum et al., 2005) or moraines (Baranowski and Karlén, 1976; Dzierzek et al., 1990; Furrer et al., 1991).

Miller et al. (2017) have been widely sampling moss in the vicinity of retreating plateau ice caps located outside of Spitsbergen's national parks (Figure 1), using a helicopter to get easily from ice caps to ice cap, and reported 45 radiocarbon dates derived from their 2013 fieldwork moss collections. They found that persistent snowline lowering happened between 4.0 and 3.4 ka BP and then, series of

successive snowline lowering episodes occurred between 1710 and 1610 BP, 1540 and 1410 BP, 1280 and 1200 BP, 950 and 730 BP, and between 650 and 500 BP.

2.4.2 Bassen

Bassen is a small plateau ice cap located on top of Operafjellet, on the north side of Adventdalen, ranging in elevation between 900 and 950 m a.s.l. It is approximately 50 m thick and had an area of 0.5 km^2 in August 2020 (Figure 1 and 4.2). Snow accumulation on Bassen is probably only driven by wind but no study has looked at plateau ice cap snow accumulation processes in Svalbard. The local bedrock geology is primarily characterized by Paleogene marine sandstones and mudstones belonging to the Grumantbyen formation (Dallmann, 2015); (Svalbardkartet, NPI: https://geokart.npolar.no/Html5Viewer/index.html?viewer=Svalbardkartet).

2.4.3 Foxfonna

Upper Foxfonna is a plateau ice cap located on the south side of Adventdalen, ranging in elevation between 700 and 800 m a.s.l. It is approximately 50 m thick and had an area of 2.5 km^2 in August 2020 (Figure 1 and 4.6). It has several outlet glaciers, Lower Foxfonna, Rieperbreen and Foxbreen, that become increasingly independent from the ice cap as the ice is recessing. The local bedrock geology is characterized by Paleogene marine sandstones and mudstones of the Grumantbyen formation (Dallmann, 2015).

2.4.4 Frostisen South Basin

Frostisen South Basin (Frostisen SB) is a small sub-ice cap located in Dickson Land on the North side of Isfjorden. It used to be connected to the larger Frostisen plateau ice cap in the North, up to sometime between 1990 and 2011, and one unnamed small outlet glacier in the East, up to sometime between 2011 and 2020 (Figure 1 and 4.9). Frostisen SB is ranging in elevation between 500 and 600 m a.s.l. and had an area of 0.6 km^2 in August 2020. The local bedrock geology is characterized by Middle Triassic black shales from the Botneheia formation and the Late Triassic immature sandstones of the Storfjorden subgroup (Dallmann, 2015). From this point onwards, Frostisen South Basin will be referred to as Frostisen.

3 Methods

3.1 Site selection

A range of potential sites have been explored using aerial imagery from 2009 and 2011 provided by the Norwegian Polar Institute (NPI) via *toposvalbard* (https://toposvalbard.npolar.no/). All small size ice caps lying on plateaux or gently sloping ground on top of mountains in central Spitsbergen, with no obvious structural deformations due to ice movements and apparently undisturbed ground emerging from their margins, were considered as potential sites for fieldwork. Retreating ice margins where no extensive reworking by lateral meltwater channels could be observed, exposing patterned ground and sometimes even vegetation were considered as ideal field sites as they are good proxies for cold based ice. A total number of 32 potential sites were identified. A first selection was made by ruling out the ice caps that would need the use of a helicopter or a several days hike coupled with camping to get to, as this would have been challenging in terms of financing, safety and logistics. The ice caps that had been investigated by Miller et al. (2017) were also disregarded. Out of the five sites left, three were successfully reached during the field campaign, adverse weather and sea conditions having forced the field team to turn around on the way to the other two (Table 3.1).

Table 3.1. The five ice caps that were selected for the field campaign. The areas and number of outlet glaciers were valid in 2009-2011.

Site name	Region	Elevation (m a.s.l.)	Ice cap area (km^2)	Number of outlet glaciers	Successfully reached ?
Bassen	Adventdalen area	890-950	0.6	0	Yes
Foxfonna	Adventdalen area	680-800	3.1	2	Yes
Frostisen	South Dickson Land	450-600	1.0	2	Yes
Templet	South Bünsow Land	700-750	1.3	2	No
Sindballefjellet	South Bünsow Land	700-810	1.0	3	No

3.2 Fieldwork

3.2.1 Sampling

Vegetation samples were taken as close as possible to the ice margin to avoid modern carbon contamination by colonisation by modern vegetation, spontaneous plant regrowth (La Farge et al., 2013) (cf. Section 2.3.4) and fungal development. Sampling within the current year's retreat area should limit the development of these phenomena. However, in the field, it is usually impossible to discern the extent of this recent retreat and therefore sampling should ideally be conducted without risks of contamination within a couple of meters from the ice margin, according to present retreat

rates observed in Spitsbergen (e.g., Rachlewicz et al., 2007; Nuth et al., 2010; Möller and Kohler, 2018; Holmlund, 2021). Samples can potentially be taken further away from the ice margin, if a larger distribution of age points is required, along a transect perpendicular to the ice margin for example, but they should then be thoroughly examined under low power microscope for any sign of colonisation, regrowth (bright green sprouts in both cases) or fungal presence (usually in the form of crust) (Figure 4.5).

While the field sampling aimed at gathering *in situ* samples from all species that could be observed at each sampling area, the vegetation targeted for radiocarbon dating was restricted to bryophytes, the main reason for this choice being that flowering plants were found only at a few sites at Frostisen, and neither at Bassen nor Foxfonna. Samples were collected at Bassen and Frostisen during a field campaign between August 19th and 21st 2020. Adverse weather conditions in the form of strong wind and heavy rain and snow prevented the field team from conducting as thorough fieldwork as was wished for, but samples were successfully collected at both sites. The samples from Foxfonna were collected in summer 2019 by Andrew Hodson (FX19-M1 and M2), while FX20-M1 was collected during a dark season field expedition in late November 2020 thanks to the coordinates recorded by Hodson the previous summer, enabling a visit to the site and successful excavation of moss from beneath the snowpack.

3.2.2 Sample storage and conservation

After collection, the samples were kept cool out of direct sunlight during the rest of the field day. Once back in Longyearbyen, they were air dried at room temperature overnight to evaporate the water surplus and then stored frozen in one of UNIS's freezer rooms at -19°C until the start of the lab work. Care was taken not to completely dehydrate them as desiccated moss becomes water repellent and might be hard to rehydrate for processing the samples (Stark, 2017).

3.3 Lab work

3.3.1 Species identification and abundance quantification

The samples were examined under low power microscopy and the species present in the samples identified. In the case of Frostisen where a thick, multispecies paleo-tundra was found, a species abundance quantification had to be established for each sample. This was done by visual estimation of the different species volume proportion in each sample, the proportions being then

reported as percentages. The bryophytes were identified following Hill et al. (2006) with the exception of the Polytrichaceae family for which Long et al. (1985) was used. The lichens were identified according to Zhurbenko and Brackel (2013) and the vascular plants according to the Svalbard Flora (Rønning, 1996).

3.3.2 Choice of the material to date

The small monospecific samples from Bassen and Foxfonna did not offer many possibilities in the choice of material to send for radiocarbon dating but, whenever possible, the greenest and better-looking moss stems were preferred for the subsampling. For consistency, a single species recurrent in all four samples from Frostisen was chosen. *Tomenthypnum nitens* was chosen, as it was shown not to have any specific age deviation by Humlum et al. (2005) and being the only species present in all samples in sufficient proportion to provide the 5 mg of material required by the dating laboratory. The apices of the chosen moss stems, of a length of ca. 5 mm from each apex for the small Bassen and Foxfonna samples and up to 1 cm for the taller Frostisen mosses, were targeted to ensure that the youngest material was dated (La Farge et al., 2013).

FR20-M5 was subsampled five times to investigate the potential age variation within one sample and establish how reliable the other ages would be. The apical parts from three different moss patches were chosen for three of the replicas, whereas the last two were taken from the middle and the lower part of the 10 cm long stems of one previously sampled moss patch to investigate the age differences along the stems (Figure 4.12).

3.3.3 Sample preparation

The samples were first completely rehydrated with double distilled milliQ water. The parts to be dated were selected under low power microscope (using different magnification levels according to the species), isolated from the bulk of the sample and thoroughly cleaned using fine tweezers and DI water to remove minerogenic and other plant debris. The cleaned subsamples were then put into small glass vials and placed in the drying oven at 40 °C until complete dehydration (around two hours).

3.3.4 Radiocarbon dating

A good understanding of radiocarbon dating methodologies, the assumptions on which they are based, and the different error sources is essential to properly evaluate the radiocarbon-derived chronologies on which this study is based.

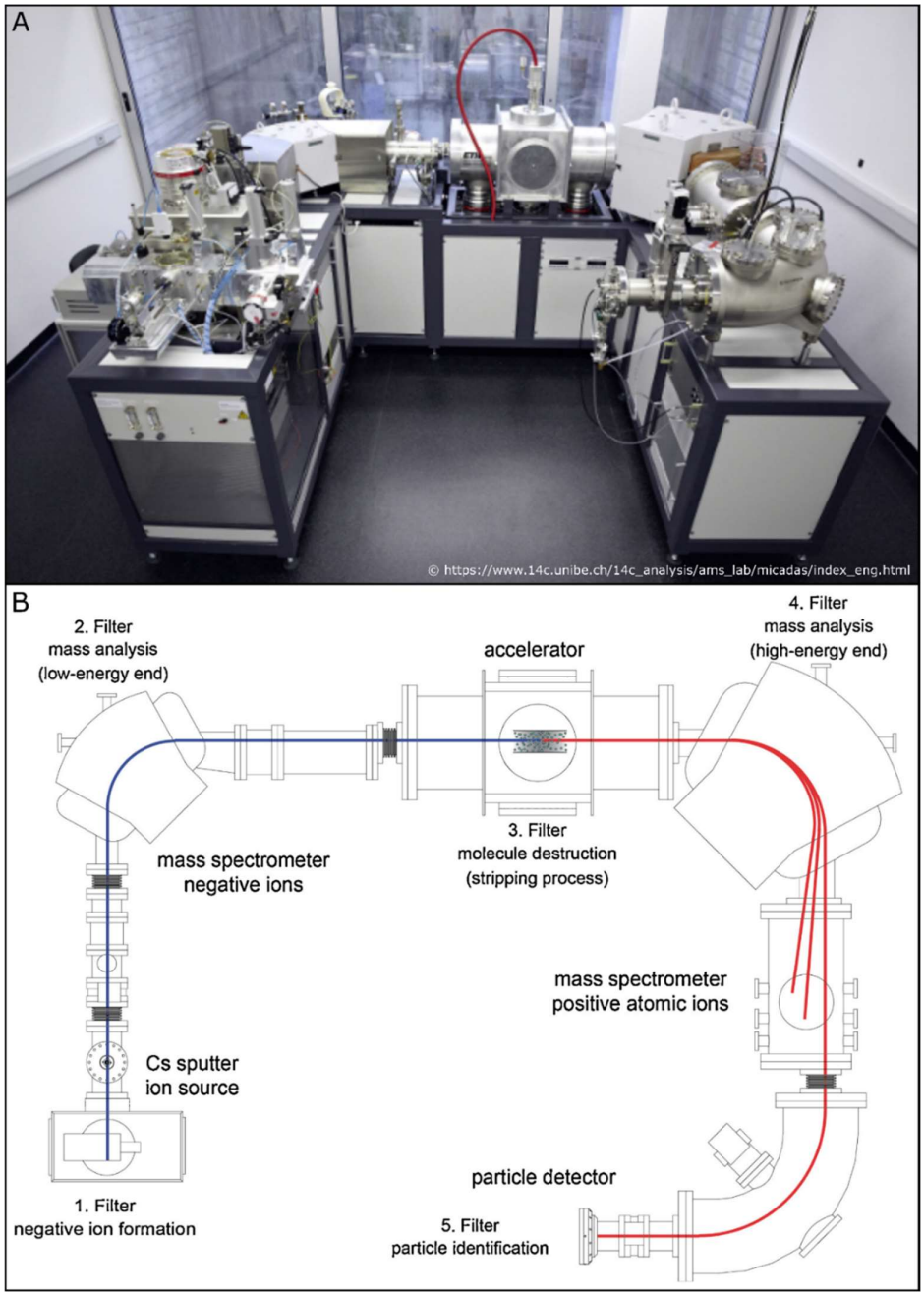

Figure 3.1. MICADAS AMS system. A. Photograph of the system at the LARA lab in Bern University. B. General layout of a typical AMS system. This example shows a representation of the ETH Zurich MICADAS system (drawing from Synal, 2013).

3.3.4.1 The formation of ^{14}C

The natural carbon present in Earth's atmosphere (410 ppm (Williams, 2020) is composed of two stable isotopes, ^{12}C (98.9%) and ^{13}C (1.1%) and of traces of the radioactive ^{14}C (radiocarbon)

(Santos, 2012). Radiocarbon has a half-life $t_{1/2} = 5730 \pm 40$ years (Godwin, 1962) and is produced in the upper atmosphere by the capture of slow neutrons, produced by cosmic background radiation, by nitrogen nuclei (the atmosphere contains 78.08% of nitrogen N_2 (Williams, 2020), inducing the following nuclear reaction:

$$^{14}\mathrm{N} + \mathrm{n} \rightarrow {}^{14}\mathrm{C} + \mathrm{p}$$

The neutrons are the product of a nuclear reaction induced by cosmic rays' action on the outer layer of the Earth's atmosphere. After their formation, ^{14}C atoms are rapidly oxidized into carbon dioxide (CO_2) via the two following reactions:

$$^{14}\mathrm{C} + \mathrm{O}_2 \rightarrow {}^{14}\mathrm{CO} + \mathrm{O}$$

$$^{14}\mathrm{CO} + \mathrm{HO} \rightarrow {}^{14}\mathrm{CO}_2 + \mathrm{H}$$

Carbon dioxide has an average residence time of about 5 years in the atmosphere (Starr, 1993) allowing the newly produced $^{14}CO_2$ to be mixed almost evenly in all parts of this reservoir before it is captured by the biosphere and the oceans. ^{14}C atoms are fixed into plant tissues by photosynthesis and into the rest of the living biosphere through the food web.

3.3.4.2 The radiocarbon dating method

In 1960, the Nobel Prize in chemistry was allocated to the American physical chemist Willard F. Libby for "his method to use ^{14}C for age determination in archaeology, geology, geophysics, and other branches of science" (Libby, 1946; Arnold and Libby, 1949, 1951). The method is based on the assumption that there has been a stable carbon isotope ratio in the atmosphere through time and on the fact that when ^{14}C is no longer replenished in an organism, after its death for example, its amount will decrease with time according to its half-life as it decays back to ^{14}N. Libby demonstrated that according to the measurement of the remaining ^{14}C from a dead or inactive organism, the time elapsed since its death could thus be inferred.

After measuring the present day $(^{14}\mathrm{C}/^{12}\mathrm{C})_t$ ratio, the exponential decrease in isotope ratio allows for age (t) determination by solving the following equation:

$$(^{14}\mathrm{C}/^{12}\mathrm{C})_t = (^{14}\mathrm{C}/^{12}\mathrm{C})_{t=0}\mathrm{e}^{-\lambda \mathrm{t}}$$

where the decay constant is related to the half-life by the relation $\lambda = (ln2)/t_{1/2}$. The calculation of the age then requires knowing the initial ratio $(^{14}\mathrm{C}/^{12}\mathrm{C})_{t=0}$. However, as there have been changes in the atmospheric $^{14}C/^{12}C$ ratio over time, the obtained ^{14}C ages, expressed in ^{14}C years BP (before 1950 CE (Godwin, 1962)), do not equal calendar years and therefore require calibration (Stuiver and Reimer, 1986, 1993). Radiocarbon ages are calculated using an internationally agreed upon reference value for the $(^{14}\mathrm{C}/^{12}\mathrm{C})_{t=0}$ ratio and the ^{14}C half-life determined by Libby $t_{1/2} = 5568 \pm 30$ in 1951 for a matter of consistency as recommended by Godwin in 1962 when his research group established a new value for the half-life of ^{14}C.

3.3.4.3 Accelerator Mass Spectrometry (AMS)

In 1977, the ^{14}C dating method faced a breakthrough with the development of the AMS technique which allowed the amount of $^{14}C/^{12}C$ in the sample to be measured directly using mass spectrometry techniques. The necessary sample size for a measurement with this method was reduced by at least a factor of 1,000 compared to the sizes required for decay counting methods that had been used until then (Muller, 1977; Nelson et al., 1977). In addition, samples could then be measured in a few minutes instead of the initial few days necessary for natural decay counting of long-lived radioisotopes.

The first MICADAS (MIni CArbon DAting System) system was developed at the University of Zürich and became operational in 2004 (Synal et al., 2007) (Figure 3.1). Once loaded into the MICADAS system the carbon atoms are first ionized before being accelerated, the different isotopes being subsequently separated according to their mass (Synal, 2013). All the radiocarbon analysis for this study were conducted at the LARA Accelerator Mass Spectrometry (AMS) laboratory of the University of Bern (https://www.14c.unibe.ch/14c_analysis/ams_lab) where the samples were first oxidized to CO_2 and then converted to graphite before being loaded into their MICADAS system for dating.

3.3.4.4 Calibration

Calibration of the obtained radiocarbon age is done by matching this age with a calibration curve. Calibration curves are established by reconstructing yearly $^{14}C/^{12}C$ palaeo-ratios using records that can be dated independently. As dendrochronology allows for precise dating of tree rings by counting them individually, comparing these calendar years with the ^{14}C ages of the same rings is the

method that has been used preferentially, whenever a tree ring record was available (Linick et al., 1985). The tree ring based calibration curve extends all the way back to 13.9 ka BP. Floating tree-ring chronologies, lacustrine and marine sediments, speleothems and coral records allowed for the expansion of the latest calibration curve back to 55 000 ka BP (Reimer et al., 2020). The calibration software that are used to calibrate radiocarbon ages also apply the correction needed from Libby's ^{14}C half-life to Godwin's half-life that is still the agreed upon value today (Godwin, 1962). These softwares return the different intercepts of the given radiocarbon ages with the calibration curve (Figure 3.2) and calculate a median calibrated age for 1σ and/or 2σ confidence intervals.

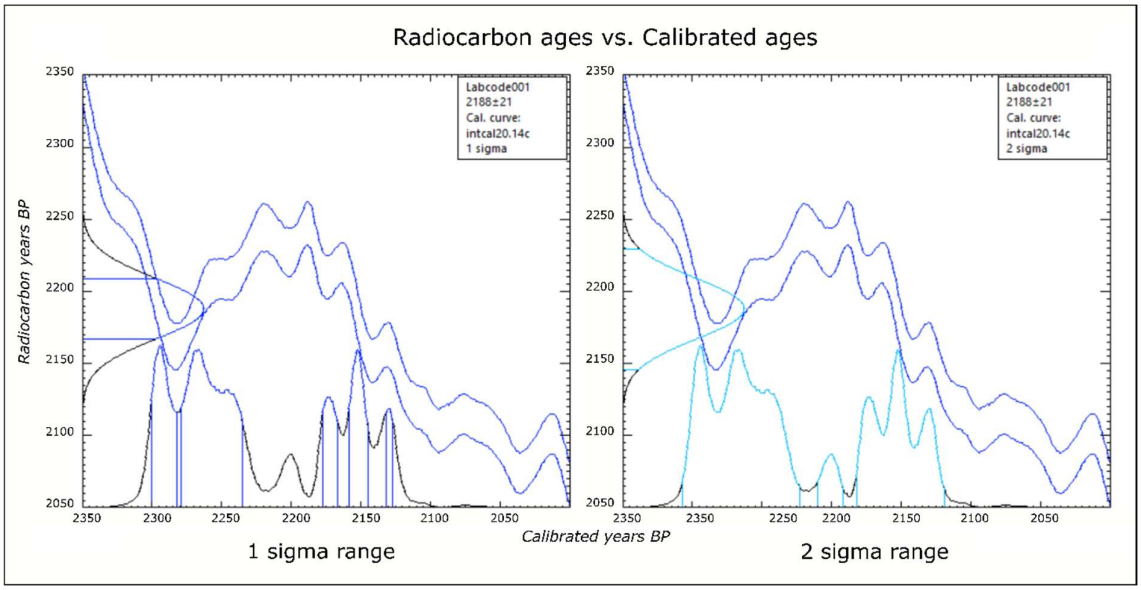

Figure 3.2. Intersection between the probability range of a radiocarbon age and the Intcal20 calibration curve. Example of B20-M2 radiocarbon dated to be 2188±21 radiocarbon years old. Calibration results from the Calib 8.4 program.

The radiocarbon dates from this study were calibrated using the Calib 8.4 program and the IntCal20 calibration curve (Reimer et al., 2020). Calibrated ages are presented as 2σ (95%) probability ranges expressed in calibrated years BP. In the text and figures, the median calibrated ages rounded up to the closest 5 years are used, + and – the range between the median age and the upper and lower probable ages, also rounded up to the closest 5 years.

3.4 Ice retreat mapping

3.4.1 Ice marginal positions

The ArcMap 10.7.1 software produced by ESRI was used to plot and analyse ice margin position variations during the past century for each of the ice caps. All geographical data presented are referenced to the WGS84 datum.

3.4.1.1 Bassen

Oblique aerial images from 1936 provided by the Norwegian Polar Institute (NPI), and aerial orthophotographs from 2009 were used to digitally retrace two former ice margin positions. The ice margin was traced by foot with a hand GPS in 2015 (Wesley R. Farnsworth, personal communication) and 2020 (this field campaign), providing precise ice marginal positions for these two years.

3.4.1.2 Frostisen

Plotting the Norwegian Polar Institute's glacier outlines shapefiles reconstructed from aerial imagery from 1936 (oblique) and 1990 (orthorectified) (available online at https://geodata.npolar.no/arcgis/rest/services/Temadata/I_Isbreer_Overflatetyper_og_utstrekning_Svalbard) allowed ice margin position definition for these given years, while the images used for the reconstruction are not in open access (1990) or difficult to process due to the view angle and the low definition of the ice cap because the photographs were taken from a long distance (1936). A position for 2011 was obtained by tracing the visible ice margin from aerial photographs (NPI) and the field GPS data was used for 2020.

3.4.1.3 Foxfonna

The glacier outline shapefiles from the NPI were used for ice margin position reconstruction for 1936 and 1990. The position for 2009 was reconstructed by tracing the visible ice margin from aerial photographs. As the fieldwork was executed during the dark season while a substantive snow cover was already in place, *in situ* ice margin tracking was impossible. Sentinel 2 satellite (10 x 10 m image mosaic) imagery from the summer of 2020 was therefore used to reconstruct the latest ice margin position (toposvalbard.no).

3.4.2 Retreat and area loss rates and ice cap survival estimates

Ice cover areas for each of the year-specific ice cover data acquired were calculated using the area measuring tool in ArcMap. Average annual surface loss rates for the different time periods were then calculated in Microsoft Excel®. Based on the percentage of the 2020 ice surface area that was lost annually during the last measurement period (n=5 for Bassen, n=11 for Foxfonna and n=9 years for Frostisen), ice cap survival estimates were calculated. These results are based on linear extrapolation of current ice loss rates and are therefore considered to correspond to the maximum time the ice cap might survive as the data shows that ice loss rates have accelerated through time. As ice retreat is not homogenous along one ice cap margin, and one retreat rate (even averaged) is therefore hardly representative for an ice cap, local retreat rates were calculated for each sampling site.

3.5 Database

3.5.1 Data gathering and recalibration of ages

The VEGLAS (VEGetation buried by GLAciers in Svalbard) database was created to gather all radiocarbon ages corresponding to palaeovegetation dated in relation to ice advance timing in Svalbard. The SVALHOLA database (Farnsworth et al., 2020), gathering all dates for Svalbard since the inset of deglaciation, has been a useful tool to find dates from old studies that are not directly related to cold-based ice advance, but where vegetation layers were found preserved between different generations of glacial sediments (Baranowski and Karlén, 1976; Dzierzek et al., 1990; Furrer et al., 1991). Each date was entered into an Excel spreadsheet and is attributed to the source publication and documented with all information relevant to its interpretation in terms of ice advance (Table 3.2). All ages presented in the database were recalibrated using Calib 8.4 and the IntCal20 calibration curve (Reimer et al., 2020). The recalibrated ages are presented as 2σ (95%) probability ranges expressed in calibrated years BP. In the text and figures, the median calibrated ages rounded up to the closest 5 years are used, + and - the range between the median age and the upper and lower 2σ ages, also rounded up to the closest 5 years.

3.5.2 Quality index

As the data gathered within the VEGLAS database was acquired up to 45 years ago and dating techniques and standards have evolved during this time span, there is a need to assess the reliability of each radiocarbon age included in the database. The definition of the different criteria used to define

a 3-point scale quality index (QI) was primarily based on the criteria used for other database gathering radiocarbon ages from periglacial environments, such as the SVALHOLA (Svalbard), the DATED-1 (Svalbard, Barents Sea, Kara Sea and Fennoscandia) and the BRITICE-CHRONO (Britain and Ireland) databases (Hughes et al., 2016; Small et al., 2017; Farnsworth et al., 2020). A few extra criteria specific to ice advance over vegetation were added to the standard ones mentioned above (Table 3.3). Based on Hughes et al. (2016), a QI ranging between 1 and 3 was given according to how well the different criteria were matched by each date. To be given QI 1 all criteria were satisfied, for QI 2 most of the criteria were satisfied and for QI 3 no (or few) criterion was satisfied. All gathered data had already been given a quality index in at least the SVALHOLA database. However, some ages that were found to be hardly reliable by this study were attributed a QI of 1 in the SVALHOLA database (see discussion chapter), therefore all QI were reassessed carefully for each date included in the VEGLAS database.

Table 3.2. Metadata recorded for each date included in the VEGLAS database (adapted from Hughes et al., 2016).

VEGLAS ID	Unique database identification number composed of the first letter of the name of the first author, the two last digits of the publication year and the sample number
Location	Region Site name Latitude and longitude coordinates: °N, °E (WGS84)
Sample characteristics	Sampling year Elevation (m a.s.l.) Distance from ice margin (m) Ice cover thickness (m), if applicable
Dated material	Sample field number and/or Laboratory ID number Type of vegetation Species
Stratigraphic context or setting	Context relative to the ice margin: ice marginal, sub-glacial, sub-morraine Glacial context: ice advance, ice free
Dating method	^{14}C, AMS
Quality index	Reliability of the age: 1 = reliable; 2 = possibly reliable; 3 = unlikely to be reliable (see Table 2 for criteria)
Ages	Uncalibrated radiocarbon age and error δ^{13}C (‰) Calibrated/calendar age and errors (2 σ probability range), radiocarbon ages calibrated to INTCAL20 (Reimer et al. 2020) Number of intersections with the callibration curve Lower and higher calibrated ages Generic age, in cal. ka BP
Comments	Any additional pertinent comments (e.g. reliability of date)
Citation information	Source reference (author, year) SVALHOLA database reference (Farnsworth et al., 2020)

Table 3.3. Age quality control criteria (based on La Farge et al., 2013; Reimer et al., 2020; Wohlfarth, 2009). Ages within VEGLAS are given a quality index (QI) rating based on the criteria specific to the dating method used. QI 1, all criteria are satisfied; QI 2, most of the criteria are satisfied; QI 3 no (or few) criterion is satisfied. Partly modified from Hughes et al., 2016.

- Sample *in situ*, i.e. no post-depositional disturbance or reworking
- Known and uncontaminated sample material
- Samples taken within the year's retreat area or carefully checked for any regrowth sign
- Samples taken within the LIA maximum ice extent
- Details of stratigraphical setting given
- Uncalibrated radiocarbon age given with error margins to enable recalibration using the latest calibration curve
- Multiple and/or stratigraphically consistent ages
- Precise ages: errors < 10% age
- Considered by original authors to be reliable

4 Results

4.1 Retreat rates

Linear retreat rates were not measured based on field monitoring, but approximated from the reconstructed ice margin positions. Retreat rates are asymmetrical and can vary greatly along the ice margin of a single ice cap. Local retreat rates range between 1.7 and 24.8 m yr^{-1} between 2011 and 2020 at Frostisen SB, between 0 and 11.2 m yr^{-1} between 2015 and 2020 at Bassen and between 1.2 and 19.0 m yr^{-1} between 2009 and 2020 at Foxfonna. To produce meaningful values despite these great local variations, ice area loss rates for the different time periods between the ice margin reconstructions were investigated in lieu of linear retreat rates. For each year during the time periods described above Frostisen, Bassen, and Foxfonna have been losing respectively 8.31 %, 2.10 % and 2.15 % of their 2020 areas. Derived from the calculated area loss yearly rates, an estimation of the maximal survival time of each ice cap was calculated based on linear extrapolation of current ice loss rates (Table 4.1).

Table 4.1. Ice surface area changes between 1936 and 2020 and derived ice surface loss rate calculations and indicatory estimated survival time of the ice caps, based on surface area changes only, therefore not taking into account volume changes which would be more accurate but are beyond the focus of this study.

	Year	Ice surface area (km2)	Area loss (km2)	Number of years	Loss rate (km2.yr^{-1})	Loss rate (% of 2020)	Projected ice cap survival time (yrs)
Bassen	1936	0.914					
	2009	0.629	0.285	73	0.004		
	2015	**0.563**	0.066	6	0.011		
	2020	**0.510**	***0.054***	***5***	***0.011***	***2.10***	***48***
Foxfonna	1936	4.216					
	1990	3.603	0.613	54	0.011		
	2009	**3.144**	0.460	19	0.024		
	2020	**2.542**	***0.601***	***11***	***0.055***	***2.15***	***47***
Frostisen SB	1936	2.074					
	1990	1.687	0.387	54	0.007		
	2011	**1.074**	0.613	21	0.029		
	2020	**0.614**	***0.459***	***9***	***0.051***	***8.31***	***12***

4.2 Vegetation samples

At all sites, vegetation was found in an exceptionally well-preserved state, with stems bearing intact and apparently healthy leaves as well as numerous roots. All the vegetation that was sampled

was found *in situ*, and still rooted into the palaeo-soil that was emerging from the retreating ice margins or solidly attached to rock surfaces.

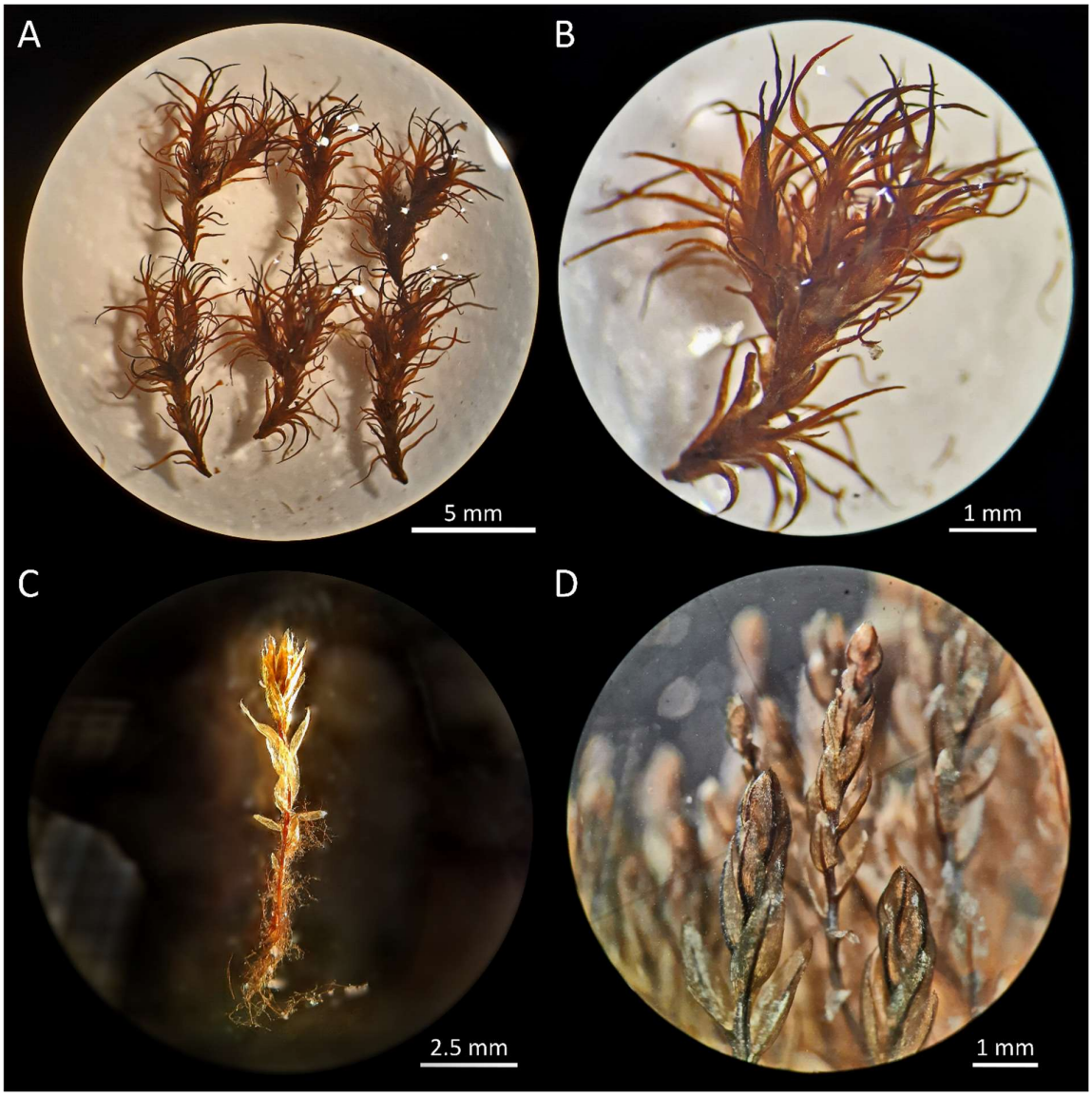

Figure 4.1. View under the low power microscope during sample preparation for radiocarbon dating. A and B: Tomenthypnum nitens *from sample FR20-M5. C. A single stem of* Pohlia obtusifolia *from sample FX19-M2 with its intact root system. D. Apical part of some stems of* Pohlia obtusifolia *from FX19-M2.*

4.2.1 Bassen

Bassen is a barren plateau essentially covered by loose cobble-sized sandstone clasts. Vegetation was encountered only on the west side of the plateau, on the leeside of the ice cap relative

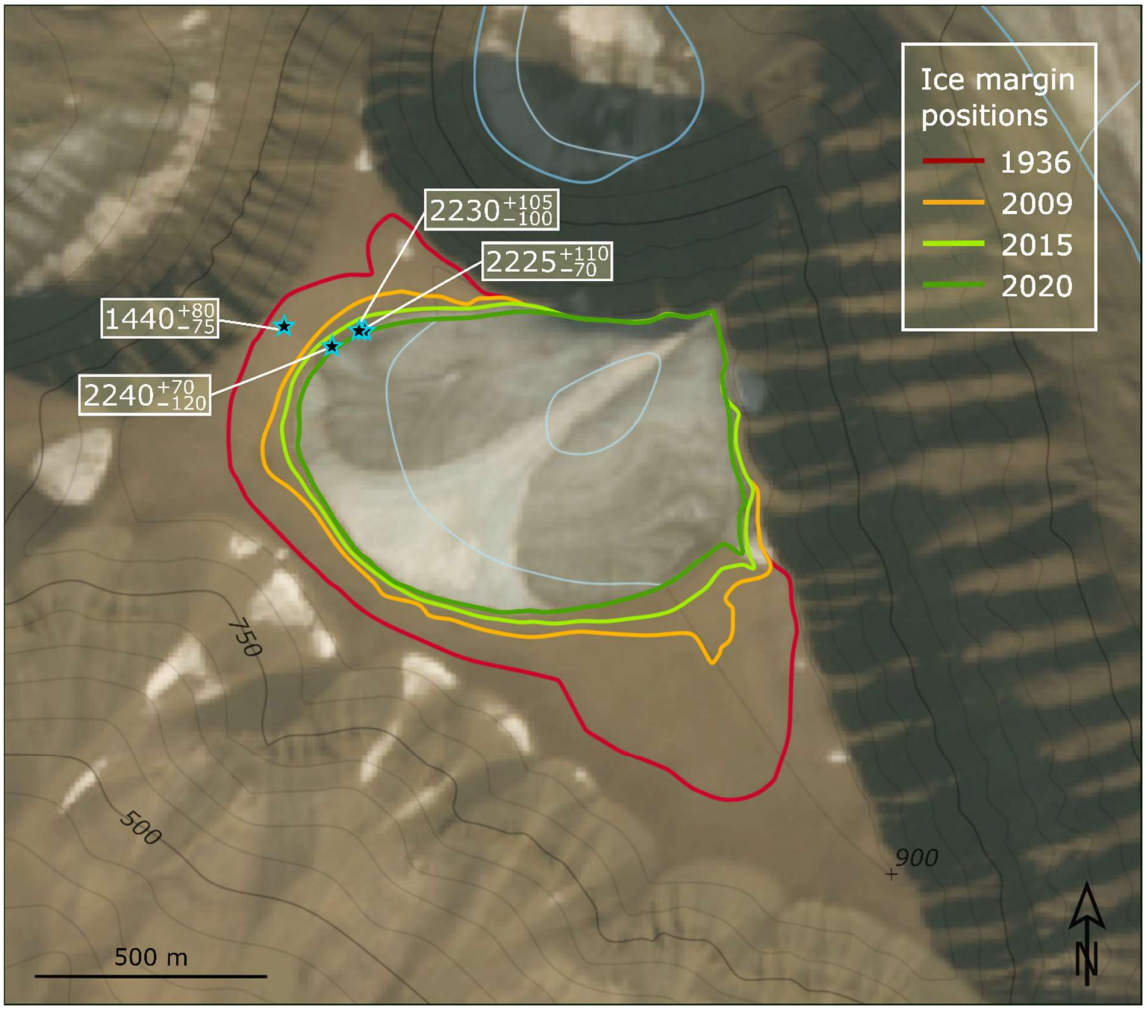

Figure 4.2. Map of the Bassen ice cap with evolution of its ice margin position from 1936 to 2020. Sample locations are marked with blue stars. Base map modified from toposvalbard.no.

to the prevailing wind direction and four moss samples were taken (Figure 4.2). At the proximity of the ice margin, sporadic moss patches of 1 to 3 cm in diameter were found growing on sandstone clasts (Figure 4.3). Two samples, B20-M2 and B20-M3 were taken within 1.5 m distance from the ice margin, c. 80 m from each other, marking the two far ends of the area where moss patches were found along the ice margin. B20-M4 was taken along the same perpendicular line to the ice margin as B20-M3, 4m further away from the ice. B20-M2, M3 and M4 are composed of several moss patches collected within a few square meters, as a single moss patch would not have provided enough material for radiocarbon dating. B20-M5 was collected a greater distance from the present ice margin (110m) as, beside what was sampled at the margin (B20-M2, B20-M3 and B20-M4), it was the only apparently dead moss that

was encountered on the plateau. The moss patches found in the area where B20-M5 was sampled were numerous and up to 10 cm in diameter. Between 2015 and 2020, the ice margin of Bassen retreated at a rate of c. 6 m yr^{-1} in the area where B20-M2, B20-M3 and B20-M4 were sampled. Close to the ice margin, numerous lichens of different species (unidentified) were observed covering large rocky areas (Figure 4.4).

Figure 4.3. A. Bassen ice cap viewed from the south, looking northwards. B. Position of B20-M2 relative to the ice margin. C. Sample B20-M2.

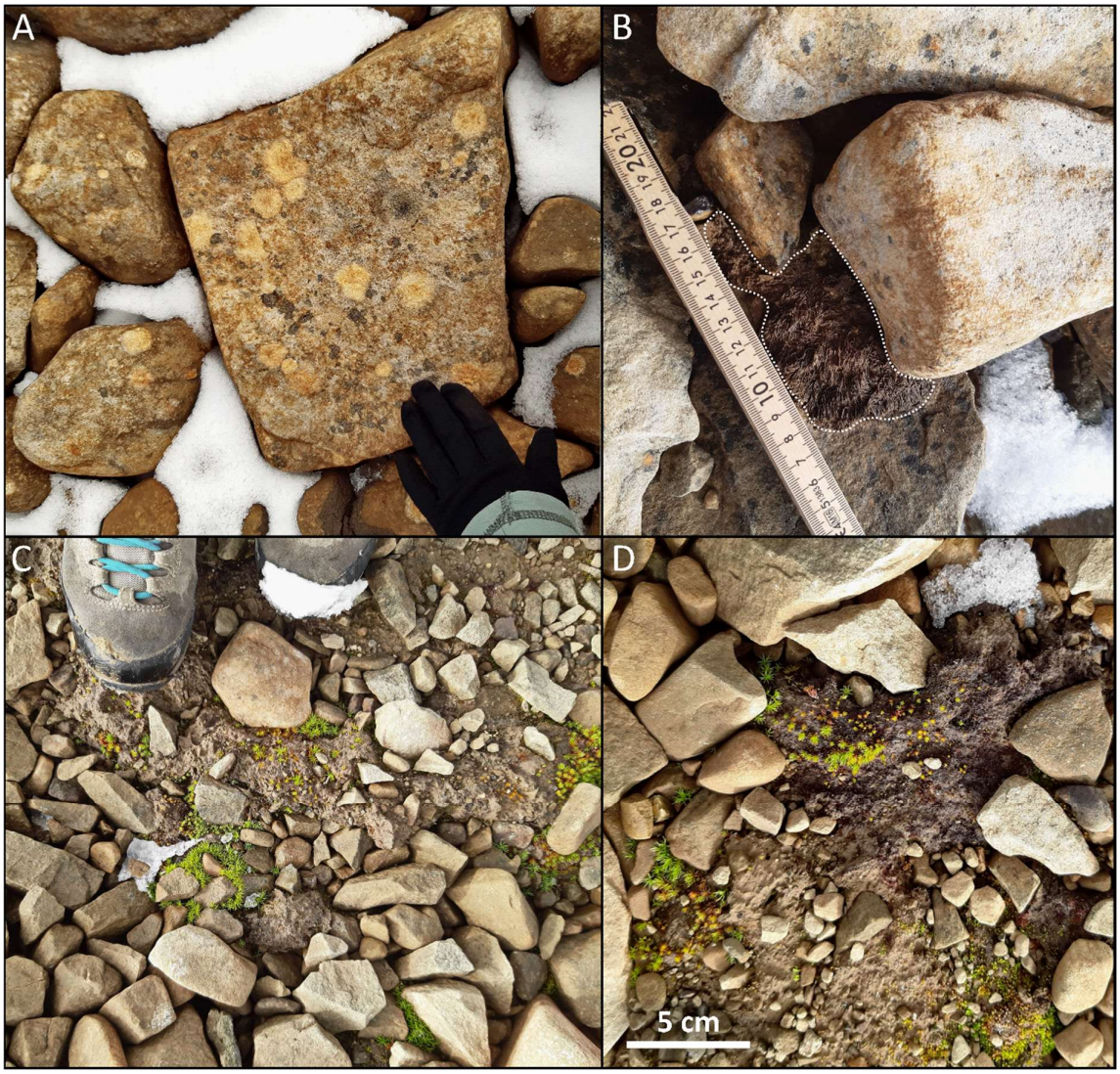

Figure 4.4. A. Rocks covered by lichens exposed by the retreating ice at Bassen. B. Sample B20-M5, sampled 110 meters from the ice margin. C and D. Live moss from the Polytrichaceae family using dead moss from a different family exposed by Bassen ice cap as a substrate to grow on, c. 100 m from the ice margin.

All samples were monospecific when buried under the ice (Table 4.2), but two fresh (bright green) stems of *Pogonatum urnigerinum* were found growing on a part of the dead B20-M5 moss patch (Figure 4.5). A whitish fungal crust also covered approximately one square centimetre of the sample. However, a large part of the sample didn't show any sign of colonisation or other bio-contamination and was subsampled for radiocarbon dating. Some tens of meters further out from where M5 was collected, large patches of dead moss (species unidentified) were being recolonised by moss of the *Polytrichaceae* family (Figure 4.4).

Table 4.2. Species list from the 4 samples collected at Bassen.

Sample ID	Group	Species	Relative proportion *
B20-M2	Bryophyte	*Andreaea blyttii*	100%
B20-M3	Bryophyte	*Andreaea obovata*	100%
B20-M4	Bryophyte	*Andreaea obovata*	100%
B20-M5	Bryophyte	*Andreaea obovata*	98%
	Bryophyte	*Pogonatum urnigerinum* **	2%

* visual estimation of the volumic proportion of each species

** new growth, using A. obovota as substrate to develop

The local linear average retreat rate between 1936 and 2009 is 1.37 m y^{-1} at the position where B20-M5 was sampled, some 38 m away from the 1936 ice margin position. Thus, these 38 m correspond to 28 years, which would mean that the area was deglaciated by 1964. However, the retreat rates during the 1936-2009 period can hardly have been constant and must have varied with

Figure 4.5. Fresh growth of Pogonatum urnigerinum*. Observed under a low power microscope. These two stems were growing using the* Andreaea obovata *from sample B20-M5 as a substrate. White fungal development can be observed above the green sprouts.*

time according to summer air temperatures (Figure 4.6), with a probable increase from a few cm per year during the cold 1960s to close to 3 m yr^{-1} in the 2000s as the local retreat rate between 2009 and 2015 was 3.2 m yr^{-1}. Therefore, the likeliness that 1964 is a too early estimation is high, and it is more likely that the deglaciation of B20-M5 occurred in the 1970s, the moss having then been exposed at most for 50 years.

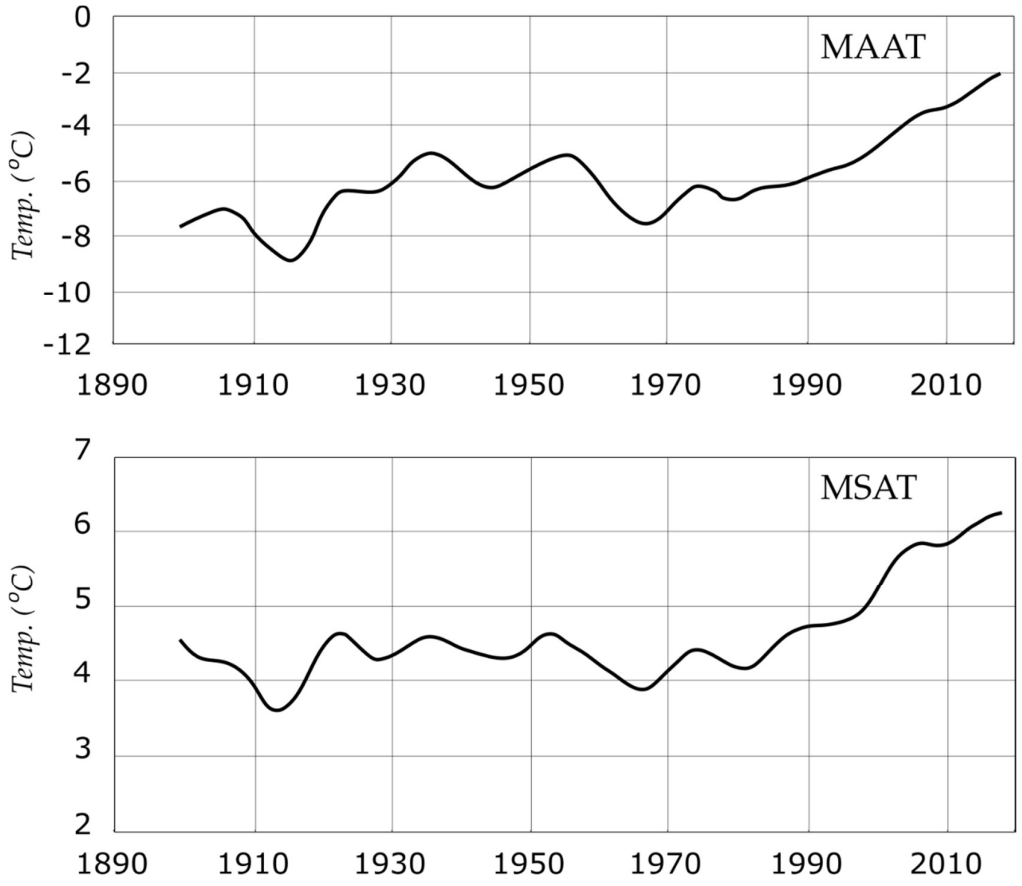

Figure 4.6. Mean air temperature (MAT) for the composite Svalbard Airport series during the period September 1898-December 2012 for annual means (MAAT) and summer (June, July and August; MSAT). Individual years are filtered by a Gaussian low-pass filter with standard deviation of three years in its distribution, corresponding to a rectangular filter of about 10 years. (The ends of the curves are not significant. Forthe last year, 2018, 38% of the weights will lie on unknown future observations; for the sixth last year, 2012, it is only 5%.). Modified from Nordli et al., 2020.

4.2.2 Foxfonna

The surface of Foxfonna plateau is, similar to Bassen, covered by loose sandstone clasts and is little vegetated in proximity to the ice cap. Two samples, FX19-M1 and FX19-M2, were collected along the eastern margin of the ice cap in the late summer of 2019 and a third sample, FX20-M1, was collected along the same margin on November 23rd 2020 where it was found rooted between rocks.

Between 2009 and 2020, the ice margin of Foxfonna retreated at a rate of c. 2.2 m yr^{-1} in the area where FX19-M2 and FX20-M1 were sampled and at a rate of c. 9.0 m yr^{-1} in the area where FX19-M1 was sampled (Figure 4.7).

Table 4.3. Species list for the 3 samples collected at Foxfonna.

Sample ID	Group	Species	Relative proportion *
FX19-M1	Bryophyte	*Pohlia sp.*	100%
FX19-M2	Bryophyte	*Pohlia obtusifolia*	80%
	Bryophyte	*Oncophorus wahlenbergii*	20%
FX20-M1	Bryophyte	*Pohlia sp.*	100%

* visual estimation of the volumic proportion of each species

FX19-M1 and FX20-M1 were found to be monospecific, but two different moss species were found to be forming FX19-M2 (Table 4.3).

4.2.3 Frostisen South Basin

Frostisen South Basin is located in a gentle depression of the terrain and the receding ice margin is therefore retreating downwards, exposing shale rich ground. An impressive amount of vegetation was found around its margins with, in some areas, a continuous 10-30 cm thick layer of mature vegetation covering the recently deglaciated ground and continued under the ice (Figures 2.3 and 4.7). Lateral meltwater channels, that cut into the ice close to the margins and reach all the way to below the ice on the north and west sides of the ice cap, allowed the sampling of vegetation that was still covered by ice at all sampling sites. All vegetation was still deeply rooted into the underlying, shale rich soil.

FR20-M1 was sampled on the east side of the ice cap, under a few centimetres of ice. Around 500 m further away along the ice margin, on the north side of the basin, a melt water channel cut deeply into the ice, forming a small ice cave. FR20-M2 and FR20-M3 were taken around 5 m apart in the melt water channel, under 50 cm of ice, just outside of the cave, and FR20-M5 was taken some 10 m into the cave under c. 2 m of ice (Figures 4.8 and 4.9). For these 3 later samples, as the vegetation emerging from the ice was very species rich, an attempt was made to gather as many species of bryophytes, vascular plants and lichens as possible found within one square meter (Table 4.4).

However, no further observations were made in the field due to harsh weather conditions. Between 2011 and 2020, the ice margin of Frostisen retreated at a rate of c. 6.5 m yr^{-1} in the area where FR20-M2, FR20-M3 and FR20-M5 were sampled and at a rate of c. 9.2 m yr^{-1} in the area where FR20-M1 was sampled.

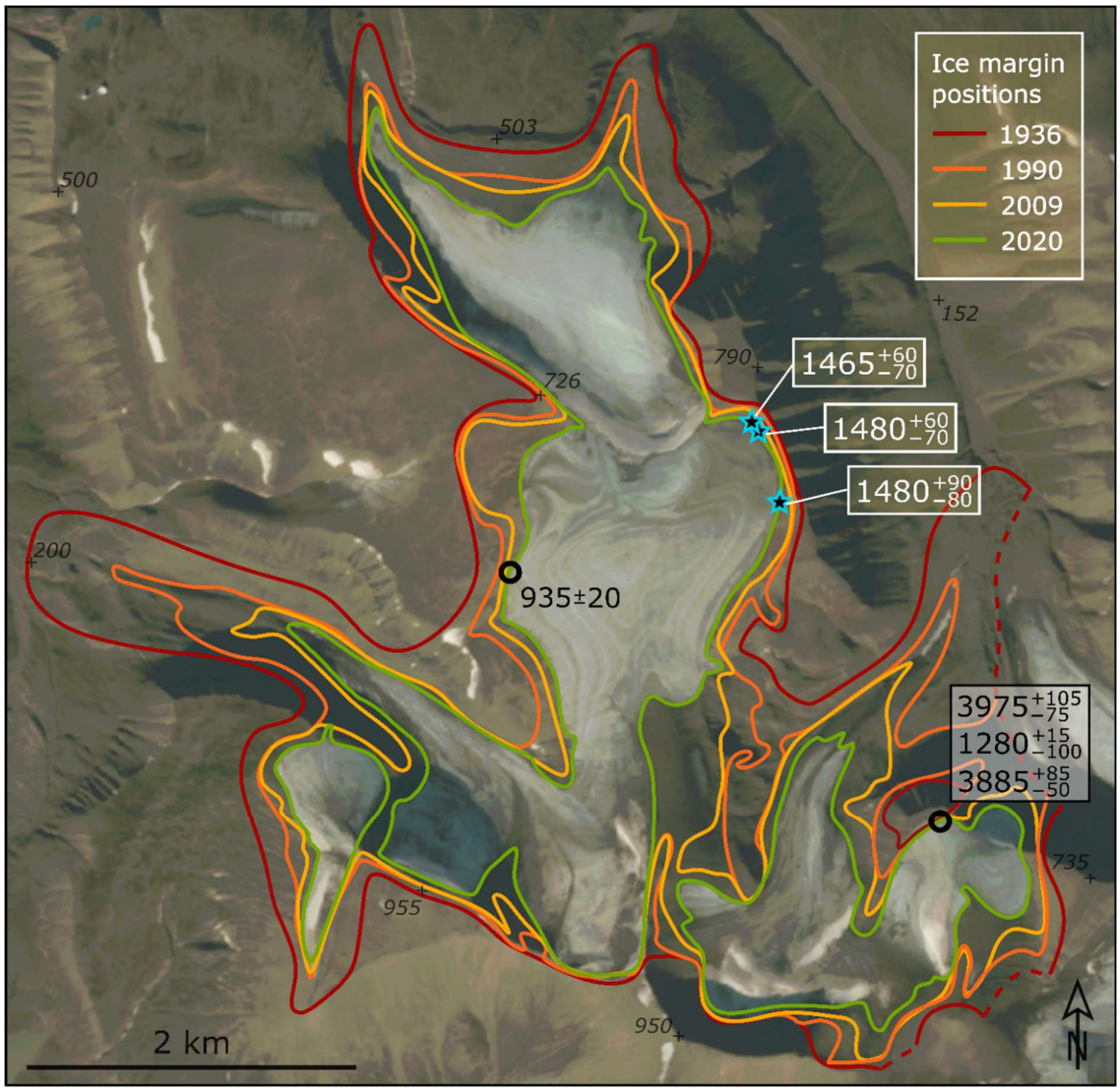

Figure 4.7. Map of the Foxfonna ice cap with evolution of its ice margin position from 1936 to 2020. Sample locations are marked with blue stars. Black circles mark the sample locations from Miller et al, 2017. Base image modified from toposvalbard.no.

A large number of glacier mice was found on the surface of the ice cap. Their sizes varied from a couple of centimetres and up to around 10 cm (Figure 4.11). Glacier mice, or jökla-mýs (Eythórsson, 1951) are small balls of moss up to 10 cm in diameter that form on some glacier surfaces. Their growth

initiates around a clast lying on the ice surface and, when the moss gets bigger, protects the underlying ice surface by thermal insulation, resulting in the moss becoming elevated on a pedestal as the surrounding ice melts. Eventually, the moss falls from this pedestal and can be rolled over on the ice

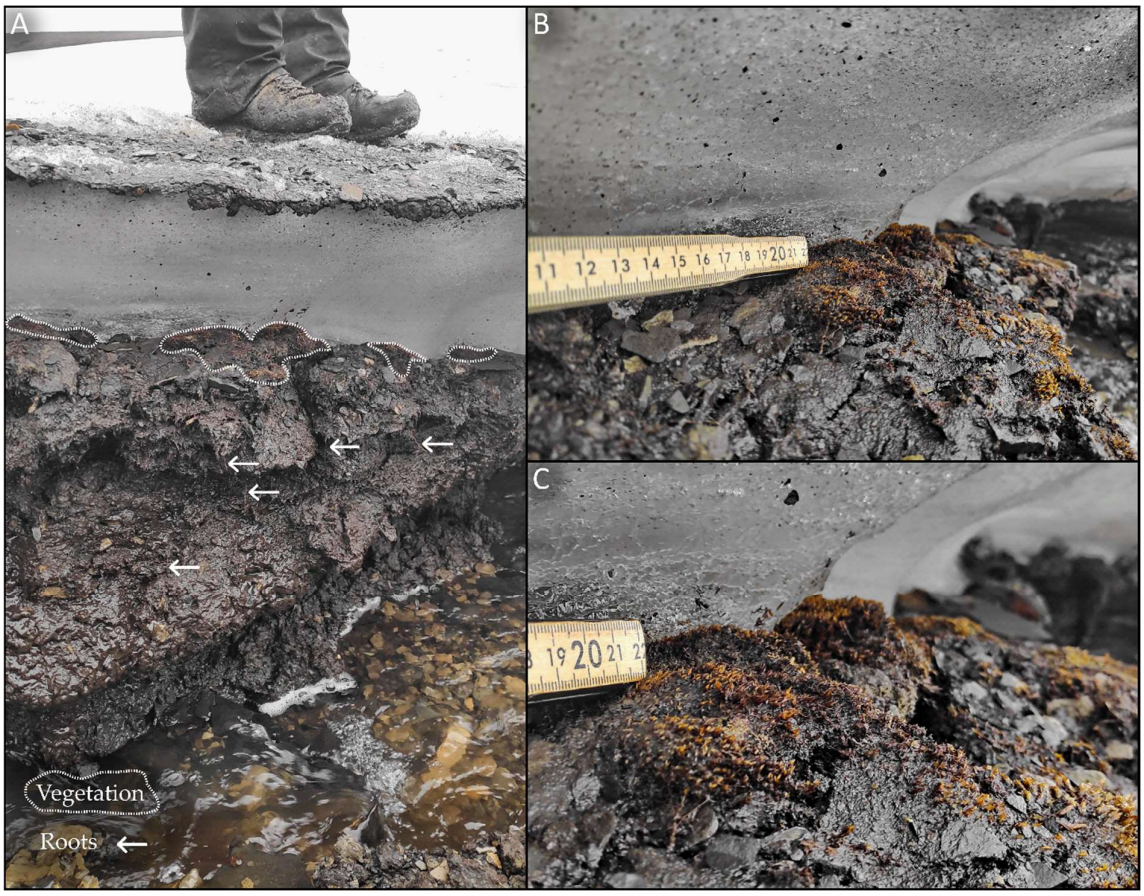

Figure 4.8. The ice margin of Frostisen locally eroded by a lateral meltwater channel exposing a palaeosoil horizon buried under the ice cap. A. The emerging vegetation layer was deeply rooted into the palaeosoil. White arrows highlight some of the in-situ *roots exposed by the erosion. B and C. Closer view on some of the moss patches still trapped under the ice. Photograph credit: Jóhanna Kristín Jóhannesdóttir.*

surface by winds and downslope movements, progressively exposing all its faces and becoming rounder (Porter et al., 2008). A wide range of moss species can form glacier mice as their formation appears to be a result of the unusual environment rather than specific species of moss (Coulson and Midgley, 2012). At Frostisen, some glacier mice were also found lying on recently deglaciated surfaces (Figure 4.11). They appeared to have continued growing on their new substrate.

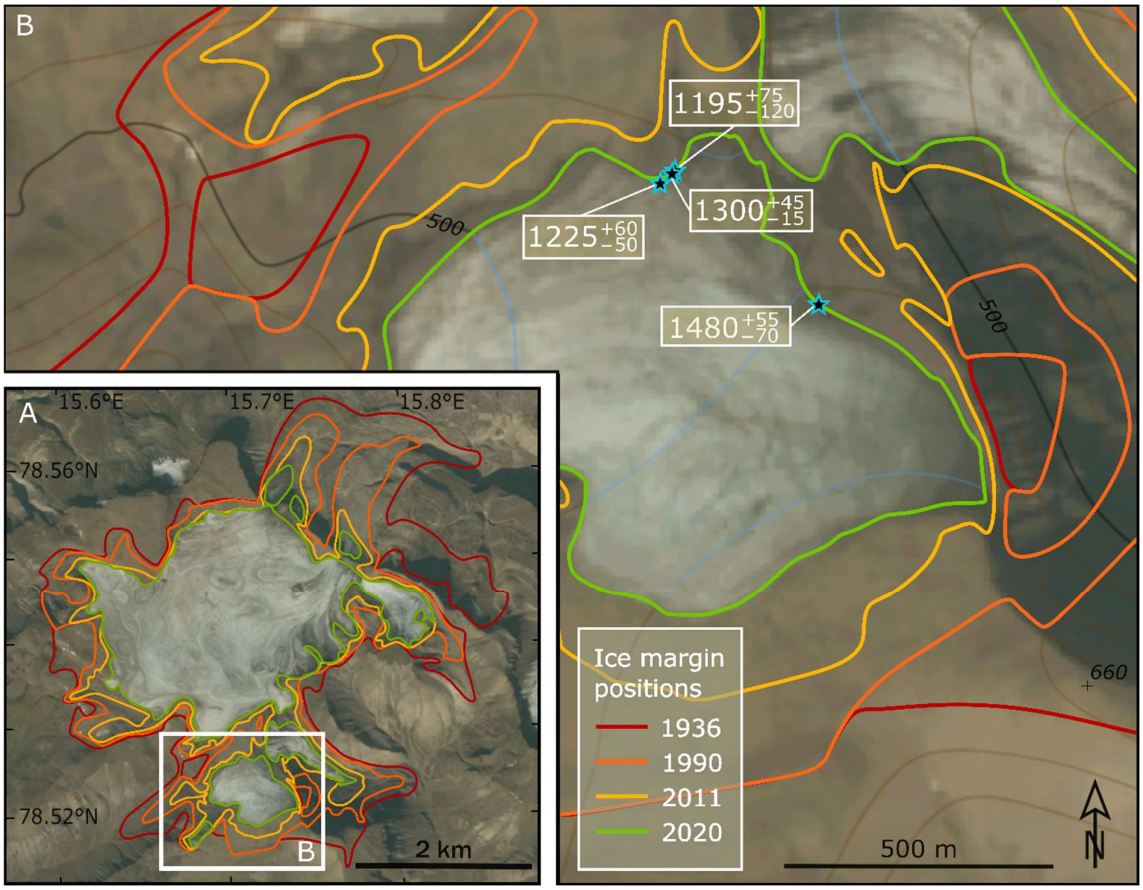

Figure 4.9. Map of the Frostisen ice cap with evolution of its ice margin position from 1936 to 2020. A. Position of the now independent South basin relative to the whole ice cap. B. Frostisen South basin. Sample locations are marked with blue stars. Base map and image modified from toposvalbard.no.

4.3 Radiocarbon dating

A total of 11 moss samples were judged suitable for dating, 4 from Bassen, 3 from Foxfonna and 4 from Frostisen (Figure 4.13; Table 4.5). Each of the samples was radiocarbon dated once except for FR20-M5 which was subsampled 5 times to investigate the potential age variations within one sample and therefore the reliability of the rest of the obtained ages. The apical, middle and bottom (excluding roots) centimetre of ten centimetres long stems of *Tomenthypnum nitens* were sampled as shown in figure 4.12 (respectively FR20-M5a, b and c) in order to investigate the age variations within a single moss individual. The two last replicates (FR20-M5d and e) correspond to the apical parts of two other

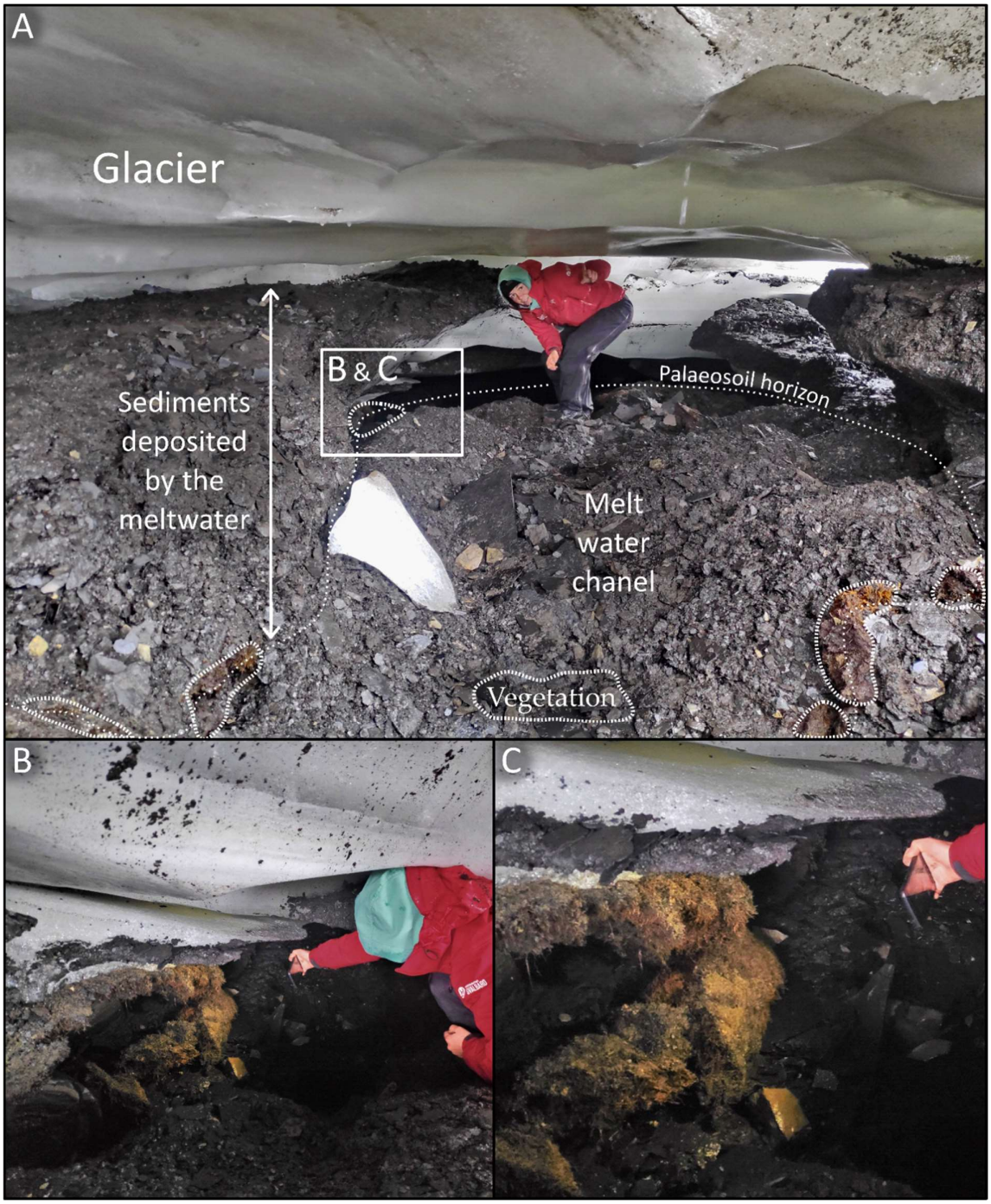

Figure 4.10. Sampling site FR20-M5, inside a small meltwater channel cutting a few meters into the margin of the ice of Frostisen. A. View from the opening of the cave, where the emerging vegetation layer is partly covered by glacial sediments deposited by the meltwater. B and C. Close up look at the sample location, where the palaeosoil was still covered by c. 2 m of ice. Photograph credit: Jóhanna Kristín Jóhannesdóttir.

patches of *Tomenthypnum nitens.* FR20-M5a was very dirty compared to the rest of the samples, with a coating of tiny shale particles sticking to the stems and leaves. Thorough cleaning under the microscope did not succeed in completely removing this shale coating. As FR20-M5a appears to be an older outlier (Figure 4.13 and Table 4.5), an average age of FR20-M5b to M5e, named M5avg, was calculated using the 4 uncalibrated ^{14}C ages and then calibrated on its own. This combined average age has been used for all the data analysis.

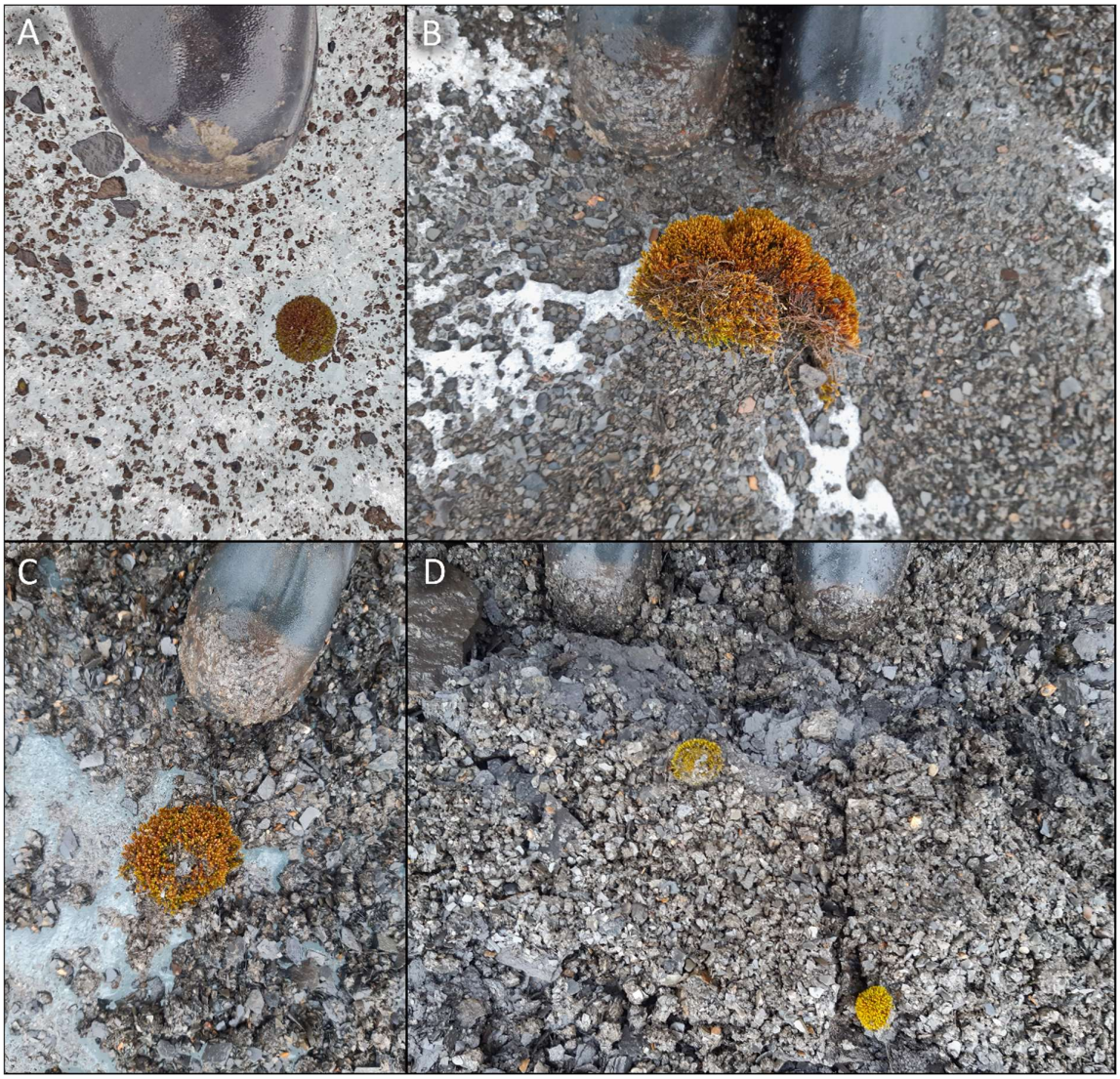

Figure 4.11. Different glacier mice encountered at Frostisen. A, B and C. Glacier mice of a range of sizes found on the ice surface. D. Two glacier mice lying on the ground after complete melt of the underlying ice.

Table 4.4. Species list for the 4 samples collected at Frostisen South Basin.

Sample ID	Group	Species	Relative proportion *
FR20-M1	Bryophyte	*Campylium stellatum*	1%
	Bryophyte	*Ditrichum flexicaule*	97%
	Bryophyte	*Hylocomium splendens*	1%
	Bryophyte	*Tomentypnum nitens*	1%
	Lichen	*Polytrichiastrum alpinum*	< 1%
FR20-M2	Bryophyte	*Bryum* sp.1 **	30%
	Bryophyte	*Bryum* sp.2 **	< 1%
	Bryophyte	*Campylium stellatum*	3%
	Bryophyte	*Kiaeria starkei*	30%
	Bryophyte	*Orthothecium chryseon*	35%
	Bryophyte	*Pohlia wahlenbergii*	1%
	Bryophyte	*Warnstorfia fluitans*	1%
	Vascular plant	Poales	< 1%
	Vascular plant	*Saxifraga oppositifolia* ssp. *oppositifolia*	< 1%
	Lichen	*Stereocaulon alpinum*	< 1%
FR20-M3	Bryophyte	*Bryum* sp. **	35%
	Bryophyte	*Oncophorus wahlenbergii*	5%
	Bryophyte	*Polytrichiastrum alpinum*	2%
	Bryophyte	*Sarmentypnum sarmentosum*	7%
	Bryophyte	*Tomentypnum nitens*	7%
	Vascular plant	Poales	17%
	Vascular plant	*Saxifraga oppositifolia* spp. *oppositifolia*	20%
	Lichen	Crustose lichen 1	2%
	Lichen	Crustose lichen 2	< 1%
	Lichen	*Peltigera* sp.	< 1%
	Lichen	*Stereocaulon* cf. *alpinum*	5%
FR20-M5	Bryophyte	*Abietinella abietina*	< 1%
	Bryophyte	*Brachythecium* cf. *turgidum* ***	< 1%
	Bryophyte	*Campyliumstellatum*	1%
	Bryophyte	*Ditrichum flexicaule*	1%
	Bryophyte	*Hypnum bambergeri*	1%
	Bryophyte	*Myurella julacea*	< 1%
	Bryophyte	*Pohlia* cf. *wahlenbergii* ***	< 1%
	Bryophyte	*Sanionia uncinata*	< 1%
	Bryophyte	*Tomentypnum nitens*	85%
	Vascular plant	*Salix polaris* (leaves and twigs)	5%
	Vascular plant	*Saxifraga oppositifolia* spp. *oppositifolia*	7%
	Lichen	Crustose lichen	< 1%
	Lichen	*Peltigera* sp.	< 1%

* visual estimation of the volumic proportion of each species
** no species identification possible without spores
*** some uncertainty in the species identification

Table 4.5. All ages produced by this study, presented with the related characteristics from the field sites and the results from the laboratory analysis. Simplified generic ages rounded to the closest 0.1 ka BP plus and minus a centennial error are given in the last column and will be used further in the text.

Site	Field ID	Sampling year	Latitude N.	Longitude E.	Elevation (m a.s.l.)	Distance to ice margin (m)	Ice cover thickness (m)	Species	Quality Index	Lab ID	^{14}C age	$\pm 1\sigma$ (y)	δ^{13}‰	Median calibrated age BP 2σ	Error + 2σ (y)	Error - 2σ (y)	Lower cal. age BP 2σ	Upper cal. age BP 2σ	Generic age (cal. ka BP)
Bassen	B20-M2	2020	78.22055	16.04775	890	1	-	*Andreaea blyttii*	1	BE-14410.1.1	2188	21	-24.2	2241	67	121	2120	2308	2.2±0.1
	B20-M3	2020	78.22085	16.050867	894	1.5	-	*Andreaea obovata*	1	BE-14411.1.1	2234	23	-24.7	2224	109	71	2153	2333	2.2±0.1
	B20-M4	2020	78.2209	16.05064	894	5.5	-	*Andreaea obovata*	1	BE-14412.1.1	2224	35	-27	2228	108	100	2128	2336	2.2±0.1
	B20-M5	2020	78.22095	16.043383	883	110	-	*Andreaea obovata*	1	BE-14413.1.1	1552	34	-26.6	1442	79	79	1363	1521	1.4±0.1
Frostisen	FR20-M1	2020	78.524306	15.725472	558	0	0.05	*Tomentypnum nitens*	1	BE-14414.1.1	1613	21	-23.6	1478	57	66	1412	1535	1.5±0.1
	FR20-M2	2020	78.526556	15.713306	545	0	0.5	*Orthothecium chryseon*	1	BE-14415.1.1	1243	21	-25.4	1193	77	120	1073	1270	1.2±0.1
	FR20-M3	2020	78.52644	15.71211	544	0	0.5	*Tomentypnum nitens*	1	BE-14416.1.1	1392	21	-27.1	1302	42	17	1285	1344	1.3±0.1
	FR20-M5a	2020	78.526472	15.712417	543	-3	2	*Tomentypnum nitens*	2	BE-14417.1.1	1528	34	-27.9	1399	118	82	1317	1517	1.4±0.1
	FR20-M5b	2020	78.526472	15.712417	543	-3	2	*Tomentypnum nitens*	1	BE-14418.1.1	1272	21	-21.8	1227	54	73	1154	1281	1.2±0.1
	FR20-M5c	2020	78.526472	15.712417	543	-3	2	*Tomentypnum nitens*	1	BE-14419.1.1	1295	21	-23.4	1224	62	48	1176	1286	1.2±0.1
	FR20-M5d	2020	78.526472	15.712417	543	-3	2	*Tomentypnum nitens*	1	BE-14420.1.1	1302	21	-25.5	1224	64	47	1177	1288	1.2±0.1
	FR20-M5e	2020	78.526472	15.712417	543	-3	2	*Tomentypnum nitens*	1	BE-14421.1.1	1328	21	-28.3	1270	26	93	1177	1296	1.3±0.1
	FR20-M5avg	2020	78.526472	15.712417	543	-3	2	*Tomentypnum nitens*	1	BE-14418-21	1299	21	-	1224	63	48	1176	1287	1.2±0.1
Foxfonna	FX20-M1	2020	78.13362	16.20745	789	1.5	-	*Pohlia sp.*	1	BE-14916.1.1	1620	25	-25.7	1480	59	68	1412	1539	1.5±0.1
	FX19-M1	2019	78.12963	16.21327	758	1	-	*Pohlia sp.*	1	BE-15300.1.1	1620	37	-27,8	1482	89	81	1401	1571	1.5±0.1
	FX19-M2	2019	78.13403	16.2068	788	1	-	*Pohlia obtusifolia.*	1	BE-15301.1.1	1575	25	-28,5	1463	62	68	1395	1525	1.5±0.1

The three samples collected at the ice margin on the north-west side of Bassen gave statistically indistinguishable calibrated ages of 2.2 ± 0.1 ka BP. The sample collected away from the ice margin was dated to be approximately 800 years younger than the vegetation collected at the ice margin and has a calibrated age of 1.4 ± 0.1 ka BP. The three samples collected on the east margin of Foxfonna, similarly to the sample from Bassen's ice margin, are statistically indistinguishable and fall well within each other's error margins, at 1.5 ± 0.1 cal. ka BP. The ages obtained from Frostisen South Basin show more variations than the ones from Bassen and Foxfonna. The age of the vegetation collected at the east margin of the basin is of 1.5 ± 0.1 cal. ka BP. The three ages originating from vegetation collected in the melt water channel at the north margin were found to be 1.2 ± 0.1, 1.3 ± 0.1 and 1.2 ± 0.1 cal. ka BP.

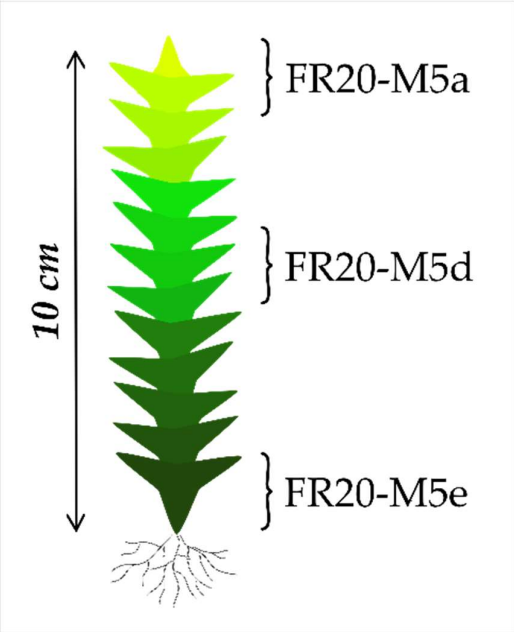

Figure 4.12. Relative position of the a, d and e radiocarbon dates replicates along the moss stems for sample FR20-M5. Replica b and c were taken, similarly to replicate a, on the apical part of stems from two other moss patches.

4.4 Database

A total of 95 radiocarbon dates, originating from 6 studies, are gathered in the VEGLAS database, including 16 dates contributed by this study (Table 4.6). Among the collected dates, 56 were given a quality index (QI) of 1, and 44 of these QI 1 dates correspond to vegetation killed by direct ice advance (Tables 4.5 and 4.6) and were used for the data interpretation. 23 of the dates correspond to vegetation buried not directly under glacial ice, but under glacial sediments such as till and moraine. The spatial distribution of the dates across Svalbard is unequal. All the dates originate from Spitsbergen, with the highest concentration in Central Spitsbergen (Figure 4.14).

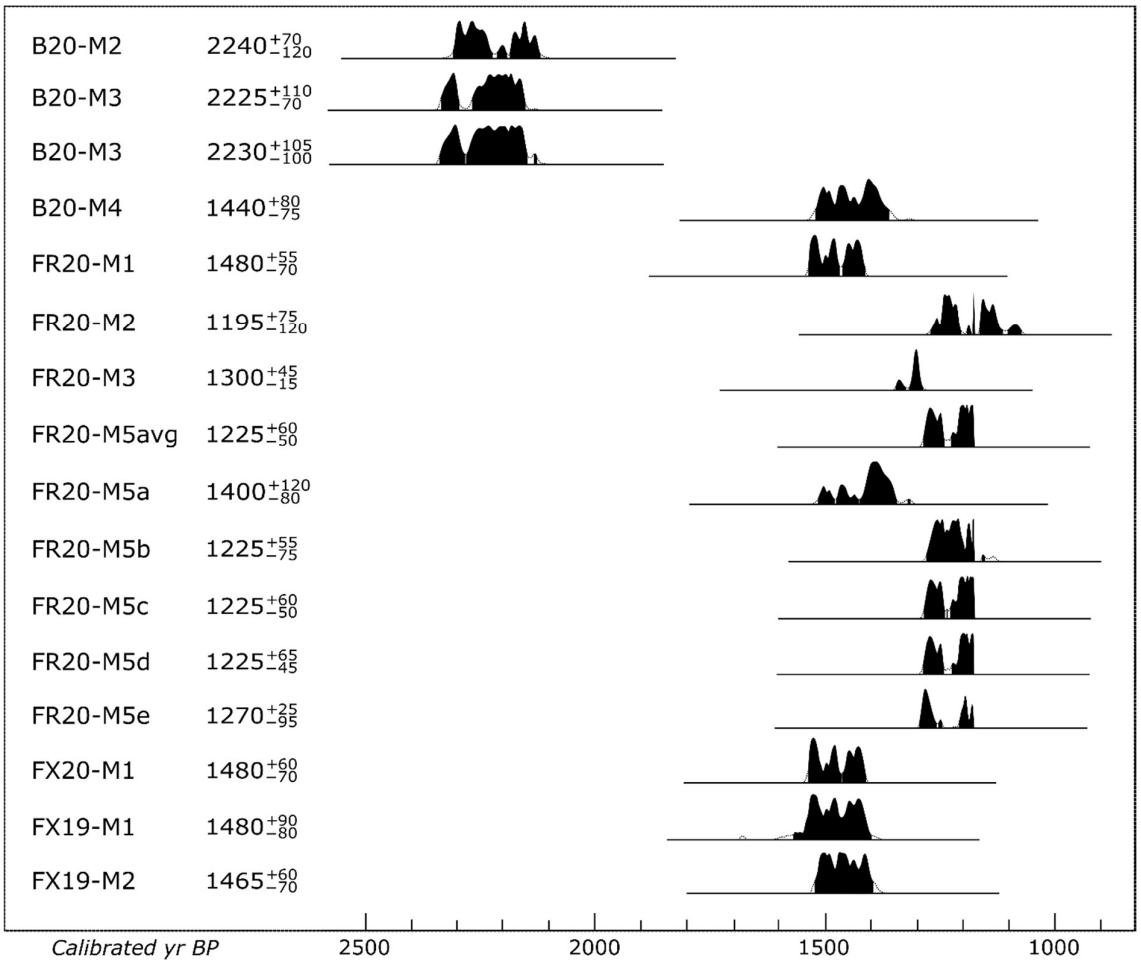

Figure 3.13. Probability distribution of the calibrated radiocarbon ages with the 95.4% (2σ) probability range highlighted in black. All calibrations were performed by Calib 8.4 (Stuiver and Reimer, 1993), using the Intcal20 calibration curve (Reimer et al., 2020).

Table 4.6. Ages from the VEGLAS database that are related to direct ice advance and were given a quality index of 1. When the GPS positions and the distances from the ice margins given by Miller et al., 2017 were inconsistent, estimations of real distances from the ice margins were established based on the GPS positions and added into bracket besides the distances given in the source paper (extract from the VEGLAS database, found at: https://www.dropbox.com/scl/fi/ueor4u1qk9kc8txaydpc2/VEGLAS-database.xlsx?dl=0&rlkey=ffop6yxs1u7r9hsdhjmwycpts).

VEGLAS database ID	Field ID	Sampling year	Geographic area	Latitude N.	Longitude E.	Elevation (m a.s.l.)	Distance to ice margin (m)	Ice cover thickness (m)	Species	Lab ID	^{14}C age	±1σ (y)	δ^{13}‰	Median callibrated age BP 2σ	Error +2σ	Error -2σ	Lower cal age BP 2σ	Upper cal age BP 2σ	Generic age (ka BP)	Publication
B76-01	-	1973	South Spitsbergen	77.07980	15.20945	25	450	-	Rhacomitrium lanuginosum-60% - Dicranum-20%	Gd-264	760	145	-	713	243	200	513	956	0.7±0.2	Baranowski and Karlen, 1976
H05-09	-	2002	Adventdalen	78.17629	15.48215	450	c. -2000	30-35	Racomitrium ericoides	Ua-16652	1355	65	-25.2	1269	109	146	1123	1378	1.3±0.1	Humlum et al., 2005
H05-10	-	2002	Adventdalen	78.17629	15.48215	450	c. -2000	30-35	Bryum pseudotriquetrum	Ua-16653	1350	45	-25.7	1273	71	97	1176	1344	1.3±0.1	Humlum et al., 2005
H05-11	-	2002	Adventdalen	78.17629	15.48215	450	c. -2000	30-35	Pogonatum urnigerum	Ua-16651	1310	45	-25.5	1230	73	104	1126	1303	1.2±0.1	Humlum et al., 2005
M17-12	NC13-S018	2013	East Spitsbergen	78.29433	18.75873	375	0	-	-	NSRL-25290	415	15	25.5	494	14	23	471	508	0.5±0.1	Miller et al., 2017
M17-13	NC13-S019	2013	East Spitsbergen	78.29425	18.76063	373	0	-	-	NSRL-24210	825	20	29.4	717	54	34	683	771	0.7±0.1	Miller et al., 2017
M17-14	NC13-S021	2013	East Spitsbergen	78.22818	18.69335	379	0.15	-	-	NSRL-24211	850	20	29.4	748	39	56	692	787	0.7±0.1	Miller et al., 2017
M17-15	NC13-S022	2013	East Spitsbergen	78.22851	18.68557	382	0.2	-	-	NSRL-25291	480	20	24.1	518	15	16	502	533	0.5±0.1	Miller et al., 2017
M17-16	NC13-S023	2013	East Spitsbergen	78.22919	18.68466	384	0.2	-	-	NSRL-24754	670	20	24	643	27	81	562	670	0.6±0.1	Miller et al., 2017
M17-17	NC13-S024	2013	Inner Van Mijen	77.85670	16.98846	683	2	-	-	NSRL-24755	3250	20	21.1	3459	89	63	3396	3548	3.5±0.1	Miller et al., 2017
M17-18	NC13-S025	2013	Inner Van Mijen	77.85793	16.98110	673	0.1	-	-	NSRL-24212	3490	20	24.5	3762	70	67	3695	3832	3.8±0.1	Miller et al., 2017
M17-19	NC13-S026	2013	Inner Van Mijen	77.87421	16.95621	687	0	-	-	NSRL-24756	3260	20	24.6	3467	91	64	3403	3558	3.5±0.1	Miller et al., 2017
M17-22	NC13-S034	2013	Adventdalen	78.11213	16.25720	722	4	-	-	NSRL-24216	3585	20	27.4	3885	84	51	3834	3969	3.9±0.1	Miller et al., 2017
M17-23	NC13-S035	2013	Adventdalen	78.11214	16.25690	723	5	-	-	NSRL-24758	3655	20	22.5	3976	106	78	3898	4082	4.0±0.1	Miller et al., 2017
M17-25	NC13-S038	2013	Dickson Land	78.61701	16.19219	546	3	-	-	NSRL-25294	590	20	23.9	606	37	62	544	643	0.6±0.1	Miller et al., 2017
M17-26	NC13-S039	2013	Dickson Land	78.61749	16.19201	542	3	-	-	NSRL-25295	665	15	23	590	77	27	563	667	0.6±0.1	Miller et al., 2017
M17-27	NC13-S040	2013	Dickson Land	78.61750	16.19195	543	1	-	-	NSRL-24196	460	20	28.7	511	15	16	495	526	0.5±0.1	Miller et al., 2017
M17-28	NC13-S041	2013	Dickson Land	78.61704	16.19211	544	3	-	-	NSRL-24197	450	20	32	507	18	15	492	525	0.5±0.1	Miller et al., 2017
M17-29	NC13-S042	2013	Dickson Land	78.61747	16.19246	547	0.4	-	-	NSRL-25296	545	15	29.2	543	80	17	526	623	0.5±0.1	Miller et al., 2017
M17-30	NC13-S043	2013	Dickson Land	78.60451	16.00268	630	0.1	-	-	NSRL-25297	1295	15	23.9	1217	67	40	1177	1284	1.2±0.1	Miller et al., 2017
M17-31	NC13-S044	2013	Dickson Land	78.60452	16.00275	631	0.1	-	-	NSRL-24198	1230	20	27.1	1146	112	76	1070	1258	1.1±0.1	Miller et al., 2017
M17-33	NC13-S046	2013	Dickson Land	78.60549	16.00107	639	115	-	-	NSRL-24740	910	20	22.6	834	73	97	737	907	0.8±0.1	Miller et al., 2017
M17-34	NC13-S047	2013	Dickson Land	78.60509	16.00205	633	65	-	-	NSRL-24741	955	20	26	848	71	55	793	919	0.8±0.1	Miller et al., 2017
M17-35	NC13-S048	2013	Dickson Land	78.60481	16.00258	631	30	-	-	NSRL-24742	1295	20	23.9	1224	62	48	1176	1286	1.2±0.1	Miller et al., 2017
M17-36	NC13-S049	2013	Dickson Land	78.60269	16.12105	682	0.5	-	-	NSRL-24743	1745	20	23.4	1637	68	65	1572	1705	1.6±0.1	Miller et al., 2017
M17-37	NC13-S050	2013	Dickson Land	78.60280	16.12119	684	0.5	-	-	NSRL-24200	1605	20	28.7	1474	58	62	1412	1532	1.5±0.1	Miller et al., 2017
M17-38	NC13-S051	2013	Dickson Land	78.60270	16.12342	687	900 (25)	-	-	NSRL-25298	1605	15	25.7	1475	56	62	1413	1531	1.5±0.1	Miller et al., 2017
M17-39	NC13-S052	2013	Dickson Land	78.60118	16.12338	688	120 (70)	-	-	NSRL-24201	660	20	27	590	76	29	561	666	0.6±0.1	Miller et al., 2017
M17-40	NC13-S054	2013	Dickson Land	78.62405	15.82580	589	479 (1)	-	-	NSRL-24202	1565	20	25.9	1461	56	72	1389	1517	1.5±0.1	Miller et al., 2017
M17-41	NC13-S055	2013	Dickson Land	78.62429	15.82422	600	482 (20)	-	-	NSRL-24744	1580	20	25.3	1466	56	62	1404	1522	1.5±0.1	Miller et al., 2017
M17-42	NC13-S057	2013	Dickson Land	78.62460	15.82184	613	491 (80)	-	-	NSRL-24745	1735	20	23	1622	79	74	1548	1701	1.6±0.1	Miller et al., 2017
M17-43	NC13-S058	2013	Dickson Land	78.62434	15.81826	623	510 (170)	-	-	NSRL-24746	1325	20	25.5	1267	28	90	1177	1295	1.3±0.1	Miller et al., 2017
M17-44	NC13-S059	2013	Dickson Land	78.62613	15.81750	640	502 (1)	-	-	NSRL-24747	1240	20	27.1	1161	106	88	1073	1267	1.2±0.1	Miller et al., 2017

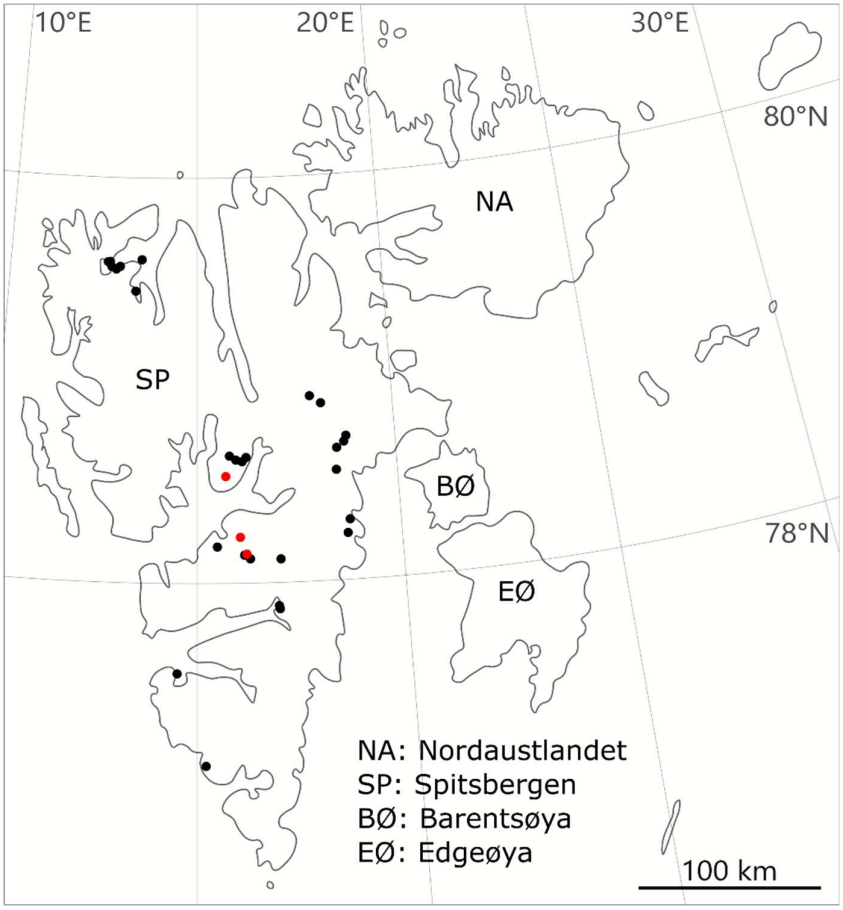

Figure 4.14. Spatial distribution of the ages gathered in the VEGLAS database. The sites from this study are marked in red.

5 Discussion

5.1 Radiocarbon ages from this study

5.1.1 Bassen

B20-M3 and B20-M4 were taken along the same line perpendicular to the ice margin, 4 m apart (M3 was taken 1.5 and M4 5.5 m from the ice margin). The objective of this sampling was to explore whether we would observe an age gradient over such short distances from the ice margin. However, the calibrated ages are within error margins of each other at 2.2 ± 0.1 ka BP (Figure 4.2, 4.13 and Table 4.5) and are therefore not significantly different. Thus, no age/distance relationship could be established at such a small scale, but B20-M5, taken 110 m away from the ice margin on the same transect as B20-M2 (Figure 4.2), is approximately 800 years younger than the three other samples taken at the ice margin. Hence, samples should be spaced by tens of meters and not just a few meters if an age transect is to be established. If ice growth rates were continuous over these 800 years, between 2.2 and 1.4 ka BP, the ice cap would have been advancing approximately 15 cm yr^{-1}. However, it is unlikely that this has been the case as the transition between the Roman Warm Period and the Dark Ages Cold Period occurs during this time period. This suggests along one ice margin. However, it is still recommended that only the apical part of the moss stems is dated as a single stem can grow over several hundreds and even thousands of years as shown by Baranowski and Karlén (1976) and Roads et al. (2014).

It is strongly recommended not to radiocarbon date samples that are still coated by shale particles after lab cleaning as part of the "dead" or ^{14}C depleted organic carbon contained in the shale has the potential to contaminate the sample during the carbon extraction process necessary for the dating, this resulting in an overestimation of the age of the sample (Aitken, 2014). This recommendation extends to particles originating from all types of organic carbon rich bedrock.

5.2 Temporal and spatial snow line descent in Svalbard

5.2.1 The problem of Miller at al. (2017)

47 % of the dates gathered in the VEGLAS database originate from Miller et al. (2017). However, the reliability of these dates is very questionable. Indeed, there are several incoherent data points presented in the paper and the given justifications for their inconsistent results are judged not

to hold up. Therefore, these apparent incoherent data points required reinterpretation in light of available geospatial evidence.

5.2.1.1 GPS coordinates and distances from the ice margins

When plotted into ArcMap, some of the GPS coordinates from Miller et al. (2017) were found not to match the reported distances from the ice margin at which the samples were collected. For five sample sites from Njordfjellet and two others from South Jotunfonna, there appeared to be a several hundred-meter offset between the reported distances and those obtained by plotting the coordinates. As it was reported by Miller et al. (2017) that in some areas partially refrozen snow prevented them from securely identify the glacier margin and seeing that the GPS positions plotted in ArcMap fit the terrain very well and seem a lot more realistic than the very long distances from the ice margins indicated, it was chosen to trust the GPS coordinates over the given distances from the ice margin. These distances were approximately remeasured according to the ice margin position observed from satellite imagery from 2011 and the local yearly retreat rates calculated for the 2011-2020 period (sampling year by Miller in 2013). However, as these estimated distances are based on assumptions, they are only given as indications and cannot be considered reliable. These new distances are presented in Table 4.6 into brackets next to the published ones (M17-38 to M17-44).

5.2.1.2 Method issues

No specific methods for sample collection are described in Miller et al. (2017), a simple reference to Miller et al. (2013) is made, stating that the methods followed are described in detail in that previous publication. However, if the methods presented by Miller et al. (2013) are precise and address various error sources, some important specifications were apparently not followed during sample collection for Miller et al. 2017 (M17).

While the given method specifies that samples should be taken within the year's retreat area of the ice in order to prevent modern carbon contamination by colonisation or regrowth, 29 % of the samples from Miller et al. (2017) were collected more than 25 m away from the ice. Once the given distances from the ice margin are corrected as explained in the previous section, there is still a remaining 22 % of samples that were collected over 25 m from the ice margins. Another important method point emphasized by Miller et al. (2013) is that multiple collections (at least two) should be made at each sample site, in order to make sure that the obtained dates are consistent with each other and can be relied on. However, at 30 % of the sites where Miller et al. (2017) has been sampling, only a single sample was dated.

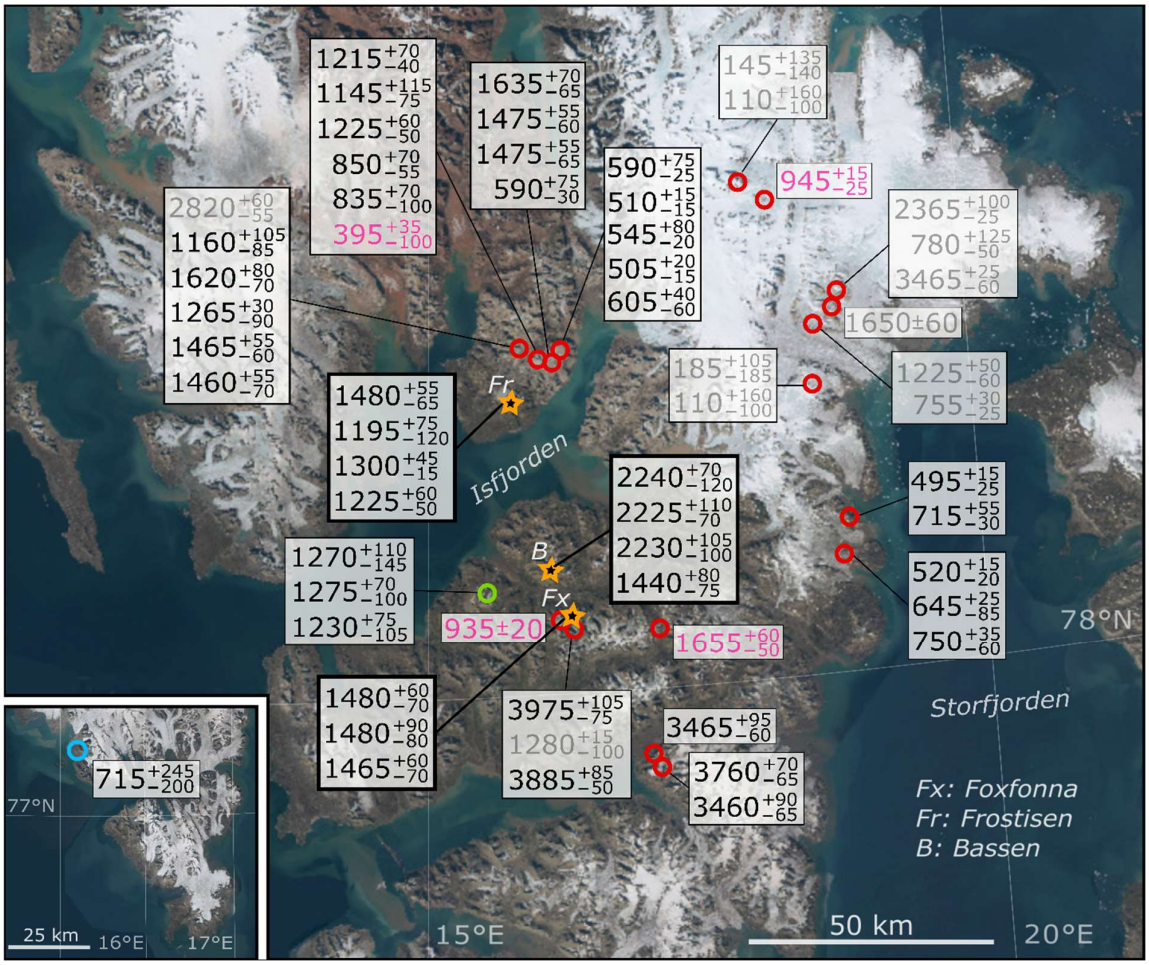

Figure 5.1. Satellite image of central Spitsbergen with recalibrated moss burial ages (cal. yrs BP) from previous studies, marked with green circle for Humlum et al., 2005, blue circle for Baranowski and Karlén, 1978 and red circles for Miller et al., 2017 and from this study, marked with yellow stars. Ages marked in black have a quality index (QI) of 1, ages in pink have a QI of 2 and ages in grey have a QI of 3 (QI 1 being the highest quality). *Base image modified from toposvalbard.no.*

5.2.1.3 Discordant ages

At two sites (Ordonnansbreen and Foxbreen), three samples were collected within a few meters distance from each other and the ages obtained after radiocarbon dating are markedly discordant. The obtained ages are 0.8 ± 0.1, 2.4 ± 0.1 and 3.5 ± 0.1 cal. ka BP for Ordonnansbreen, and 1.3 ± 0.1, 3.9 ± 0.1 and 4.0 ± 0.1 cal. ka BP for Foxbreen, which in both cases corresponds to an age difference of 2.7 ka between the youngest and oldest dates for samples collected less than 5 m apart. Similar age discrepancies are found at two other sites, Lykkebreen and Njordfjellet with respectively 0.5 ka and 1.2 ka of age difference between the youngest and oldest dates (Figure 5.1). Such large age differences within small sampling areas are surprising, in comparison with the indistinguishable ages obtained in this study between samples collected 600 m apart at Foxfonna and 80 m apart at Bassen.

Furthermore, Miller et al. (2013) show that age replicates from samples taken up to 200 m apart along ice margins on Baffin Island also give ages that are indistinguishable from each other once calibrated; a finding in line with the results from this current study.

According to Miller et al. (2017), the millennial-scale age differences obtained from a sampling site should be caused by successive advances and retreat of the ice margin - burying, exposing, and subsequently reburying the moss (Figure 5.2). However, based upon in-field observations on Bassen (this study), it is considered unlikely that mosses can be re-exposed for a sufficient period of time for other mosses to develop next to them but without suffering from harsh arctic weathering and erosion, decomposition and degradation of any sort, colonisation by other plants, bacteria or fungi and regrowth. Furthermore, based on observations from Svalbard (this study) it appears that the likelihood of precisely sampling three mosses that had been living for several thousands of years, dying, and then being preserved without suffering from any kind of alteration, recolonization, or regeneration is extremely low. This is borne out by the findings of contamination (this study) on B20-M5 by other moss species and fungi after a maximum 50 years of exposure. This specially when considering that Bassen is the highest lying ice cap that has been sampled in Svalbard at 900 m a.s.l., and the plateau surrounding the ice cap is not a life-welcoming environment with no presence of soil, cold temperatures and strong winds. Hence, it can be expected that at lower elevation and with milder temperatures, the contamination would happen even more rapidly. Moreover, Miller et al. (2013) repeatedly emphasises that the ages can only be relied on if it is assumed that the plant has continuously been covered by ice since its burial and all of their conclusions rely on this continuous ice cover component.

Based on direct observations from new ages from Svalbard (this study) and associated contamination issues, a simpler explanation of post-exposure colonization and/or regrowth resulting in younger ages or organic carbon-rich sediment contamination resulting in older ages is preferred over the complex model of burial, exposure, re-burial, and re-exposure by Miller et al. (2017). It is more probable that the oldest ages are more reliable as contamination by modern carbon (colonisation, regrowth) is more likely to happen than contamination by old/dead carbon (organic rich bedrock) as the bedrock at all sites where discordant ages are reported is mainly composed of sandstones and siliceous sediments (Dallmann, 2015). This supports the assumption that there was likely no bedrock contamination. Nevertheless, to maintain the rigour of the dataset, all discordant ages were discarded and given a quality index of 3 in the database with the exception of the two

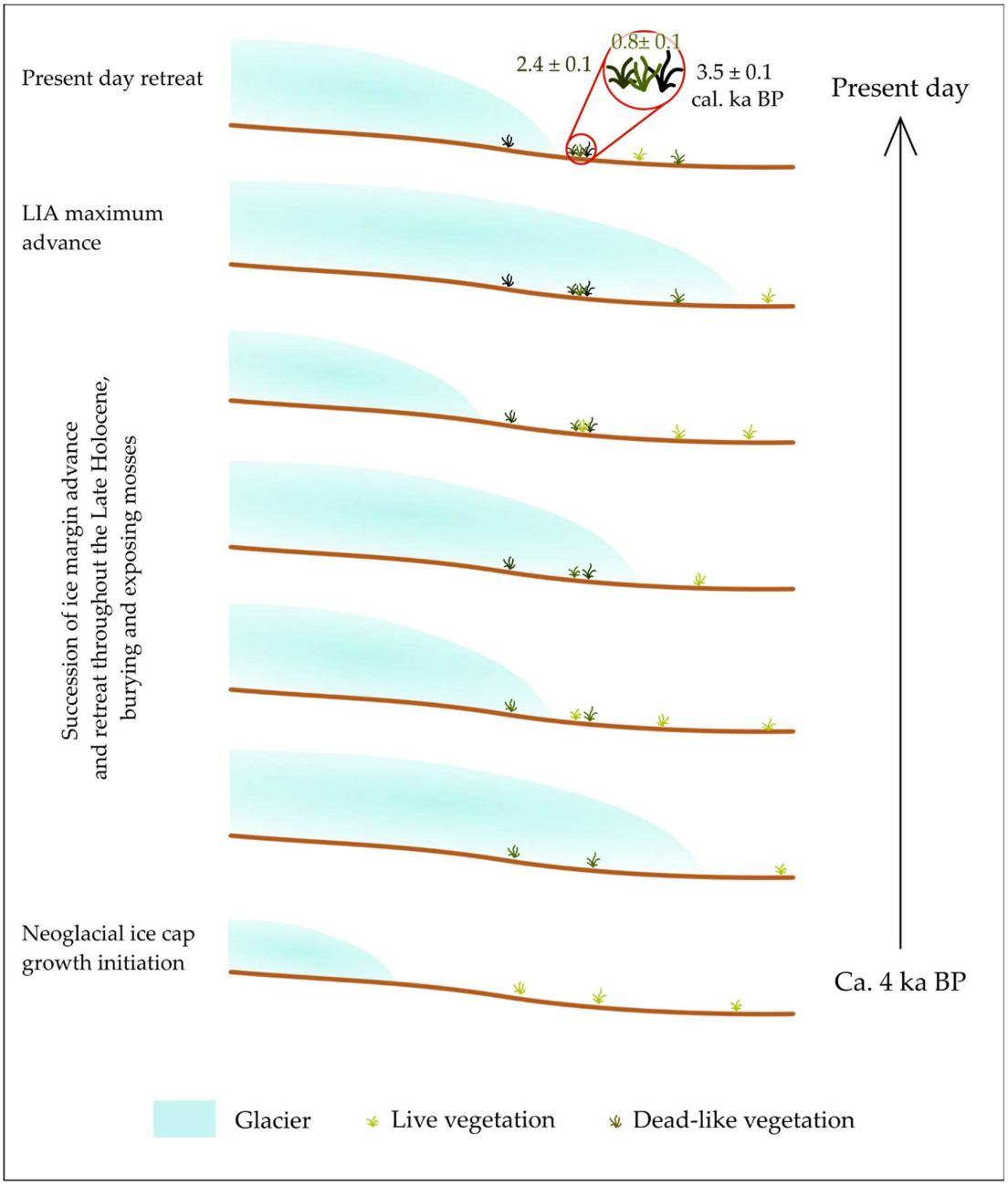

Figure 5.2. Schematic illustration of the explanation given by Miller et al. (2017) to justify the great inconsistency of some of their radiocarbon age. Example of their three median calibrated ages from Ordonnansbreen in East Spitsbergen, coming from moss patches sampled a few meters apart from each other, where they propose that ice buried moss patches can be re-exposed for an extensive amount of time after ice margin retreat and before being re-buried by later ice advance without suffering in any way from either recolonization and regrowth or harsh arctic weathering and soil erosion.

concordant older ages from Foxbreen (4.0 ± 0.1 and 3.9 ± 0.1 cal. ka BP), where only the much younger age (1.3 ± 0.1 cal. ka BP) was disregarded.

Based on the recommendations from Miller et al. (2013) and the demonstrated inconsistency of age replicates from other sites, the ages for sites where only one sample was dated were discarded and given a quality index of 2 in the database with the exception of the date from Snøvola (3.5 ± 0.1 cal. ka BP) as it is consistent with the two ages from Bjartfonna (3.5 ± 0.1 and 3.8 ± 0.1 cal. ka BP), located two kilometres further south in inner van Mijenfjorden at similar elevation.

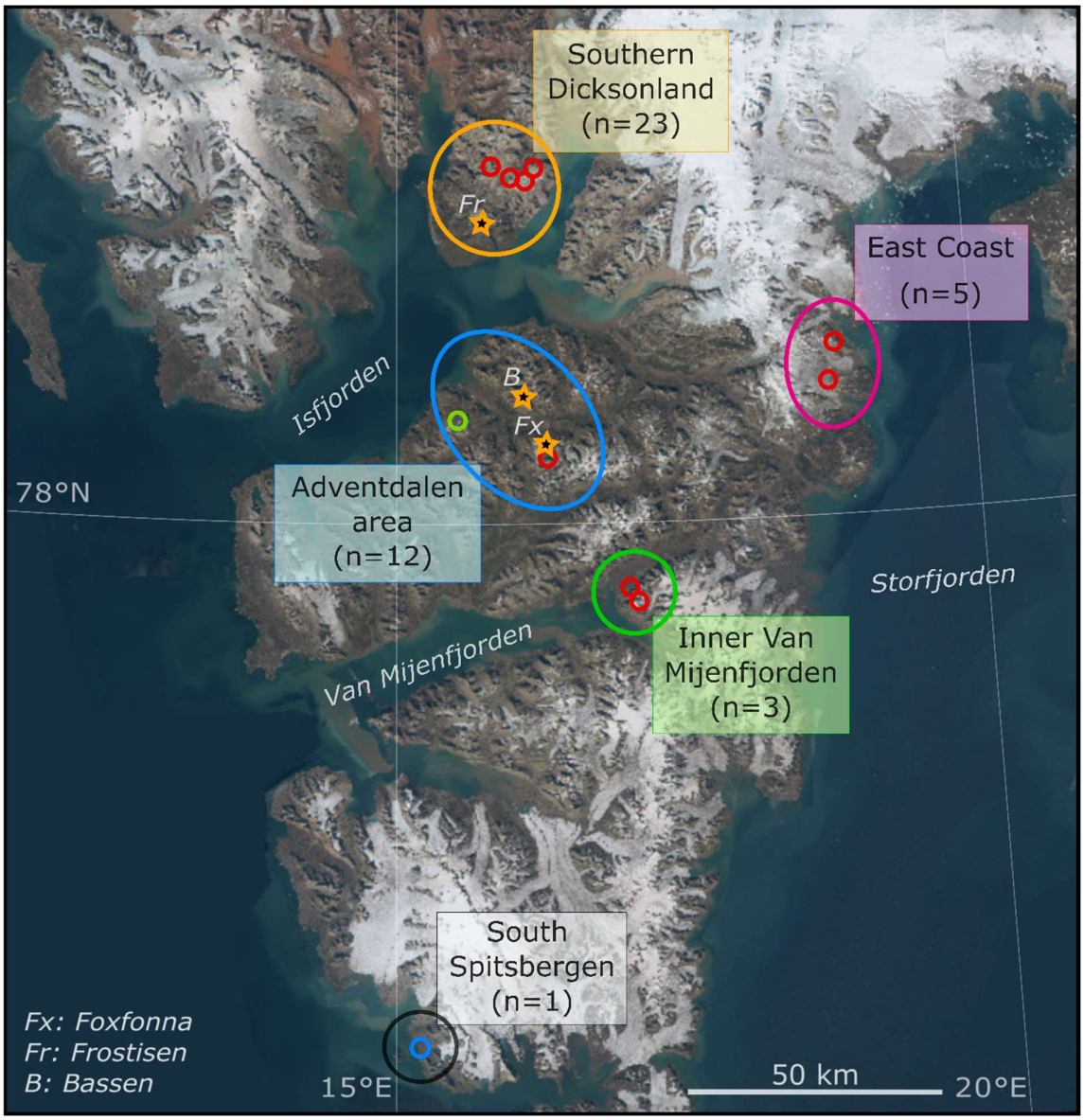

Figure 5.3. Spatial definition of the five geographic regions in which the dates of quality index 1 (QI 1) have been divided. Base image modified from toposvalbard.no.

5.2.2 General glacial advance phases

The 44 QI 1 ages related to direct ice advance were divided into five distinct geographic areas (Figure 5.3) with the highest data concentration in Southern Dickson Land with 23 dates and in Adventdalen Area with 12 dates. Two major ice advance phases can be recognised during the past 1.6 ka (Figure 5.4), a first one between 1640 and 1150 BP and a second one between 850 and 500 BP (median calibrated ages). While this first advance phase seems to match well the Dark Ages Cold Period (DACP) timing as defined by Helama et al. (2017) from 1650 to 1185 BP (Figure 5.5), the second phase predates by 300 years the global timing for the Little Ice Age (LIA) that was defined to occur between

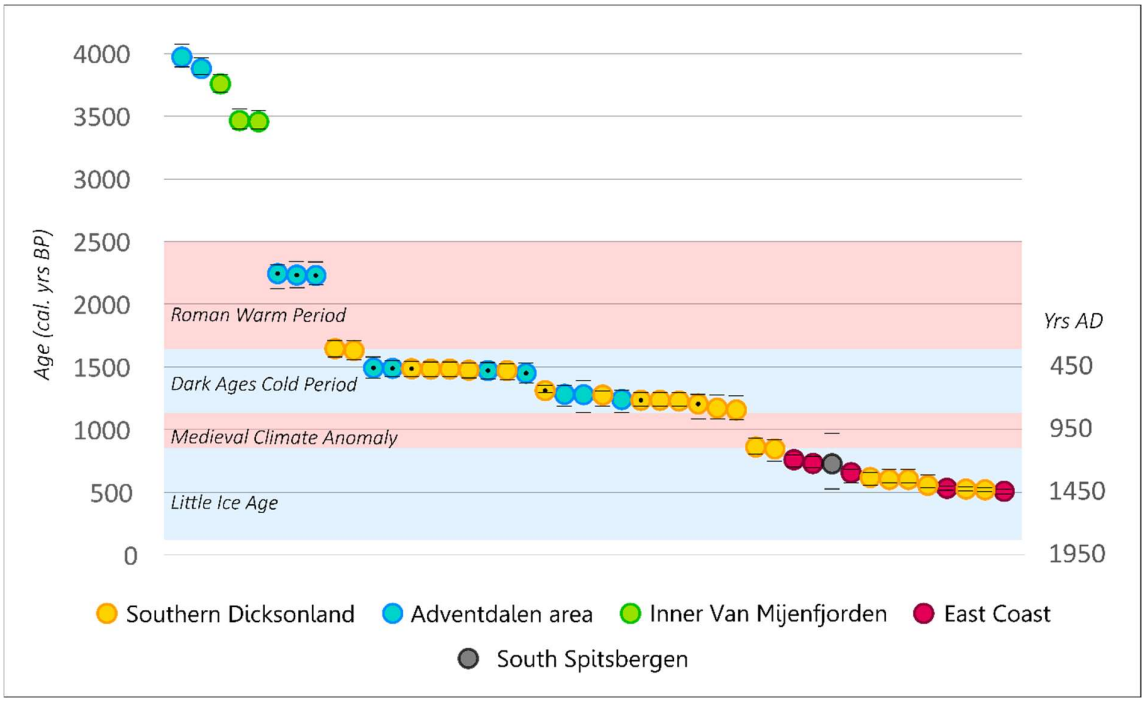

Figure 5.4. All the 44 QI 1 dates ranked in order by decreasing ages and marked with colors according to their provenance regions. The 11 dates from this study are marked with a black dot. The warm and cold periods of the Late Holocene in Svalbard as defined by this study (see Figure 26) *are highlighted in red and blue respectively.*

550 and 250 BP in the extratropical North Hemisphere (Mann et al., 2009). However, the timing and nature of the climatic variations connected to the LIA are highly variable from region to region, and the notion of it happening as a globally synchronous cold period has long been dismissed (Bradley and Jonest, 1993; Mann et al., 1999). An earlier onset of the LIA in the regions surrounding the North Atlantic than in the Alps where the climatic event was first studied has been inferred for several decades (Grove, 2001) yet, no timing for the initiation of the LIA in Svalbard has been proposed. The definition of the LIA is complex and unclear and can differ greatly according to the source. The term

has been used to describe both a climatic and a glaciological concept (Matthews and Briffa, 2005). Based on the results from this study and considering the LIA as being the most recent phase of glaciation that occurred during the Neoglacial, it is inferred that the LIA initiated around 850 BP in Svalbard (Figure 5.5), *id est* in the early twelfth century of the common era (CE), which would be the earliest onset reported in the literature (e.g., Grove, 2001; Matthews and Briffa, 2005; Miles et al., 2020).

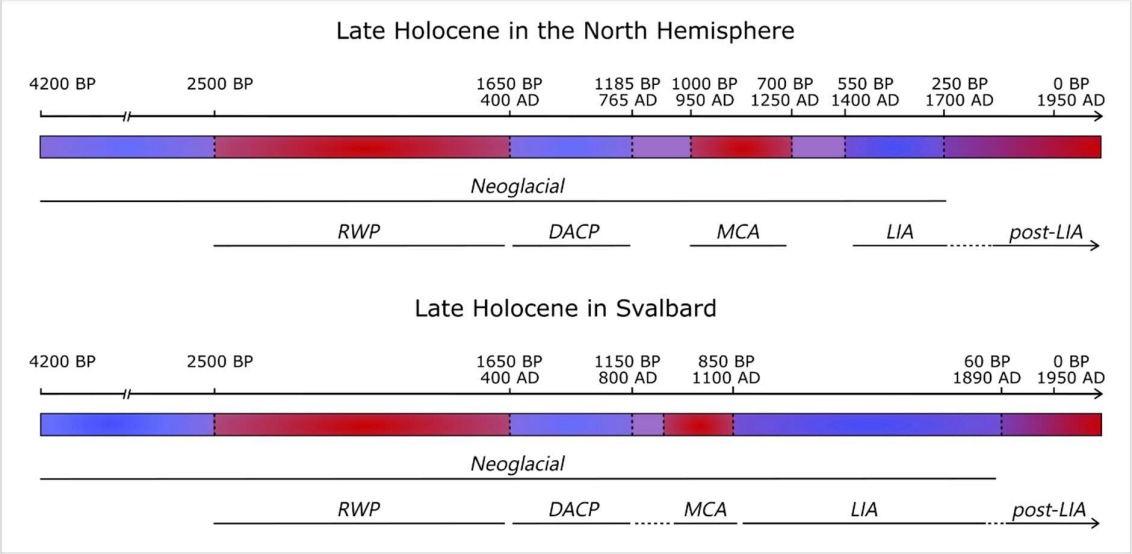

Figure 5.5. ***Late Holocene timeline****. RWP: Roman Warm Period; DACP: Dark Ages Cold Period; MCA: Medieval Climate Anomaly; LIA: Little Ice Age. Timing of the Late Holocene sub-epoch boundaries according to Walker et al., 2018, for the equivalent official Meghalayan sub-epoch.* ***North Hemisphere time boundaries****: timing of the RWP according to Wang et al., 2012; of the MCA and the LIA according to Mann et al., 2009 and of the DACP according to Helama et al., 2017.* ***Svalbard time boundaries****: timing of the RWP according to Wang et al., 2012; the rest of the time boundaries are inferred by this study's results. The termination of the LIA pre-1900 is inferred from the warming already observed in the early 1900s at the very beginning of Svalbard's historical temperature record (Førland et al., 2011; Nordli et al., 2014).*

The two described phases of ice advance are separated by a 300-year gap in data that corresponds to a phase of either ice still-stand or ice retreat. The second proposition is more realistic as glaciers have been inferred to be going through still-stand phases only during brief periods of climatic change before shifting between advance and retreat phases or vice-versa (Raina, 2013; Rana et al., 2019). This phase of ice retreat is therefore inferred to correspond to the Medieval Climate Anomaly (MCA). However, if the termination of this period can be timed with the initiation of the LIA around 850 BP, the timing of its initiation cannot be as accurately defined. Indeed, retreating ice margins during the MCA will have resulted in the exposure of vegetation buried during the latest ice advance phase of the precursory DACP, causing a loss of the data constraining the timing of the end of

this cold period. Thus, the only thing that can be stated with certainty is that around 1150 BP, ice was still advancing, and that sometimes after 1150 BP, the DACP glaciation phase ended and was succeeded by the MCA.

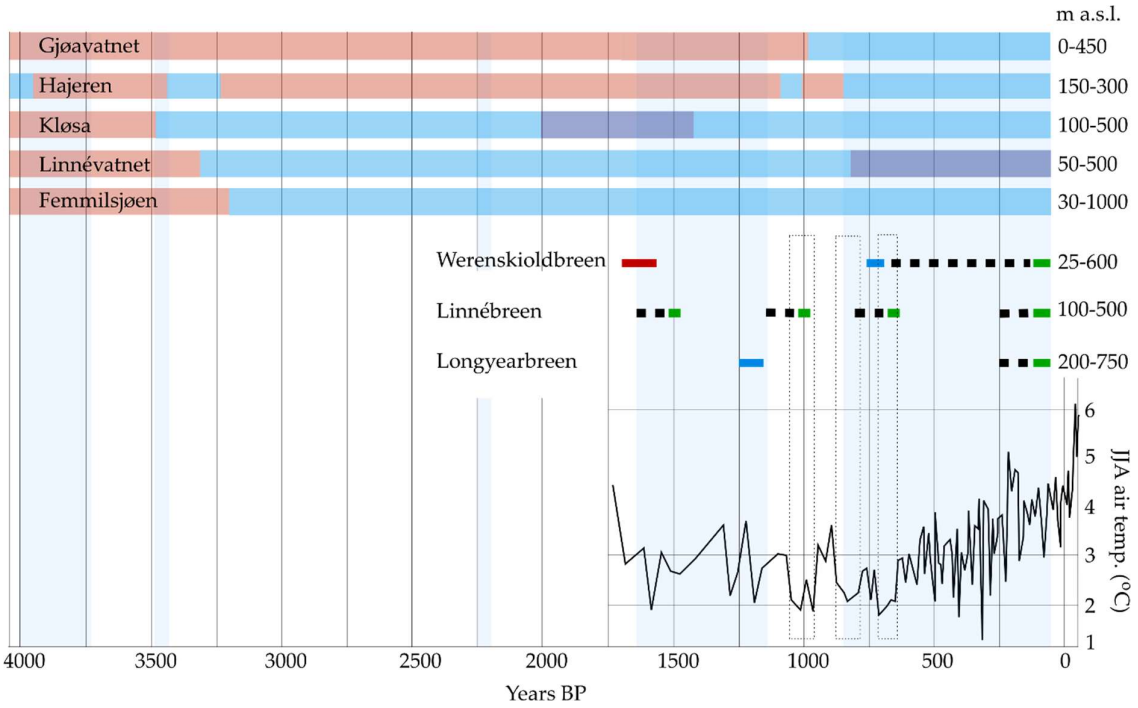

Figure 5.6. ***Comparison of the timing of the DACP and the LIA glacial advances as defined by this study's data (blue shadings) with other records from Svalbard****.* ***Top****: schematic view of Late Holocene glacial activity reconstructed from lake sediments of five proglacial lakes from western Spitsbergen (Gjøavatnet (de Wet et al., 2018), Hajeren (van der Bilt et al., 2016), Kløsa (Røthe et al., 2015), Linnévatnet (Svendsen and Mangerud, 1997) and Femmilsjøen (Allaart et al., 2021)). Blue boxes represent periods of glacial activity (dark blue suggest enhanced glacial activity), red boxes suggest no glacier was present in the catchment or glacial activity was greatly reduced (modified from Farnsworth et al., 2020). The elevation ranges indicated on the right side correspond to the glaciers present in the lakes' catchments (respectively Annabreen, 2 unnamed cirque glaciers, Karlbreen, Linnébreen and Londstaffbreen-Åsgardfonna).* ***Middle****: glacial behaviour of three glaciers (Werenskioldbreen (Baranowski and Karlén, 1976), Linnébreen (Werner, 1993) and Longyearbreen (Humlum et al., 2005)) inferred from buried vegetation, lichenometry and historical observations. Green bars represent moraine stabilization, blue bars represent glacial advance, red bars represent glacial retreat and black dots probable glacial advance inferred from the rest of the data.* ***Bottom****: Air temperature reconstructions from Kongressvatnet for June, July and August (JJA) based on* U^{K}_{37} *(modified from D'Andrea et al., 2012). Dotted rectangles denote intervals of coldest summer temperature during the past 1800 yrs.*

For similar reasons as described above, the timing of the end of the LIA cannot be inferred from this study's data. The last ice advance evidence that corresponds to vegetation buried by ice dates to ca. 500 BP. Notwithstanding, the LIA is known to have continued for several more centuries and have ended sometimes before 50 BP (1900 CE)(Figure 5.5), as inferred by the warming already

observed in the early 1900s at the beginning of Svalbard's historical temperature record (Førland et al., 2011; Nordli et al., 2014), historical observations (e.g., de Geer, 1919), and photographs (e.g., the de Geer Collection, Stockholm University). It is thus assumed that all vegetation buried by ice advance during the four later centuries of the LIA had already been exposed by the ongoing retreat and likely been removed from the landscape by weathering processes or colonised by modern vegetation. An earlier phase of ice advance is marked by five data points that fall between 3.5 ± 0.1 and 4.0 ± 0.1 cal. ka BP. However, five data points over 500 years are not judged enough to properly define and constrain in time this advance phase considering the 1.9 ka data gap separating it from the next advance phase.

This reconstruction of ice advance phases permits comparison with other climate records from Svalbard. Though proxy based climatic records exist for the Early and Mid-Holocene, most of them are inconclusive regarding trends for the Late Holocene (e.g., Kjellman et al., 2020) and therefore cannot be compared with this study's results. When comparing the two above-described advance phases to a proxy-based summer temperature reconstruction for the past 1800 years from a sediment core taken from Kongressvatnet in Western Spitsbergen (D'Andrea et al., 2012) (Figure 5.6), no relation between ice advance and summer temperature can be established. This absence of correlation can be interpreted in two ways. A first option would be that the temperature series from Kongressvatnet is not representative for the rest of Spitsbergen as there is a strong east-west temperature and precipitation gradient across Spitsbergen (Førland et al., 2011). Another explanation would be that the main factor driving glacial advances in Svalbard is not summer temperature as advanced by Miller et al. (2017). Winter precipitations also play an important role in the mass balance of a glacier (Copland, 2011) and an increased amount of snowfall due to a milder and wetter climate as suggested by D'Andrea et al. (2012) could well be the change in climatic conditions behind the two last ice advance phases of the Neoglaciation in Svalbard. A study from Southern Norway showed that the last phase of the LIA advance of glaciers in this area was caused mainly by an increase in winter precipitation (Nesje and Dahl, 2003).

When extending the comparison to three glaciers and five lakes records from which some data is available during the past 4.0 ka (Figure 5.6), the LIA seems to have coincided with widespread glacial advance, at least along the west coast of Spitsbergen, where all of these records but two are originated from. However, the DACP does not seem to have seen as synchronous advances. This might be explained by the fact that the two lakes records that do not show advance during the DACP (Gjøavatnet and Hajeren) are connected to very small low-lying glaciers in north-west Spitsbergen that might need more favourable climatic conditions than the other glaciers to exist.

Once the ages plotted against elevation (Figure 5.7), they appear to be clustering according to their provenance regions, suggesting that there is some geographic and elevation control over the ice advance timing in Spitsbergen with the earliest advances starting at higher elevation and slowly reaching lower and lower elevations as the Neoglacial progresses. These results are not surprising given the elevation-controlled environmental lapse rate. This clear trend of ice growth initiating at high elevation and propagating to lower elevation with time is more or less pronounced whether considering the whole dataset or discarding the earliest advances at around 4 ka BP (Figure 5.7). Miller et al. (2017) have attempted linear regressions to show this time/elevation trend in their data with low correlation coefficients (r = 0.62) following exclusion of the inconvenient data, that was lowering too much the coefficient, as outliers. With reassessing the reliability of many of their ages, the relevance of this attempt at statistical analysis must be considered equivocal, especially when considering that once ice growth has initiated at one elevation, the advance continues at this same elevation while propagating to lower levels.

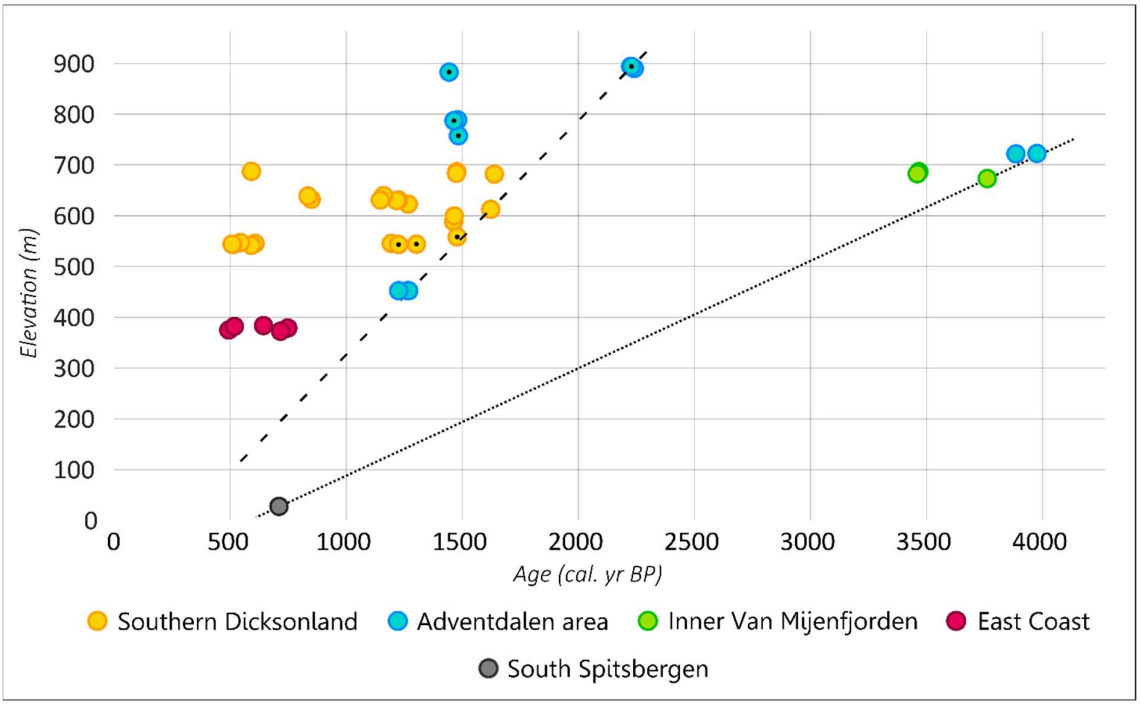

Figure 5.7. QI 1 ages plotted against elevation and color coded according to their provenance regions. The ages from this study are marked with a black dot. The dotted line shows that ice advance started at higher elevation before spreading to lower ground, all ice caps continuing to expand after ice growth initiation. The dashed line shows the same but more pronounced trend when ignoring the oldest age cluster and the lowest elevation point that can appear as an outlier.

5.2.3 Focus on Central Spitsbergen

The Adventdalen Area and Southern Dickson Land regions, located in Central Spitsbergen, represent 80 % of the usable data from VEGLAS. However, the database gathers ages from vegetation that was collected from a few hundreds of meters away from the ice margin and up to two kilometres beneath an active glacier, this making ice extent comparisons with present day ice limits complex. When focussing only on ages from vegetation collected at or very close to the ice margin, a picture of when glaciers last had the same extent as that maximum rates of ice advance could have considerably exceeded the 15 cm yr^{-1} calculated average rate.

5.2.4 Foxfonna

All three dates are very consistent and fall well within each other's error margins at 1.5 ± 0.1 cal. ka BP (Figure 4.7, 4.13 and Table 4.5). However, unlike the work conducted at Bassen and Frostisen, the whole margin of the ice cap was not investigated; the data acquired during field work conducted either in the dark season or beyond the scope of this study. Therefore, further investigation of vegetation that might be present elsewhere along the ice margin could provide more information on the spatial growth patterns of Foxfonna.

5.2.5 Frostisen

FR20-M5 subsamples b to e show very consistent ages and fall well within each other's error margins at 1.2 ± 0.1 cal. ka BP (Figure 4.10, 4.13 and Table 4.5), but FR20-M5a appears to be an outlier, being ca. 175 years older than the four other subsamples. As this sample only was still dirty, the moss stems and leaves coated with a thin layer of micro shale particles, when sent to the lab for dating, it is assumed that during the carbon extraction process, some of the dead carbon from the shale particles contaminated the organic carbon from the moss and by doing so biased the radiocarbon age of the sample, making it appear older than it actually was. For this reason, FR20-M5a was discarded and the average age for FR20-M5 used in the analysis was calculated using the uncalibrated ages of subsamples b to e prior to calibration.

Subsamples b and c, taken respectively in the middle and lower sections of a 10 cm high moss patch, do not show a significant age discrepancy with subsamples d and e that were taken for the apical part of separate moss patches. Thus, it should be possible to date whole stems without causing any age alteration even though it is not recommended as different moss species have various growth rates and individuals from a same species can also have different growth rates according to eg. moisture availability and temperature (Zechmeister, 1995).

The age discrepancy between FR20-M2, M3 and M5avg, which date respectively back to 1.2 ± 0.1, 1.3 ± 0.1 and 1.2 ± 0.1 cal. ka BP and FR20-M1 that is approximately 250 years older (1.5 ± 0.1 cal. ka BP) indicates that the ice advanced following a different spatial pattern compared to its current retreat. This is unlike that observed in the data from Bassen and Foxfonna. Such a difference may be explained by the fact that in the two later cases, the samples are only originating from one side of the ice caps and therefore a wider spread of samples along the whole ice margin might show different trends.

5.2.6 Recommendations for sampling and material selection

If an age transect is to be established, it should be established along an axis perpendicular to the ice margin and samples should be spaced by tens of meters and not just a few meters in order to observe significant potential age variations. The ages obtained from a transect made by Miller et al. (2017, Fig. 8a) show that, in that specific case, significant age differences were obtained when the samples were spaced more than 50 m from each other; however, this minimum distance probably varies from ice cap to ice cap.

The absence of significant age discrepancy between B20-M2, 3 and 4 and the FR20-M5 subsamples coming from moss patches collected within a c. 3x3 m square allows us to conclude that if vegetation is not abundant enough, the moss collection for a single sample can be extended over several square meters without affecting its age. These observations are strongly supported by the results from Miller et al. (2013) who showed that there is no greater age variation within one moss patch than between moss patches collected up to 200 m away from each other at the same elevation they have today can be derived (Figure 5.8). In Central Spitsbergen, vegetation was sampled directly at the margin of eight different ice caps or sub-ice caps (this study and Miller et al., 2017) (Figure 5.8). The corresponding ages from five of these eight ice caps cluster well during the DACP, while the three remaining ones appear to be clear outliers, having last reached a similar size to today 2.3 ka and 0.6 ka before the DACP and 0.5 ka after the DACP. The oldest outlier is the small ice cap located above Foxbreen (and referred to as Foxbreen from this point onwards) which reached a similar size to today around 4.0 ka BP. The nearby Bassen ice cap, which is the only ice cap from the database to have advanced during the so called Roman Warm Period around 2.2 thousand years ago (Figure 5.4 and 5.8) also shows this outlier behaviour, as does the basin of north-east Jotunfonna, being the only ice cap in Central Spitsbergen to have reached a size close to today as late as ca. 500 BP during the LIA.

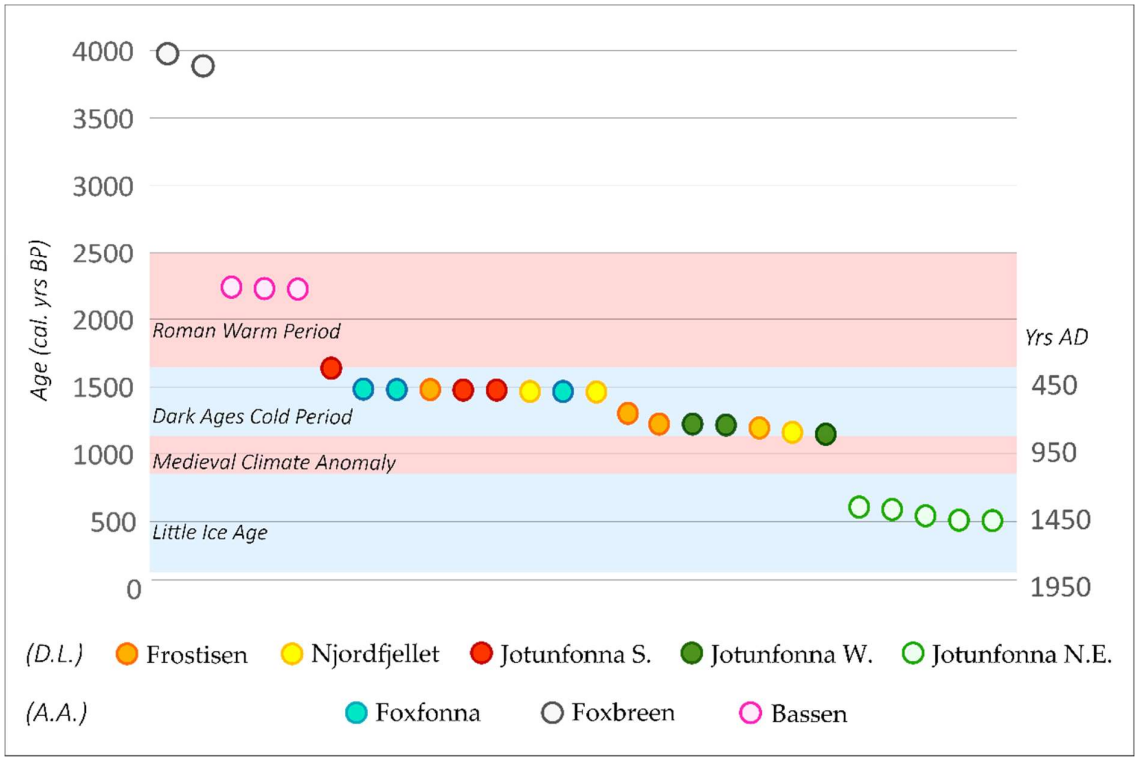

Figure 5.8. *Ages from central Spitsbergen (Dickson Land (D.L.) and Adventdalen Area (A.A.)) from mosses that were collected at or very close to the ice margin, ranked in order by decreasing ages and marked with colors according to their provenance ice cap (n=26). The warm and cold periods of the Late Holocene in Svalbard as defined by this study are highlighted in red and blue respectively. The graph shows when the ice caps previously occupied similar dimensions to today (2013-2020). We observe a cluster during the DACP for five of the eight ice caps, while North-East Jotunfonna, Bassen and Foxbreen appear clearly as outliers.*

The fact that, out of eight ice caps located within a 30 km radius, three clearly did not grow according to the trend set by the five others, indicates that a number of Spitsbergen's ice caps exhibit very individual behaviour and that even within a small dataset, numerous outliers should be expected. These individual behaviours may be related to different snow accumulation processes and local wind patterns as wind reworking is a major factor in local snow distribution patterns (Humlum, 2002; Dadic et al., 2010a, 2010b). However, it is not yet fully understood how these ice caps can have behaved so differently when being so close neighbours (Foxbreen and Foxfonna are only located two kilometres apart and at similar elevation but advanced to their modern position with 2500 years of interval). Close investigations of the ice caps that do not behave according to the general trend, coupling field observations and snow accumulation processes modelling, could shed light on the processes driving these individual behaviours.

The high occurrence of outliers has some important repercussions for the interpretation of data related to vegetation buried by glacial advances in Svalbard and one must be aware of this factor when interpreting results where unexpected complexity may arise. The only solid interpretation that can be made from a data point is that a specific ice margin was advancing over a specific location at a specific time. Generic region-wide conclusions should not be drawn from the data obtained from a single ice cap given their potential for unpredictable individual responses to differing forcing mechanisms. Thus, it is recommended to compare any new data obtained in the future with the data gathered within the VEGLAS database in order to derive a comprehensive overview of ice cap advance timing in Svalbard.

5.2.7 Future perspectives

With the exception of unpredictable outliers, it is not anticipated that any datable vegetation younger than what has already been sampled will be recovered given that vegetation exposed by the retreating ice is relatively quickly removed from the landscape (Miller et al., 2013). However, as the latest recorded advances to modern position are from the East Coast region, sampling at the margin of the low-lying ice caps in this area may bring a new perspective and fill in the data gap in the latest part of the LIA record. Regardless of the interest in trying to find vegetation younger than 550 years old, sampling ice caps in a wider geographical range would increase the understanding of Neoglacial ice advance timing over the archipelago as it is expected to have not been synchronous considering the strong climatic gradient present across Svalbard. As ice margins are receding, older and older vegetation will be exposed by the ice, allowing for a better definition of the ice advance phases that predate the DACP.

While Miller et al. (2017) conclude that no snow line lowering happened between 3.4 and 1.7 ka BP and qualify this conclusion as robust despite the small size of their dataset, only 3 out of the 11 ages obtained during this study fall during this time interval, questioning the alleged robustness of their conclusion. As these three ages correspond to the moss sampled at the margin of only one ice cap - Bassen, they have been shown by this study to be outliers and not match the general ice advance phases displayed by most of the other ice caps in the gathered dataset. However, given the high occurrence of ice caps not behaving according to the general trend in Spitsbergen, it is expected that a more detailed analysis of these outlying data points based on a geographically-expanded dataset in the futures may show response patterns to apparent in the current dataset. The conclusion made by Miller et al. (2017) that no glacier advance happened between 3.4 and 1.7 ka BP, may be challenged, where records from plateau icefields on Baffin Island (Anderson et al., 2008; Miller et al., 2012; Briner

et al., 2014) may not be directly analogous to those on Svalbard where different (and steeper) environmental gradients occur.

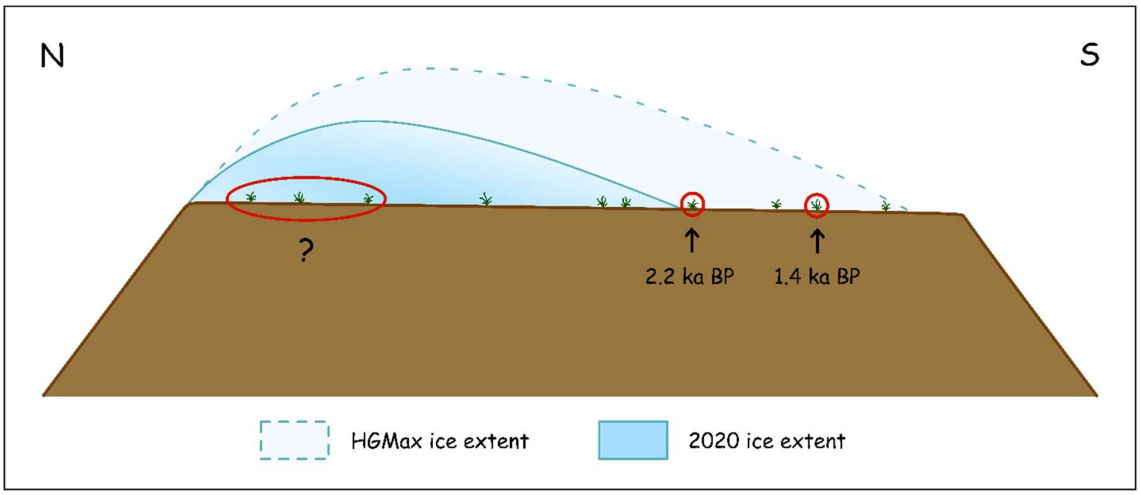

Figure 5.9. Schematic transversal view of the asymmetric Bassen ice cap. The question mark highlights the range of potential locations for the oldest moss buried by the ice cap and the black arrows the relative position of the vegetation sampled in this study. The ice cap extent in 2020 and a reconstitution of its maximal extent during the Neoglaciation (HGMax) are shown in blue.

Can moss dates from retreating cold-based ice margins be used to answer the question of when the Neoglaciation initiated in Svalbard? Currently, it would appear that there is insufficient data to accomplish this. Numerous ice caps across the archipelago have exhibited asymmetric growth patterns and are now retreating following different spatial patterns. This leaves the question of where to find the oldest vegetation buried under the ice open and a likely different answer for each of the ice caps found in Svalbard. When taking the example of Bassen ice cap, which is a simple system, located on an even plateau, and with no outlet glaciers (Figure 5.9), it is not possible to pinpoint from modern observations where the ice cap started to develop and therefore where the oldest vegetation might have been buried by the ice. This may be beneath the top of the existing ice dome but could also possibly be further towards the edge of the plateau where the ice cap or its precursor snow patch is likely to have started to develop. Even if the location of the oldest vegetation under the ice could be determined, the issue of how to access it would remain. Some attempts of coring or drill the ice hoping to find vegetation at the bottom of the drill hole could be made, but besides being strenuous, complicated and onerous, such an approach has a low probability of successful recovery given the very low spatial frequency of observed mosses melting out from the current ice margin of some ice caps (eg. Bassen and Foxfonna). The sole realistic way of accessing the oldest vegetation buried under an

ice cap, and hence determining the timing of the initiation of its Neoglacial development, is to wait for the whole ice cap to melt out completely. According to the simple life expectancy calculation made for the three ice caps that were the focus of this study (Table 4.1), a large number of small ice caps will have disappear in 50 years' time, so the question of the timing of the start of the Neoglaciation in Svalbard may be resolved in this time frame.

Considering that the oldest ages that are currently available are 3.8 ± 0.1, 3.9 ± 0.1 and 4.0 ± 0.1 cal. ka BP, correspond to vegetation taken along the margin of ice caps that are today still up to two kilometres wide, it is expected that at least locally the onset of the Neoglaciation predates the beginning of the Late Holocene 4.2 thousand years ago. The occurrence of these old ages at the margin of these ice caps could suggest that they survived the Holocene Glacial Minimum (HGMin) as has been the case on Baffin Island where it is common to find vegetation with non-finite ages, and therefore having been covered by ice since before the LGM, melting out of the margin of ice caps (Pendleton et al., 2019). However, while this hypothesis cannot be ruled out for Svalbard, it is considered unlikely for the archipelago's small plateau ice caps given that the HGMin saw extensive ice retreat in Svalbard, including the probable complete melt out of the large Åsgardfonna ice cap (Allaart et al., 2020).

5.3 Perspectives on recolonisation processes, error sources and palaeovegetation

5.3.1 Recolonisation of recently deglaciated areas and resulting error sources

A range of processes related to recolonisation of recently deglaciated surfaces by vegetation can lead to various kinds of errors, both regarding interpretation of the origin of the present vegetation and regarding contamination of the sampled vegetation by modern carbon. Since the publication of the research of La Farge et al. (2013), awareness about the regrowth potential of apparently dead bryophytes has greatly increased. However, only a thorough examination of the collected samples under a low power microscope can rule out the possibility that a moss sample has started to regrow, photosynthesise, and fix modern carbon. Another source of contamination by modern carbon, less discussed but likely of more frequent occurrence, is recolonisation. Indeed, even dead moss exposed by the retreating ice provides an organic substrate that can facilitate the colonisation of the newly deglaciated ground by other plant species, providing for example an easy habitat for wind transported spores. This phenomenon being more obvious in soil-barren environments such as Bassen plateau, where cases of colonisation by new bryophyte species on dead moss patches exposed by ice retreat can be observed. Indeed, at this site, modern moss growth was only observed on top of dead moss patches (Figures 4.3 and 4.4). Here again, while some of the recolonisation, especially if extensive, can

easily be observed in the field, an examination of each sample under a low power microscope is required to make sure that no modern growth is occurring. Recolonisation can in most cases be easily distinguished from regrowth as the colonising species often differs from the dead substrate species. In these two cases of contamination by modern growth, the older the sample, the more impact a small amount of modern carbon will have on the age of the sample (Aitken, 2014).

In addition to bryophytes, other preserved organisms are observed appearing from beneath retreating ice margins. Besides the observations of *in situ* lichens being exposed by retreating ice at Bassen and Frostisen, there are several occurrences of similar observations in the literature. Bergsma et al. (1984) mentions well preserved lichens from his field site and from older reference papers unpublished online (Beschel, 1961; Smith and Norden, 1961) and so does Hilty (1959) and Miller et al. (2013). Thus, when cold ice is involved, the concept of lichen kill-zones marking the maximum extent of LIA advances should be considered carefully. Bergsma's lichens emerging from the ice are described as "faded" and he could allegedly quite easily determine a kill-zone by looking at how fresh the lichens looked. The lichens observed at Bassen were equally faded (Figure 4.4), however, there are cases when the described lichens look as fresh as live ones, such as the ones found at Frostisen in Miller et al. (2013, Figure 1c) and Hilty (1959). It is not known whether these lichens have the potential to achieve cryobiosis and therefore survive their long burial under the ice. Bergsma et al. (1984) assessed freshly exposed lichens for CO_2 efflux using infrared gas analysis, but no respiration was indicated, and the lichens were accordingly considered dead. The degradation time of these dead lichens after exposure by the ice is also unknown, but is expected to be site and substrate dependent as well as reliant on local microclimate factors such as wind.

The preservation of lichens also has implications for the lichenometry geochronological method as it is not necessarily possible to determine whether a lichen is dead without measuring CO_2 efflux. Not knowing if a lichen has been preserved under the ice for an undetermined period of time or not and therefore if its size or diameter can be an indication of how long terrain has been deglaciated, as the potential to confuse lichenometric chronologies where this has occurred. Glacier mice (round shaped moss growing on the surface of glaciers) can be found on freshly deglaciated ground where the retreating ice left them and might then be mistaken for mosses emerging from below the ice. This is especially the case that once on the ground, they can develop a root system into the palaeosoil if there is one in place. They are often bright green and easily distinguishable from formerly ice buried moss, but mistakes could be made if one is not aware of their existence.

Lévesque and Svoboda (1999) underline the destructive nature of climatic cooling events such as the LIA on vulnerable polar ecosystems, emphasizing the fact that vegetation is killed by newly formed ice or perennial snow that eventually covers it as a result of a cooling climatic event and that after deglaciation the recolonisation of these vegetation-dead areas is extremely slow. A whole contradictory new perspective is brought to light, however, with the long-term high preservation potential of vegetated ground once covered by cold based ice. Mature, species rich layers of vegetation can be exposed by retreating ice margins (e.g., Frostisen) in environments where no or very little live plants are found today, as the coldest phases of the Neoglaciation destroyed the vegetation that had been growing around the ice caps under more favourable climatic conditions. Therefore, the local release of thick layers of mostly dead vegetation in nearly barren environments represents a major step in the recolonisation process. As shown by Lafarge et al. (2013) and Roads et al. (2014), mosses have a high potential for regeneration and can regrow from any part of a dead moss. Even if the mature plants are dead, there is likely an abundance of seeds and spores among them that are dormant and can start to develop using the dead vegetation as a nutrient rich substrate. Modern seeds and spores transported from lower lying grounds by wind, birds, foxes or reindeers, can also use the dead vegetation as substrate, as was the case on the dead moss patches found on the periphery of Bassen ice cap (in this specific case, the colonising spores were likely wind transported).

5.3.2 Potential for palaeovegetation reconstruction

The vegetation found melting out of the ice at Frostisen is far more developed, species rich and mature in comparison to that which can be found today in the same area and at similar elevation. This implies that the vegetation layer and the underlying soil have been developing over a longer ice-free period, likely thousands of years, during which the ground was not glaciated and the climatic conditions favourable to vegetation development. It is probable that this vegetation has been developing since the deglaciation of the plateau in the Early Holocene, until being covered by ice during the Neoglaciation while the surrounding and likely as-mature vegetation died and was removed from the landscape by weathering processes.

A similar phenomenon was observed on the Bassen plateau where, approximately 70 m from the ice margin, large dead moss patches showing extensive colonisation were found in a more soil-rich environment than the rest of the rocky plateau in the centre of poorly-developed sorted circles. This implies that where soil was available, large moss patches were living on the plateau prior to the Neoglaciation while today, the only live vegetation found on the plateau is growing on the dead moss exposed by the retreating ice.

The presence of vegetation more mature than that which is observed today prior to the neoglaciation does not indicate that summer temperatures were warmer than today at that time, solely that summer temperature were favourable to the development of the plant species found in the vegetation layer during a long enough period of time for these plants to have to opportunity to settle there. A careful examination of the vegetation emerging from the ice at Frostisen with thorough species inventory and precise abundance quantification for each one of them will allow for local reconstitution of the climatic conditions necessary for its development.

5.3.3 A question of terminology

The terms “kill-date” or “kill-ages” are used in nearly all the literature referring to radiocarbon ages obtained from vegetation that was buried under cold-based ice (e.g., Miller et al., 2013, 2017; Briner et al., 2014; Schweinsberg et al., 2015). However, Cannone et al. (2017) have shown that upon exposure by ice under which they had been buried for several centuries, mosses were still alive for a short period of time (approximately one growing season), before dying of exhaustion while trying to repair damage done to their tissues by the long burial. Their radiocarbon ages thus corresponding to the moment they stopped exchanging carbon with the atmosphere, *id est* when they got buried by snow or ice. Hence, there is a need to change the “kill-date” or “kill-age” denominations into the more accurate terms of “burial date” or “burial age” at least when referring to mosses, as they stay alive until some month after re-exposure by the retreating ice. As it is not known how long other families of plants might survive upon burial by ice, and considering that it is unlikely that they die immediately after this event, the use of “burial” in place of “kill” is recommended in every instance.

The mosses have been shown by Cannone et al. (2017) to be alive (meaning able to perform cellular respiration), which is far from meaning that they are healthy enough to perform photosynthesis. As cellular respiration does not involve any modern carbon intake, but in the contrary contributes to release its own carbon into the atmosphere (see the following equation for cellular respiration, (O’Leary and Plaxton, 2016)), the fact that mosses are still alive should not have influence on their burial age.

$$C_6H_{12}O_6 + 6O_2 \rightarrow 6CO_2 + 6H_2O$$

5.3.4 Exciting perspectives

There has been little research worldwide on moss survival after long term burial under ice and their subsequent regeneration abilities. The few regrowth experiments that have been done were

conducted on moss buried by LIA advances in Arctic Canada and in Antarctica (La Farge et al., 2013; Cannone et al., 2017), apart from Roads et al. (2014) that managed to regrow moss that had been trapped in the permafrost of a maritime Antarctic island for 1.5 thousand years. There is however no published evidence from regrowth of any older moss. If any successful regrowth was obtained from moss collected in Svalbard, it would provide important data on moss regrowth potential with increased burial time and therefore on the probability of finding regrowth in the field in Svalbard as no field evidence has been reported so far for the archipelago.

6 Conclusion

- Preservation of mature layers of vegetation under cold ice can help live vegetation to recolonize an area after deglaciation, as seeds and spores can use the dead vegetation as a nutrient-rich substrate to develop on. This colonisation process is responsible for contamination of the dead vegetation, that is the focus of the ice advance dating method used for this study, by new growth and hence modern carbon, becoming a major error source when radiocarbon dating this palaeovegetation.

- Despite the small size of the dataset gathered within this study (44 ages from 13 ice caps), it was shown that a relatively large minority of these ice caps do not seem to behave according to the main trend set by the other ice caps and can thus be qualified as outliers. This observation complicating the interpretation process of ages related to vegetation buried under ice in Svalbard, as a high number of concordant ages are required to set a trend that can be generalized to the whole of Svalbard, and timings given by isolated data points have to be considered carefully.

- In regard to the data currently available, it is not possible to determine when the Neoglaciation initiated in Svalbard, and only a complete disappearance of the ice caps will allow for sampling of the oldest vegetation buried under them and hence determine when and where the start of the Neoglaciation occurred. As the oldest ages gathered within VEGLAS are close to 4.0 ka BP and correspond to vegetation sampled at the margin of still sizable ice caps, it is expected that, at least locally, the onset of the Neoglaciation predates the beginning of the Late Holocene 4.2 thousand years ago.

- Two distinct ice advance periods were defined by this study, based on radiocarbon ages from vegetation that had been buried under cold based ice caps. A first advance phase occurred during the Dark Ages Cold Period (DACP) between 1650 and 1150 BP and a second during the Little Ice Age (LIA) between 850 and 500 BP. A phase of ice margin retreat corresponding to the Medieval Climate Anomaly is inferred to have occur between these two ice advance phases.

- As most ice caps from the VEGLAS database have current sizes similar to the ones they reached sometimes after the onset of the DACP, data is lacking prior to this event. The low concentration of data points before 1650 BP is does not allow for precise definition of the timing of the earliest ice advance phases, but ice advances occurred at least locally between 4.0 and 3.7 ka BP, around 3.5 ka BP and around 2.2 ka BP. As ice margins are receding, older and older vegetation will be exposed, allowing for a better constraint on the timing of ice advance phases that predate the DACP, helping with the understanding of the complex climatic and glacial fluctuations that characterize the Late Holocene in Svalbard.

- The onset of the LIA happened ca. 300 years earlier in Svalbard than previously defined for the north hemisphere, supporting earlier claims that the LIA initiated several centuries earlier in the North Atlantic region than elsewhere in the north hemisphere.

7 References

Aitken, M.J., 2014. Science-Based Dating in Archaeology. Routledge.

Allaart, L., Müller, J., Schomacker, A., Rydningen, T.A., Håkansson, L., Kjellman, S.E., Mollenhauer, G., Forwick, M., 2020. Late Quaternary glacier and sea-ice history of northern Wijdefjorden, Svalbard. Boreas 49, 417–437. https://doi.org/10.1111/bor.12435

Allaart, L., Schomacker, A., Larsen, N.K., Nørmark, E., Rydningen, T.A., Farnsworth, W.R., Retelle, M., Brynjólfsson, S., Forwick, M., Kjellman, S.E., 2021. Glacial history of the Åsgardfonna Ice Cap, NE Spitsbergen, since the last glaciation. Quat. Sci. Rev. 251, 106717. https://doi.org/10.1016/j.quascirev.2020.106717

Anderson, R.K., Miller, G.H., Briner, J.P., Lifton, N.A., DeVogel, S.B., 2008. A millennial perspective on Arctic warming from 14C in quartz and plants emerging from beneath ice caps. Geophys. Res. Lett. 35. https://doi.org/10.1029/2007GL032057

Andrews, T.D., MacKay, G., 2012. [Introduction]: The Archaeology and Paleoecology of Alpine Ice Patches: A Global Perspective. Arctic 65, iii–vi.

Arnold, J.R., Libby, W.F., 1951. Radiocarbon Dates. Science 113, 111–120.

Arnold, J.R., Libby, W.F., 1949. Age Determinations by Radiocarbon Content: Checks with Samples of Known Age. Science 110, 678–680.

Ballantyne, C.K., Stone, J.O., 2015. Trimlines, blockfields and the vertical extent of the last ice sheet in southern Ireland. Boreas 44, 277–287. https://doi.org/10.1111/bor.12109

Baranowski, S., Karlén, W., 1976. Remnants of Viking Age Tundra in Spitsbergen and Northern Scandinavia. Geogr. Ann. Ser. Phys. Geogr. 58, 35–40. https://doi.org/10.1080/04353676.1976.11879922

Bartels, D., Salamini, F., 2001. Desiccation Tolerance in the Resurrection Plant Craterostigma plantagineum. A Contribution to the Study of Drought Tolerance at the Molecular Level. Plant Physiol. 127, 1346–1353.

Beierlein, L., Salvigsen, O., Schöne, B.R., Mackensen, A., Brey, T., 2015. The seasonal water temperature cycle in the Arctic Dicksonfjord (Svalbard) during the Holocene Climate Optimum derived from subfossil Arctica islandica shells. The Holocene 25, 1197–1207. https://doi.org/10.1177/0959683615580861

Berben, S.M.P., Husum, K., Navarro-Rodriguez, A., Belt, S.T., Aagaard-Sørensen, S., 2017. Semi-quantitative reconstruction of early to late Holocene spring and summer sea ice conditions in the northern Barents Sea. J. Quat. Sci. 32, 587–603. https://doi.org/10.1002/jqs.2953

Bergsma, B.M., Svoboda, J., Freedman, B., 1984. Entombed Plant Communities Released by a Retreating Glacier at Central Ellesmere Island, Canada. Arctic 37, 49–52.

Beschel, 1961. Botany: and some remarks on the history of vegetation and glacierization., in: Arctic Research Expedition to Axel Heiberg Island, Queen Elizabeth Islands. Preliminary Report 1959-1960. Montreal: McGill University., pp. 179–199.

Birks, H.H., 1991. Holocene vegetational history and climatic change in west Spitsbergen - plant macrofossils from Skardtjørna, an Arctic lake. The Holocene 1, 209–218. https://doi.org/10.1177/095968369100100303

Blake, W., 1981. Neoglacial Fluctuations of Glaciers, Southeastern Ellesmere Island, Canadian Arctic Archipelago. Geogr. Ann. Ser. Phys. Geogr. 63, 201–218. https://doi.org/10.2307/520833

Borém, A., Diola, V., Fritsche-Neto, R., 2014. Chapter 1 - Plant Breeding and Biotechnological Advances, in: Borem, A., Fritsche-Neto, R. (Eds.), Biotechnology and Plant Breeding. Academic Press, San Diego, pp. 1–17. https://doi.org/10.1016/B978-0-12-418672-9.00001-5

Bradley, R.S., Bakke, J., 2019. Is there evidence for a 4.2 ka BP event in the northern North Atlantic region? Clim. Past 15, 1665–1676. https://doi.org/10.5194/cp-15-1665-2019

Bradley, R.S., Jonest, P.D., 1993. “Little Ice Age” summer temperature variations: their nature and relevance to recent global warming trends. The Holocene 3, 367–376. https://doi.org/10.1177/095968369300300409
Briner, J.P., Lifton, N.A., Miller, G.H., Refsnider, K., Anderson, R., Finkel, R., 2014. Using in situ cosmogenic 10Be, 14C, and 26Al to decipher the history of polythermal ice sheets on Baffin Island, Arctic Canada. Quat. Geochronol. 19, 4–13. https://doi.org/10.1016/j.quageo.2012.11.005
Cannone, N., Corinti, T., Malfasi, F., Gerola, P., Vianelli, A., Vanetti, I., Zaccara, S., Convey, P., Guglielmin, M., 2017. Moss survival through in situ cryptobiosis after six centuries of glacier burial. Sci. Rep. 7, 4438. https://doi.org/10.1038/s41598-017-04848-6
Cavalieri, D.J., Parkinson, C.L., 2012. Arctic sea ice variability and trends, 1979–2010. The Cryosphere 6, 881–889. https://doi.org/10.5194/tc-6-881-2012
Cerri, M., Tinganelli, W., Negrini, M., Helm, A., Scifoni, E., Tommasino, F., Sioli, M., Zoccoli, A., Durante, M., 2016. Hibernation for space travel: Impact on radioprotection. Life Sci. Space Res. 11, 1–9. https://doi.org/10.1016/j.lssr.2016.09.001
Christiansen, H.H., Etzelmüller, B., Isaksen, K., Juliussen, H., Farbrot, H., Humlum, O., Johansson, M., Ingeman-Nielsen, T., Kristensen, L., Hjort, J., Holmlund, P., Sannel, A.B.K., Sigsgaard, C., Åkerman, H.J., Foged, N., Blikra, L.H., Pernosky, M.A., Ødegård, R.S., 2010. The thermal state of permafrost in the nordic area during the international polar year 2007–2009. Permafr. Periglac. Process. 21, 156–181. https://doi.org/10.1002/ppp.687
Clegg, J.S., 2001. Cryptobiosis — a peculiar state of biological organization. Comp. Biochem. Physiol. B Biochem. Mol. Biol. 128, 613–624. https://doi.org/10.1016/S1096-4959(01)00300-1
Copland, L., 2011. Retreat/Advance of Glaciers, in: Singh, V.P., Singh, P., Haritashya, U.K. (Eds.), Encyclopedia of Snow, Ice and Glaciers. Springer Netherlands, Dordrecht, pp. 934–939. https://doi.org/10.1007/978-90-481-2642-2_446
Corbett, L.B., Bierman, P.R., Rood, D.H., 2016. Constraining multi-stage exposure-burial scenarios for boulders preserved beneath cold-based glacial ice in Thule, northwest Greenland. Earth Planet. Sci. Lett. 440, 147–157. https://doi.org/10.1016/j.epsl.2016.02.004
Coulson, S.J., Midgley, N.G., 2012. The role of glacier mice in the invertebrate colonisation of glacial surfaces: the moss balls of the Falljökull, Iceland. Polar Biol. 35, 1651–1658. https://doi.org/10.1007/s00300-012-1205-4
Curry, A., 2014. Racing the thaw. Science 346, 157–159. https://doi.org/10.1126/science.346.6206.157
Dadic, R., Mott, R., Lehning, M., Burlando, P., 2010a. Wind influence on snow depth distribution and accumulation over glaciers. J. Geophys. Res. Earth Surf. 115. https://doi.org/10.1029/2009JF001261
Dadic, R., Mott, R., Lehning, M., Burlando, P., 2010b. Parameterization for wind–induced preferential deposition of snow. Hydrol. Process. 24, 1994–2006. https://doi.org/10.1002/hyp.7776
Dallmann, W.K., 2015. Geoscience atlas of Svalbard, 292. Norsk Polarinstitutt.
D’Andrea, W.J., Vaillencourt, D.A., Balascio, N.L., Werner, A., Roof, S.R., Retelle, M., Bradley, R.S., 2012. Mild Little Ice Age and unprecedented recent warmth in an 1800 year lake sediment record from Svalbard. Geology 40, 1007–1010. https://doi.org/10.1130/G33365.1
Davis, P.T., Briner, J.P., Coulthard, R.D., Finkel, R.W., Miller, G.H., 2006. Preservation of Arctic landscapes overridden by cold-based ice sheets. Quat. Res. 65, 156–163. https://doi.org/10.1016/j.yqres.2005.08.019
De Geer, G., 1919. Om Spetsbergens natur i Sveagruvans omnejd. (The natural environment of Spitsbergen in the area of Sveagruva.). Ymer.

de Wet, G.A., Balascio, N.L., D'Andrea, W.J., Bakke, J., Bradley, R.S., Perren, B., 2018. Holocene glacier activity reconstructed from proglacial lake Gjøavatnet on Amsterdamøya, NW Svalbard. Quat. Sci. Rev. 183, 188–203. https://doi.org/10.1016/j.quascirev.2017.03.018

Dickson, J.H., Oeggl, K., Handley, L.L., 2003. The Iceman Reconsidered. Sci. Am. 288, 70–79.

Dickson, R.R., Osborn, T.J., Hurrell, J.W., Meincke, J., Blindheim, J., Adlandsvik, B., Vinje, T., Alekseev, G., Maslowski, W., 2000. The Arctic Ocean Response to the North Atlantic Oscillation. J. Clim. 13, 2671–2696. https://doi.org/10.1175/1520-0442(2000)013<2671:TAORTT>2.0.CO;2

Dzierzek, J., Nitychoruk, J., Rzetkowska, A., 1990. Geological-geomorphological analysis and 14C dating of submoraine organogenic deposits within the Renardbreen outer margin, Wedel Jarlsberg Land, Spitsbergen. Polar Res. 8, 275–281. https://doi.org/10.1111/j.1751-8369.1990.tb00389.x

Ebbesen, H., Hald, M., Eplet, T.H., 2007. Lateglacial and early Holocene climatic oscillations on the western Svalbard margin, European Arctic. Quat. Sci. Rev., Early Holocene climate oscillations - causes and consequences 26, 1999–2011. https://doi.org/10.1016/j.quascirev.2006.07.020

Eythórsson J., 1951. Correspondence. Jökla-mýs. J. Glaciol. 1.

Farnell, R., Hare, P.G., Blake, E., Bowyer, V., Schweger, C., Greer, S., Gotthardt, R., 2004. Multidisciplinary Investigations of Alpine Ice Patches in Southwest Yukon, Canada: Paleoenvironmental and Paleobiological Investigations. Arctic 57, 247–259.

Farnsworth, W.R., Allaart, L., Ingólfsson, Ó., Alexanderson, H., Forwick, M., Noormets, R., Retelle, M., Schomacker, A., 2020. Holocene glacial history of Svalbard: Status, perspectives and challenges. Earth-Sci. Rev. 208, 103249. https://doi.org/10.1016/j.earscirev.2020.103249

Farnsworth, W.R., Ingólfsson, Ó., Noormets, R., Allaart, L., Alexanderson, H., Henriksen, M., Schomacker, A., 2017. Dynamic Holocene glacial history of St. Jonsfjorden, Svalbard. Boreas 46, 585–603. https://doi.org/10.1111/bor.12269

Farnsworth, W.R., Ingólfsson, Ó., Retelle, M., Allaart, L., Håkansson, L.M., Schomacker, A., 2018. Svalbard glaciers re-advanced during the Pleistocene–Holocene transition. Boreas 47, 1022–1032. https://doi.org/10.1111/bor.12326

Farnsworth, W.R., Ingólfsson, Ó., Retelle, M., Schomacker, A., 2016. Over 400 previously undocumented Svalbard surge-type glaciers identified. Geomorphology 264, 52–60. https://doi.org/10.1016/j.geomorph.2016.03.025

Fjeldskaar, W., Bondevik, S., Amantov, A., 2018. Glaciers on Svalbard survived the Holocene thermal optimum. Quat. Sci. Rev. 199, 18–29. https://doi.org/10.1016/j.quascirev.2018.09.003

Flink, A.E., Noormets, R., Fransner, O., Hogan, K.A., ÓRegan, M., Jakobsson, M., 2017. Past ice flow in Wahlenbergfjorden and its implications for late Quaternary ice sheet dynamics in northeastern Svalbard. Quat. Sci. Rev. 163, 162–179. https://doi.org/10.1016/j.quascirev.2017.03.021

Flink, A.E., Noormets, R., Kirchner, N., Benn, D.I., Luckman, A., Lovell, H., 2015. The evolution of a submarine landform record following recent and multiple surges of Tunabreen glacier, Svalbard. Quat. Sci. Rev. 108, 37–50. https://doi.org/10.1016/j.quascirev.2014.11.006

Førland, E.J., Benestad, R., Hanssen-Bauer, I., Haugen, J.E., Skaugen, T.E., 2011. Temperature and Precipitation Development at Svalbard 1900–2100. Adv. Meteorol. 2011, 1–14. https://doi.org/10.1155/2011/893790

Forman, S.L., Lubinski, D.J., Ingólfsson, Ó., Zeeberg, J.J., Snyder, J.A., Siegert, M.J., Matishov, G.G., 2004. A review of postglacial emergence on Svalbard, Franz Josef Land and Novaya Zemlya, northern Eurasia. Quat. Sci. Rev., Quaternary Environments of the Eurasian North (QUEEN) 23, 1391–1434. https://doi.org/10.1016/j.quascirev.2003.12.007

Furrer, G., Stapfer, A., Glaser, U., 1991. Zur nacheiszeitlichen Gletschergeschichte des Liefdefjords (Spitzbergen) (Ergebnisse der Geowissenschaftlichen Spitzbergenexpedition 1990). Geogr. Helvetica 46, 147–155. https://doi.org/10.5194/gh-46-147-1991

Godwin, H., 1962. Half-life of Radiocarbon. Nature 195, 984–984. https://doi.org/10.1038/195984a0
Goldthwait, R.P., 1960. Study of ice cliff in Nunatarssuaq. Greenl. Tech. Rep. Cold Reg. Res. Eng. Lab. 47, 63.
Grosjean, M., Suter, P.J., Trachsel, M., Wanner, H., 2007. Ice-borne prehistoric finds in the Swiss Alps reflect Holocene glacier fluctuations. J. Quat. Sci. 22, 203–207. https://doi.org/10.1002/jqs.1111
Grove, J.M., 2001. The Initiation of the "Little Ice Age" in Regions Round the North Atlantic. Clim. Change 48, 53–82. https://doi.org/10.1023/A:1005662822136
Hagen, J.O. (Ed.), 1993. Glacier atlas of Svalbard and Jan Mayen, Meddelelser / Norsk Polarinstitutt. Nork Polarinstitutt, Oslo.
Hald, M., Ebbesen, H., Forwick, M., Godtliebsen, F., Khomenko, L., Korsun, S., Ringstad Olsen, L., Vorren, T.O., 2004. Holocene paleoceanography and glacial history of the West Spitsbergen area, Euro-Arctic margin. Quat. Sci. Rev., Holocene climate variability - a marine perspective 23, 2075–2088. https://doi.org/10.1016/j.quascirev.2004.08.006
Hare, P.G., Greer, S., Gotthardt, R., Farnell, R., Bowyer, V., Schweger, C., Strand, D., 2004. Ethnographic and Archaeological Investigations of Alpine Ice Patches in Southwest Yukon, Canada. Arctic 57, 260–272.
Hare, P.G., Thomas, C.D., Topper, T.N., Gotthardt, R., 2012. The Archaeology of Yukon Ice Patches: New Artifacts, Observations, and Insights. Arctic 65, 118–135.
Helama, S., Jones, P.D., Briffa, K.R., 2017. Dark Ages Cold Period: A literature review and directions for future research. The Holocene 27, 1600–1606. https://doi.org/10.1177/0959683617693898
Hill, M.O., Bell, N., Bruggeman-Nannenga, M.A., Brugués, M., Cano, M.J., Enroth, J., Flatberg, K.I., Frahm, J.-P., Gallego, M.T., Garilleti, R., Guerra, J., Hedenäs, L., Holyoak, D.T., Hyvönen, Ignatov, M.S., Lara, F., Mazimpaka, V., Muñoz, J., Söderström, L., 2006. An annotated checklist of the mosses of Europe and Macaronesia. J. Bryol. 28, 198–267. https://doi.org/10.1179/174328206X119998
Hilty, R.E., 1959. MEASUREMENTS OF ICE TUNNEL DEFORMATION CAMP RED ROCK, GREENLAND. SNOW ICE AND PERMAFROST RESEARCH ESTABLISHMENT WILMETTE IL.
Hisdal, V., 1985. Geography of Svalbard, 81 pp. Oslo Nor. Polarinst.
Holmlund, E.S., 2021. Aldegondabreen glacier change since 1910 from structure-from-motion photogrammetry of archived terrestrial and aerial photographs: utility of a historic archive to obtain century-scale Svalbard glacier mass losses. J. Glaciol. 67, 107–116. https://doi.org/10.1017/jog.2020.89
Hormes, A., Gjermundsen, E.F., Rasmussen, T.L., 2013. From mountain top to the deep sea – Deglaciation in 4D of the northwestern Barents Sea ice sheet. Quat. Sci. Rev. 75, 78–99. https://doi.org/10.1016/j.quascirev.2013.04.009
Hughes, A.L.C., Gyllencreutz, R., Lohne, Ø.S., Mangerud, J., Svendsen, J.I., 2016. The last Eurasian ice sheets - a chronological database and time-slice reconstruction, DATED-1. Boreas 45, 1–45. https://doi.org/10.1111/bor.12142
Humlum, O., 2002. Modelling late 20th-century precipitation in Nordenskiold Land, Svalbard, by geomorphic means. Nor. Geogr. Tidsskr. - Nor. J. Geogr. 56, 96–103. https://doi.org/10.1080/002919502760056413
Humlum, O., Elberling, B., Hormes, A., Fjordheim, K., Hansen, O.H., Heinemeier, J., 2005. Late-Holocene glacier growth in Svalbard, documented by subglacial relict vegetation and living soil microbes. The Holocene 15, 396–407. https://doi.org/10.1191/0959683605hl817rp
Humlum, O., Instanes, A., Sollid, J.L., 2003. Permafrost in Svalbard: a review of research history, climatic background and engineering challenges. Polar Res. 22, 191–215. https://doi.org/10.3402/polar.v22i2.6455

Isaksen, K., Nordli, ø., Førland, E.J., Łupikasza, E., Eastwood, S., Niedźwiedź, T., 2016. Recent warming on Spitsbergen-Influence of atmospheric circulation and sea ice cover: RECENT WARMING ON SPITSBERGEN. J. Geophys. Res. Atmospheres 121, 11,913-11,931. https://doi.org/10.1002/2016JD025606

Ishikawa, M., Murata, T., Sato, Y., Nishiyama, T., Hiwatashi, Y., Imai, A., Kimura, M., Sugimoto, N., Akita, A., Oguri, Y., Friedman, W.E., Hasebe, M., Kubo, M., 2011. Physcomitrella Cyclin-Dependent Kinase A Links Cell Cycle Reactivation to Other Cellular Changes during Reprogramming of Leaf Cells. Plant Cell 23, 2924–2938. https://doi.org/10.1105/tpc.111.088005

Iverson, N.R., McCracken, R.G., Zoet, L.K., Benediktsson, í. ö., Schomacker, A., Johnson, M.D., Woodard, J., 2017. A Theoretical Model of Drumlin Formation Based on Observations at Múlajökull, Iceland: A Model of Drumlin Formation. J. Geophys. Res. Earth Surf. 122, 2302–2323. https://doi.org/10.1002/2017JF004354

Jaedicke, C., Gauer, P., 2005. The influence of drifting snow on the location of glaciers on western Spitsbergen, Svalbard. Ann. Glaciol. 42, 237–242. https://doi.org/10.3189/172756405781812628

James, T.D., Murray, T., Barrand, N.E., Sykes, H.J., Fox, A.J., King, M.A., 2012. Observations of enhanced thinning in the upper reaches of Svalbard glaciers. The Cryosphere 6, 1369–1381. https://doi.org/10.5194/tc-6-1369-2012

Kjellman, S.E., Schomacker, A., Thomas, E.K., Håkansson, L., Duboscq, S., Cluett, A.A., Farnsworth, W.R., Allaart, L., Cowling, O.C., McKay, N.P., Brynjólfsson, S., Ingólfsson, Ó., 2020. Holocene precipitation seasonality in northern Svalbard: Influence of sea ice and regional ocean surface conditions. Quat. Sci. Rev. 240, 106388. https://doi.org/10.1016/j.quascirev.2020.106388

Kleman, J., 1994. Preservation of landforms under ice sheets and ice caps. Geomorphology 9, 19–32. https://doi.org/10.1016/0169-555X(94)90028-0

Kohler, J., James, T.D., Murray, T., Nuth, C., Brandt, O., Barrand, N.E., Aas, H.F., Luckman, A., 2007. Acceleration in thinning rate on western Svalbard glaciers. Geophys. Res. Lett. 34. https://doi.org/10.1029/2007GL030681

Kohler, J., Nordli, Ø., Brandt, O., Isaksson, E., Pohjola, V., Martma, T., Aas, H.F., 2002. Svalbard temperature and precipitation, late 19th century to the present. 21.

Kopec, B.G., Feng, X., Michel, F.A., Posmentier, E.S., 2016. Influence of sea ice on Arctic precipitation. Proc. Natl. Acad. Sci. 113, 46–51. https://doi.org/10.1073/pnas.1504633113

Kutschera, W., 1994. 4.4 Radiocarbon dating of the Iceman Ötzi with accelerator mass spectrometry. Inst. Isot. Res. Nucl. Phys. Univ. Vienna 1–9.

Kutschera, W., Rom, W., 2000. Ötzi, the prehistoric Iceman. Nucl. Instrum. Methods Phys. Res. Sect. B Beam Interact. Mater. At. 164–165, 12–22. https://doi.org/10.1016/S0168-583X(99)01196-9

La Farge, C., Williams, K.H., England, J.H., 2013. Regeneration of Little Ice Age bryophytes emerging from a polar glacier with implications of totipotency in extreme environments. Proc. Natl. Acad. Sci. 110, 9839–9844. https://doi.org/10.1073/pnas.1304199110

Larsen, E., Lysså, A., Rubensdotter, L., Farnsworth, W.R., Jensen, M., Nadeau, M.J., Ottesen, D., 2018. Lateglacial and Holocene glacier activity in the Van Mijenfjorden area, western Svalbard. arktos 4, 1–21. https://doi.org/10.1007/s41063-018-0042-2

Laskar, J., Robutel, P., Joutel, F., Gastineau, M., Correia, A.C.M., Levrard, B., 2004. A long-term numerical solution for the insolation quantities of the Earth. Astron. Astrophys. 428, 261–285. https://doi.org/10.1051/0004-6361:20041335

Lee, C.M., 2012. Withering Snow and Ice in the Mid-latitudes: A New Archaeological and Paleobiological Record for the Rocky Mountain Region. Arctic 65, 165–177.

Lévesque, E., Svoboda, J., 1999. Vegetation re-establishment in polar “lichen-kill” landscapes: a case study of the Little Ice Age impact. Polar Res. 18, 221–228. https://doi.org/10.1111/j.1751-8369.1999.tb00297.x

Lewis, J.K., Bischof, J.C., Braslavsky, I., Brockbank, K.G.M., Fahy, G.M., Fuller, B.J., Rabin, Y., Tocchio, A., Woods, E.J., Wowk, B.G., Acker, J.P., Giwa, S., 2016. The Grand Challenges of Organ Banking: Proceedings from the first global summit on complex tissue cryopreservation. Cryobiology 72, 169–182. https://doi.org/10.1016/j.cryobiol.2015.12.001

Libby, W.F., 1946. Atmospheric Helium Three and Radiocarbon from Cosmic Radiation. Phys. Rev. 69, 671–672. https://doi.org/10.1103/PhysRev.69.671.2

Linick, T.W., Suess, H.E., Becker, B., 1985. La Jolla Measurements of Radiocarbon in South German Oak Tree-Ring Chronologies. Radiocarbon 27, 20–32. https://doi.org/10.1017/S0033822200006901

Long, D.G., Mogensen, G.S., Crum, H.A., Murray, B.M., 1985. Illustrated Moss Flora of Arctic North America and Greenland. Kommissionen for Videnskabelige Undersøgelser i Grønland.

Lønne, I., 2005. Faint traces of high Arctic glaciations: an early Holocene ice-front fluctuation in Bolterdalen, Svalbard. Boreas 34, 308–323. https://doi.org/10.1111/j.1502-3885.2005.tb01103.x

Lovelock, C.E., Jackson, A.E., Melick, D.R., Seppelt, R.D., 1995. Reversible Photoinhibition in Antarctic Moss during Freezing and Thawing. Plant Physiol. 109, 955–961. https://doi.org/10.1104/pp.109.3.955

Lysså, A., Larsen, E.A., Høgaas, F., Jensen, M.A., Klug, M., Rubensdotter, L., Szczuciński, W., 2018. A temporary glacier-surge ice-dammed lake, Braganzavågen, Svalbard. Boreas 47, 837–854. https://doi.org/10.1111/bor.12302

Małecki, J., 2013. Elevation and volume changes of seven Dickson Land glaciers, Svalbard, 1960–1990–2009. Polar Res. 32, 18400. https://doi.org/10.3402/polar.v32i0.18400

Mangerud, J., Svendsen, J.I., 2018. The Holocene Thermal Maximum around Svalbard, Arctic North Atlantic; molluscs show early and exceptional warmth. The Holocene 28, 65–83. https://doi.org/10.1177/0959683617715701

Mann, M.E., Bradley, R.S., Hughes, M.K., 1999. Northern hemisphere temperatures during the past millennium: Inferences, uncertainties, and limitations. Geophys. Res. Lett. 26, 759–762. https://doi.org/10.1029/1999GL900070

Mann, M.E., Zhang, Z., Rutherford, S., Bradley, R.S., Hughes, M.K., Shindell, D., Ammann, C., Faluvegi, G., Ni, F., 2009. Global Signatures and Dynamical Origins of the Little Ice Age and Medieval Climate Anomaly. Science 326, 1256–1260. https://doi.org/10.1126/science.1177303

Marchal, O., Cacho, I., Stocker, T.F., Grimalt, J.O., Calvo, E., Martrat, B., Shackleton, N., Vautravers, M., Cortijo, E., van Kreveld, S., Andersson, C., Koç, N., Chapman, M., Sbaffi, L., Duplessy, J.-C., Sarnthein, M., Turon, J.-L., Duprat, J., Jansen, E., 2002. Apparent long-term cooling of the sea surface in the northeast Atlantic and Mediterranean during the Holocene. Quat. Sci. Rev. 21, 455–483. https://doi.org/10.1016/S0277-3791(01)00105-6

Matthews, J.A., Briffa, K.R., 2005. The ‘little ice age’: re-evaluation of an evolving concept. Geogr. Ann. Ser. Phys. Geogr. 87, 17–36. https://doi.org/10.1111/j.0435-3676.2005.00242.x

Miles, M.W., Andresen, C.S., Dylmer, C.V., 2020. Evidence for extreme export of Arctic sea ice leading the abrupt onset of the Little Ice Age. Sci. Adv. 6, eaba4320. https://doi.org/10.1126/sciadv.aba4320

Miller, G.H., Briner, J.P., Refsnider, K.A., Lehman, S.J., Geirsdóttir, Á., Larsen, D.J., Southon, J.R., 2013. Substantial agreement on the timing and magnitude of Late Holocene ice cap expansion between East Greenland and the Eastern Canadian Arctic: a commentary on Lowell et al., 2013. Quat. Sci. Rev. 77, 239–245. https://doi.org/10.1016/j.quascirev.2013.04.019

Miller, G.H., Geirsdóttir, Á., Zhong, Y., Larsen, D.J., Otto-Bliesner, B.L., Holland, M.M., Bailey, D.A., Refsnider, K.A., Lehman, S.J., Southon, J.R., Anderson, C., Björnsson, H., Thordarson, T., 2012. Abrupt onset of the Little Ice Age triggered by volcanism and sustained by sea-ice/ocean feedbacks. Geophys. Res. Lett. 39. https://doi.org/10.1029/2011GL050168

Miller, G.H., Landvik, J.Y., Lehman, S.J., Southon, J.R., 2017. Episodic Neoglacial snowline descent and glacier expansion on Svalbard reconstructed from the 14C ages of ice-entombed plants. Quat. Sci. Rev. 155, 67–78. https://doi.org/10.1016/j.quascirev.2016.10.023

Möller, M., Kohler, J., 2018. Differing Climatic Mass Balance Evolution Across Svalbard Glacier Regions Over 1900–2010. Front. Earth Sci. 6. https://doi.org/10.3389/feart.2018.00128

Müller, J., Stein, R., 2014. High-resolution record of late glacial and deglacial sea ice changes in Fram Strait corroborates ice–ocean interactions during abrupt climate shifts. Earth Planet. Sci. Lett. 403, 446–455. https://doi.org/10.1016/j.epsl.2014.07.016

Muller, R.A., 1977. Radioisotope Dating with a Cyclotron. Science 196, 489–494. https://doi.org/10.1126/science.196.4289.489

Navarro, F.J., Lapazaran, J., Martín-Español, A., Otero, J., 2016. Ground-penetrating radar studies in Svalbard aimed to the calculation of the ice volume of its glaciers. Cuad. Investig. Geográfica 42, 399–414. https://doi.org/10.18172/cig.2929

Navarro, F.J., Martín-Español, A., Lapazaran, J.J., Grabiec, M., Otero, J., Vasilenko, E.V., Puczko, D., 2014. Ice Volume Estimates from Ground-Penetrating Radar Surveys, Wedel Jarlsberg Land Glaciers, Svalbard. Arct. Antarct. Alp. Res. 46, 394–406. https://doi.org/10.1657/1938-4246-46.2.394

Nelson, D.E., Korteling, R.G., Stott, W.R., 1977. Carbon-14: Direct Detection at Natural Concentrations. Science 198, 507–508. https://doi.org/10.1126/science.198.4316.507

Nesje, A., Dahl, S.O., 2003. The 'Little Ice Age' – only temperature? The Holocene 13, 139–145. https://doi.org/10.1191/0959683603hl603fa

Nesje, A., Pilø, L.H., Finstad, E., Solli, B., Wangen, V., Ødegård, R.S., Isaksen, K., Støren, E.N., Bakke, D.I., Andreassen, L.M., 2012. The climatic significance of artefacts related to prehistoric reindeer hunting exposed at melting ice patches in southern Norway. The Holocene 22, 485–496. https://doi.org/10.1177/0959683611425552

Neuman, Y., 2006. Cryptobiosis: A new theoretical perspective. Prog. Biophys. Mol. Biol. 92, 258–267. https://doi.org/10.1016/j.pbiomolbio.2005.11.001

Nordli, Ø., Przybylak, R., Ogilvie, A.E.J., Isaksen, K., 2014. Long-term temperature trends and variability on Spitsbergen: the extended Svalbard Airport temperature series, 1898–2012. Polar Res. 33, 21349. https://doi.org/10.3402/polar.v33.21349

Nordli, Ø., Wyszyński, P., Gjelten, H., Isaksen, K., Łupikasza, E., Niedźwiedź, T., Przybylak, R., 2020. Revisiting the extended Svalbard Airport monthly temperature series, and the compiled corresponding daily series 1898–2018. https://doi.org/10.33265/polar.v39.3614

Nuth, C., Kohler, J., König, M., von Deschwanden, A., Hagen, J.O., Kääb, A., Moholdt, G., Pettersson, R., 2013. Decadal changes from a multi-temporal glacier inventory of Svalbard. The Cryosphere 7, 1603–1621. https://doi.org/10.5194/tc-7-1603-2013

Nuth, C., Moholdt, G., Kohler, J., Hagen, J.O., Kääb, A., 2010. Svalbard glacier elevation changes and contribution to sea level rise. J. Geophys. Res. Earth Surf. 115. https://doi.org/10.1029/2008JF001223

Ødegård, R., Nesje, A., Isaksen, K., Andreassen, L.M., Eiken, T., Schwikowski, M., Uglietti, C., 2017. Climate change threatens archaeologically significant ice patches: Insights into their age, internal structure, mass balance and climate sensitivity. The Cryosphere 11, 17–32. https://doi.org/10.5194/tc-11-17-2017

Oeggl, K., 2009. The significance of the Tyrolean Iceman for the archaeobotany of Central Europe. Veg. Hist. Archaeobotany 18, 1–11.

Oeggl, K., Kofler, W., Schmidl, A., Dickson, J.H., Egarter-Vigl, E., Gaber, O., 2007. The reconstruction of the last itinerary of “Ötzi”, the Neolithic Iceman, by pollen analyses from sequentially sampled gut extracts. Quat. Sci. Rev. 26, 853–861. https://doi.org/10.1016/j.quascirev.2006.12.007

Oerlemans, J., Jania, J., Kolondra, L., 2011. Application of a minimal glacier model to Hansbreen, Svalbard. The Cryosphere 5, 1–11. https://doi.org/10.5194/tc-5-1-2011

O’Leary, B.M., Plaxton, W.C., 2016. Plant Respiration, in: ELS. American Cancer Society, pp. 1–11. https://doi.org/10.1002/9780470015902.a0001301.pub3

Pendleton, S.L., Miller, G.H., Lifton, N., Lehman, S.J., Southon, J., Crump, S.E., Anderson, R.S., 2019. Rapidly receding Arctic Canada glaciers revealing landscapes continuously ice-covered for more than 40,000 years. Nat. Commun. 10, 445. https://doi.org/10.1038/s41467-019-08307-w

Philipps, W., Briner, J.P., Gislefoss, L., Linge, H., Koffman, T., Fabel, D., Xu, S., Hormes, A., 2017. Late Holocene glacier activity at inner Hornsund and Scottbreen, southern Svalbard. J. Quat. Sci. 32, 501–515. https://doi.org/10.1002/jqs.2944

Pilø, L.H., Barrett, J.H., Eiken, T., Finstad, E., Grønning, S., Post-Melbye, J.R., Nesje, A., Rosvold, J., Solli, B., Ødegård, R.S., 2020. Interpreting archaeological site-formation processes at a mountain ice patch: A case study from Langfonne, Norway. The Holocene 0959683620972775. https://doi.org/10.1177/0959683620972775

Pithan, F., Mauritsen, T., 2014. Arctic amplification dominated by temperature feedbacks in contemporary climate models. Nat. Geosci. 7, 181–184. https://doi.org/10.1038/ngeo2071

Porter, P.R., Evans, A.J., Hodson, A.J., Lowe, A.T., Crabtree, M.D., 2008. Sediment–moss interactions on a temperate glacier: Falljökull, Iceland. Ann. Glaciol. 48, 25–31. https://doi.org/10.3189/172756408784700734

Pugnaire, F., Valladares, F., 1999. Handbook of Functional Plant Ecology. CRC Press.

Rachlewicz, G., Szczuciński, W., Ewertowski, M., 2007. Post-“Little Ice Age” retreat rates of glaciers around Billefjorden in central Spitsbergen, Svalbard. Pol. Polar Res. 159–186.

Raina, V.K., 2013. Global Warming and the Glacier Retreat: An Overview, in: Sinha, R., Ravindra, R. (Eds.), Earth System Processes and Disaster Management, Society of Earth Scientists Series. Springer, Berlin, Heidelberg, pp. 9–23. https://doi.org/10.1007/978-3-642-28845-6_2

Rana, N., Sharma, S., Ali, S.N., Singh, S., Shukla, A.D., 2019. Investigating the sensitivity of glaciers to climate variability since the MIS-2 in the upper Ganga catchment (Saraswati valley), Central Himalaya. Geomorphology 346, 106854. https://doi.org/10.1016/j.geomorph.2019.106854

Rasmussen, T.L., Forwick, M., Mackensen, A., 2012. Reconstruction of inflow of Atlantic Water to Isfjorden, Svalbard during the Holocene: Correlation to climate and seasonality. Mar. Micropaleontol. 94–95, 80–90. https://doi.org/10.1016/j.marmicro.2012.06.008

Rasmussen, T.L., Thomsen, E., Skirbekk, K., Ślubowska-Woldengen, M., Klitgaard Kristensen, D., Koç, N., 2014. Spatial and temporal distribution of Holocene temperature maxima in the northern Nordic seas: interplay of Atlantic-, Arctic- and polar water masses. Quat. Sci. Rev., APEX II: Arctic Palaeoclimate and its Extremes 92, 280–291. https://doi.org/10.1016/j.quascirev.2013.10.034

Reckin, R., 2013. Ice patch archaeology in global perspective: archaeological discoveries from alpine ice patches worldwide and their relationship with paleoclimates. J. World Prehistory 26, 323–385.

Reckin, R.J., 2018. Mountains as Crossroads: Temporal and Spatial Patterns of High Elevation Activity in the Greater Yellowstone Ecosystem, USA (Thesis). University of Cambridge. https://doi.org/10.17863/CAM.25441

Reimer, P.J., Austin, W.E.N., Bard, E., Bayliss, A., Blackwell, P.G., Ramsey, C.B., Butzin, M., Cheng, H., Edwards, R.L., Friedrich, M., Grootes, P.M., Guilderson, T.P., Hajdas, I., Heaton, T.J., Hogg,

A.G., Hughen, K.A., Kromer, B., Manning, S.W., Muscheler, R., Palmer, J.G., Pearson, C., Plicht, J. van der, Reimer, R.W., Richards, D.A., Scott, E.M., Southon, J.R., Turney, C.S.M., Wacker, L., Adolphi, F., Büntgen, U., Capano, M., Fahrni, S.M., Fogtmann-Schulz, A., Friedrich, R., Köhler, P., Kudsk, S., Miyake, F., Olsen, J., Reinig, F., Sakamoto, M., Sookdeo, A., Talamo, S., 2020. The IntCal20 Northern Hemisphere Radiocarbon Age Calibration Curve (0–55 cal kBP). Radiocarbon 62, 725–757. https://doi.org/10.1017/RDC.2020.41

Renssen, H., Seppä, H., Heiri, O., Roche, D.M., Goosse, H., Fichefet, T., 2009. The spatial and temporal complexity of the Holocene thermal maximum. Nat. Geosci. 2, 411–414. https://doi.org/10.1038/ngeo513

Reusche, M., Winsor, K., Carlson, A.E., Marcott, S.A., Rood, D.H., Novak, A., Roof, S., Retelle, M., Werner, A., Caffee, M., Clark, P.U., 2014. 10Be surface exposure ages on the late-Pleistocene and Holocene history of Linnébreen on Svalbard. Quat. Sci. Rev. 89, 5–12. https://doi.org/10.1016/j.quascirev.2014.01.017

Risebrobakken, B., Dokken, T., Smedsrud, L.H., Andersson, C., Jansen, E., Moros, M., Ivanova, E.V., 2011. Early Holocene temperature variability in the Nordic Seas: The role of oceanic heat advection versus changes in orbital forcing. Paleoceanography 26. https://doi.org/10.1029/2011PA002117

Roads, E., Longton, R.E., Convey, P., 2014. Millennial timescale regeneration in a moss from Antarctica. Curr. Biol. 24, R222–R223. https://doi.org/10.1016/j.cub.2014.01.053

Rogers, S.R., Fischer, M., Huss, M., 2014. Combining glaciological and archaeological methods for gauging glacial archaeological potential. J. Archaeol. Sci. 52, 410–420. https://doi.org/10.1016/j.jas.2014.09.010

Rollo, F., Ubaldi, M., Ermini, L., Marota, I., 2002. Ötzi's last meals: DNA analysis of the intestinal content of the Neolithic glacier mummy from the Alps. Proc. Natl. Acad. Sci. 99, 12594–12599. https://doi.org/10.1073/pnas.192184599

Rønning, O.I., 1996. The Flora of Svalbard. Norsk polarinstitutt.

Røthe, T.O., Bakke, J., Støren, E.W.N., Bradley, R.S., 2018. Reconstructing Holocene Glacier and Climate Fluctuations From Lake Sediments in Vårfluesjøen, Northern Spitsbergen. Front. Earth Sci. 6. https://doi.org/10.3389/feart.2018.00091

Røthe, T.O., Bakke, J., Vasskog, K., Gjerde, M., D'Andrea, W.J., Bradley, R.S., 2015. Arctic Holocene glacier fluctuations reconstructed from lake sediments at Mitrahalvøya, Spitsbergen. Quat. Sci. Rev. 109, 111–125. https://doi.org/10.1016/j.quascirev.2014.11.017

Salvigsen, O., 1981. Radiocarbon Dated Raised Beaches in Kong Karls Land, Svalbard, and their Consequences for the Glacial History of the Barents Sea Area. Geogr. Ann. Ser. Phys. Geogr. 63, 283–291. https://doi.org/10.1080/04353676.1981.11880043

Santos, G., 2012. Beyond archaeology: 14C-AMS and the global carbon cycle. AIP Conf. Proc. 1423, 311. https://doi.org/10.1063/1.3688819

Schomacker, A., Farnsworth, W.R., Ingólfsson, Ó., Allaart, L., Håkansson, L., Retelle, M., Siggaard-Andersen, M.-L., Korsgaard, N.J., Rouillard, A., Kjellman, S.E., 2019. Postglacial relative sea level change and glacier activity in the early and late Holocene: Wahlenbergfjorden, Nordaustlandet, Svalbard. Sci. Rep. 9, 6799. https://doi.org/10.1038/s41598-019-43342-z

Schomacker, A., Kjær, K.H., 2008. Quantification of dead-ice melting in ice-cored moraines at the high-Arctic glacier Holmströmbreen, Svalbard. Boreas 37, 211–225. https://doi.org/10.1111/j.1502-3885.2007.00014.x

Schweinsberg, A., Briner, J.P., Miller, G.H., Bennike, O., 2015. Records of Local Glacier Variability in Western Greenland During the Holocene From Lake Sediments, Ice-cap-killed Vegetation, and 10Be Dating. AGU Fall Meet. Abstr. 33, PP33A-2281.

Screen, J.A., Simmonds, I., 2010. The central role of diminishing sea ice in recent Arctic temperature amplification. Nature 464, 1334–1337. https://doi.org/10.1038/nature09051

Sessford, E.G., Strzelecki, M.C., Hormes, A., 2015. Reconstruction of Holocene patterns of change in a High Arctic coastal landscape, Southern Sassenfjorden, Svalbard. Geomorphology 234, 98–107. https://doi.org/10.1016/j.geomorph.2014.12.046

Sevestre, H., Benn, D.I., Hulton, N.R.J., Bælum, K., 2015. Thermal structure of Svalbard glaciers and implications for thermal switch models of glacier surging. J. Geophys. Res. Earth Surf. 120, 2220–2236. https://doi.org/10.1002/2015JF003517

Shen-Miller, J., Mudgett, M.B., Schopf, J.W., Clarke, S., Berger, R., 1995. Exceptional seed longevity and robust growth: ancient Sacred Lotus from China. Am. J. Bot. 82, 1367–1380. https://doi.org/10.1002/j.1537-2197.1995.tb12673.x

Shulgina, T.M., Genina, E.Y., Gordov, E.P., 2011. Dynamics of climatic characteristics influencing vegetation in Siberia. Environ. Res. Lett. 6, 045210. https://doi.org/10.1088/1748-9326/6/4/045210

Skre, O., Oechel, W.C., 1981. Moss functioning in different taiga ecosystems in interior Alaska. Oecologia 48, 50–59. https://doi.org/10.1007/BF00346987

Ślubowska-Woldengen, M., Rasmussen, T.L., Koç, N., Klitgaard-Kristensen, D., Nilsen, F., Solheim, A., 2007. Advection of Atlantic Water to the western and northern Svalbard shelf since 17,500calyr BP. Quat. Sci. Rev. 26, 463–478. https://doi.org/10.1016/j.quascirev.2006.09.009

Small, D., Clark, C.D., Chiverrell, R.C., Smedley, R.K., Bateman, M.D., Duller, G.A.T., Ely, J.C., Fabel, D., Medialdea, A., Moreton, S.G., 2017. Devising quality assurance procedures for assessment of legacy geochronological data relating to deglaciation of the last British-Irish Ice Sheet. Earth-Sci. Rev. 164, 232–250. https://doi.org/10.1016/j.earscirev.2016.11.007

Smith, D.I., Norden, I.G.C. (19th: 1960, 1961. The glaciation of northern Ellesmere Island., in: The Physical Geography of Greenland. Folia Geographica Danica, pp. 224–234.

Staiger, J.K.W., Gosse, J.C., Johnson, J.V., Fastook, J., Gray, J.T., Stockli, D.F., Stockli, L., Finkel, R., 2005. Quaternary relief generation by polythermal glacier ice. Earth Surf. Process. Landf. 30, 1145–1159. https://doi.org/10.1002/esp.1267

Stark, L.R., 2017. Ecology of desiccation tolerance in bryophytes: A conceptual framework and methodology. The Bryologist 120, 130–165. https://doi.org/10.1639/0007-2745-120.2.130

Starr, C., 1993. Atmospheric CO2 residence time and the carbon cycle. Energy, 1992 EPRI/SIO Symposium on Global Warming 18, 1297–1310. https://doi.org/10.1016/0360-5442(93)90017-8

Stuiver, M., Reimer, P.J., 1993. Extended 14C Data Base and Revised CALIB 3.0 14C Age Calibration Program. Radiocarbon 35, 215–230. https://doi.org/10.1017/S0033822200013904

Stuiver, M., Reimer, P.J., 1986. A Computer Program for Radiocarbon Age Calibration. Radiocarbon 28, 1022–1030. https://doi.org/10.1017/S0033822200060276

Svendsen, J.I., Mangerud, J., 1997. Holocene glacial and climatic variations on Spitsbergen, Svalbard. The Holocene 7, 45–57. https://doi.org/10.1177/095968369700700105

Synal, H.-A., 2013. Developments in accelerator mass spectrometry. Int. J. Mass Spectrom., 100 years of Mass Spectrometry 349–350, 192–202. https://doi.org/10.1016/j.ijms.2013.05.008

Synal, H.-A., Stocker, M., Suter, M., 2007. MICADAS: A new compact radiocarbon AMS system. Nucl. Instrum. Methods Phys. Res. Sect. B Beam Interact. Mater. At., Accelerator Mass Spectrometry 259, 7–13. https://doi.org/10.1016/j.nimb.2007.01.138

Turetsky, M.R., Bond-Lamberty, B., Euskirchen, E., Talbot, J., Frolking, S., McGuire, A.D., Tuittila, E.-S., 2012. The resilience and functional role of moss in boreal and arctic ecosystems. New Phytol. 196, 49–67. https://doi.org/10.1111/j.1469-8137.2012.04254.x

van der Bilt, W., D`Andrea, W., Bakke, J., Balascio, N., Werner, J., Hoek, W., 2016. Short-lived high-amplitude cooling on Svalbard during the Dark Ages 18, EPSC2016-15694.

van der Bilt, W., D'Andrea, W.J., Werner, J.P., Bakke, J., 2019. Early Holocene Temperature Oscillations Exceed Amplitude of Observed and Projected Warming in Svalbard Lakes. Geophys. Res. Lett. 46, 14732–14741. https://doi.org/10.1029/2019GL084384

van der Bilt, W.G.M., Bakke, J., Vasskog, K., D'Andrea, W.J., Bradley, R.S., Ólafsdóttir, S., 2015. Reconstruction of glacier variability from lake sediments reveals dynamic Holocene climate in Svalbard. Quat. Sci. Rev. 126, 201–218. https://doi.org/10.1016/j.quascirev.2015.09.003

van der Bilt, W.G.M., D'Andrea, W.J., Bakke, J., Balascio, N.L., Werner, J.P., Gjerde, M., Bradley, R.S., 2018. Alkenone-based reconstructions reveal four-phase Holocene temperature evolution for High Arctic Svalbard. Quat. Sci. Rev. 183, 204–213. https://doi.org/10.1016/j.quascirev.2016.10.006

van Pelt, W.J.J., Oerlemans, J., Reijmer, C.H., Pettersson, R., Pohjola, V.A., Isaksson, E., Divine, D., 2013. An iterative inverse method to estimate basal topography and initialize ice flow models. The Cryosphere 7, 987–1006. https://doi.org/10.5194/tc-7-987-2013

Vanderhoek, R., Dixon, E.J., Jarman, N.L., Tedor, R.M., 2012. Ice Patch Archaeology in Alaska: 2000–10. Arctic 65, 153–164.

Vedeler, M., Jørgensen, L.B., 2013. Out of the Norwegian glaciers: Lendbreen—a tunic from the early first millennium AD. Antiquity 87, 788–801. https://doi.org/10.1017/S0003598X00049462

Vinther, B.M., Buchardt, S.L., Clausen, H.B., Dahl-Jensen, D., Johnsen, S.J., Fisher, D.A., Koerner, R.M., Raynaud, D., Lipenkov, V., Andersen, K.K., Blunier, T., Rasmussen, S.O., Steffensen, J.P., Svensson, A.M., 2009. Holocene thinning of the Greenland ice sheet. Nature 461, 385–388. https://doi.org/10.1038/nature08355

Voldstad, L.H., Alsos, I.G., Farnsworth, W.R., Heintzman, P.D., Håkansson, L., Kjellman, S.E., Rouillard, A., Schomacker, A., Eidesen, P.B., 2020. A complete Holocene lake sediment ancient DNA record reveals long-standing high Arctic plant diversity hotspot in northern Svalbard. Quat. Sci. Rev. 234, 106207. https://doi.org/10.1016/j.quascirev.2020.106207

Walczowski, W., Piechura, J., 2011. Influence of the West Spitsbergen Current on the local climate. Int. J. Climatol. 31, 1088–1093. https://doi.org/10.1002/joc.2338

Walker, M., Head, M.J., Berkelhammer, M., Björck, S., Cheng, H., Cwynar, L., Fisher, D., Gkinis, V., Long, A., Lowe, J., Newnham, R., Rasmussen, S.O., Weiss, H., 2018. Formal ratification of the subdivision of the Holocene Series/Epoch (Quaternary System/Period): two new Global Boundary Stratotype Sections and Points (GSSPs) and three new stages/subseries. Episodes 41, 213–223. https://doi.org/10.18814/epiiugs/2018/018016

Walker, M., Johnsen, S., Rasmussen, S.O., Popp, T., Steffensen, J.-P., Gibbard, P., Hoek, W., Lowe, J., Andrews, J., Björck, S., Cwynar, L.C., Hughen, K., Kershaw, P., Kromer, B., Litt, T., Lowe, D.J., Nakagawa, T., Newnham, R., Schwander, J., 2009. Formal definition and dating of the GSSP (Global Stratotype Section and Point) for the base of the Holocene using the Greenland NGRIP ice core, and selected auxiliary records. J. Quat. Sci. 24, 3–17. https://doi.org/10.1002/jqs.1227

Wang, T., Surge, D., Mithen, S., 2012. Seasonal temperature variability of the Neoglacial (3300–2500BP) and Roman Warm Period (2500–1600BP) reconstructed from oxygen isotope ratios of limpet shells (Patella vulgata), Northwest Scotland. Palaeogeogr. Palaeoclimatol. Palaeoecol. 317–318, 104–113. https://doi.org/10.1016/j.palaeo.2011.12.016

Wanner, H., Beer, J., Bütikofer, J., Crowley, T.J., Cubasch, U., Flückiger, J., Goosse, H., Grosjean, M., Joos, F., Kaplan, J.O., Küttel, M., Müller, S.A., Prentice, I.C., Solomina, O., Stocker, T.F., Tarasov, P., Wagner, M., Widmann, M., 2008. Mid- to Late Holocene climate change: an overview. Quat. Sci. Rev. 27, 1791–1828. https://doi.org/10.1016/j.quascirev.2008.06.013

Werner, A., 1993. Holocene moraine chronology, Spitsbergen, Svalbard: lichenometric evidence for multiple Neoglacial advances in the Arctic. The Holocene 3, 128–137. https://doi.org/10.1177/095968369300300204

Werner, K., Müller, J., Husum, K., Spielhagen, R.F., Kandiano, E.S., Polyak, L., 2016. Holocene sea subsurface and surface water masses in the Fram Strait – Comparisons of temperature and sea-ice reconstructions. Quat. Sci. Rev., Special Issue: PAST Gateways (Palaeo-Arctic Spatial and Temporal Gateways) 147, 194–209. https://doi.org/10.1016/j.quascirev.2015.09.007

Weston Blake Jr., 1981. Neoglacial Fluctuations of Glaciers, Southeastern Ellesmere Island, Canadian Arctic Archipelago: Geografiska Annaler: Series A, Physical Geography: Vol 63, No 3-4 [WWW Document]. URL https://www.tandfonline.com/doi/abs/10.1080/04353676.1981.11880035 (accessed 1.18.21).

Wharton, D.A., 2015. Anhydrobiosis. Curr. Biol. 25, R1114–R1116. https://doi.org/10.1016/j.cub.2015.09.047

Wickström, S., Jonassen, M.O., Vihma, T., Uotila, P., 2020. Trends in cyclones in the high-latitude North Atlantic during 1979–2016. Q. J. R. Meteorol. Soc. 146, 762–779. https://doi.org/10.1002/qj.3707

Williams, D.R., 2020. Earth Fact Sheet [WWW Document]. Earth Fact Sheet NASA. URL https://nssdc.gsfc.nasa.gov/planetary/factsheet/earthfact.html (accessed 2.22.21).

Wohlfarth, B., 2009. Ice-free conditions in Fennoscandia during Marine Oxygen Isotope Stage 3? (Technical report No. SKB-TR-09-12). Swedish Nuclear Fuel and Waste Management Co., Stockholm, Sweden.

Zechmeister, H., 1995. Growth rates of five pleurocarpous moss species under various climatic conditions. J. Bryol. 18, 455–468. https://doi.org/10.1179/jbr.1995.18.3.455

Zhurbenko, M.P., Brackel, W. von, 2013. Checklist of Lichenicolous Fungi and Lichenicolous Lichens of Svalbard, Including New Species, New Records and Revisions. Herzogia 26, 323–359. https://doi.org/10.13158/heia.26.2.2013.323

Zink, A.R., Maixner, F., 2019. The Current Situation of the Tyrolean Iceman. Gerontology 65, 699–706. https://doi.org/10.1159/000501878

8 Appendix

The VEGLAS database can be accessed here:
https://www.dropbox.com/scl/fi/ueor4u1qk9kc8txaydpc2/VEGLAS-database.xlsx?dl=0&rlkey=ffop6yxs1u7r9hsdhjmwycpts